ARHGEF6 controls speed and directionality of lymphocyte migration by regulating Rac1/PAK2/LIMK1/cofilin signaling pathway

Dissertation

zur Erlangung des akademischen Grades

doctor rerum naturalium (Dr. rer. nat.)

genehmigt durch
die Fakultät für Naturwissenschaften
der Otto-von-Guericke-Universität Magdeburg

von MSc Pharmazie Dejan Mamula

geb. am 15. Dezember 1980 in Valjevo (Serbien)

Gutachter

Prof. Dr. Klaus-Dieter Fischer

Prof. Dr. Klaudia Giehl

Eingereicht am 12. April 2019

Verteidigt am 06. Dezember 2019

TABLE OF CONTENTS

List of tables and figures **v**

Summary **viii**

Zusammenfassung **ix**

1. INTRODUCTION **1**

1.1 The principle of T cell immunity 1

1.2 T cell development 3

1.3 T cell activation and motility 6

1.4 Mechanism of leukocytes migration 9

1.5 The role of Rho GTPases and RhoGEFs in T cell migration 11

1.6 PIX/GIT complex, effectors and implicated signaling pathways 13

1.7 PAK activation by Rac/Cdc42 18

1.8 Downstream regulation of actin dynamics 20

1.9 Immune phenotype of *Arhgef6*$^{-/-}$ mice 26

1.10 Aims of the study 27

2. MATERIALS AND METHODS **28**

2.1 Materials **28**

2.1.1 Membranes and plastic ware 28

2.1.2 Equipment and software tools 29

2.1.3 Kits 29

2.1.4 Chemicals and reagents for cell culture 30

2.1.5 Cells 31

2.1.6 Vectors, primers and oligos 31

2.1.7 Antibodies 32

2.1.7.1 For Western Blotting 32

2.1.7.2 For Immunocytochemistry 33

2.1.7.3 For Stimulation 35

2.1.7.4 For Flow Cytometry 36

2.1.8 Other chemicals and reagents (in alphabetical order) 36

2.2 Methods **39**

2.2.1 Cell cultures 39

2.2.2 IL-7 production 39

2.2.3 Mice 40

2.2.4 Primary cell preparations 40

2.2.4.1 Thymocyte and lymphocyte isolation 40

2.2.4.2 Counting cells by FACS 41

2.2.4.3 Purification of $CD4^+$ T cells 41

2.2.4.4 Culturing of activated $CD4^+$ T cells 41

2.2.4.5 Flow cytometry 42

2.2.4.6 Stimulation of thymocytes for western blot analysis 43

2.2.5 Electroporation of mammalian cells 44

2.2.6 Transwell migration (HSB2 and Jurkat cells) 44

2.2.7 Biochemistry 45

2.2.7.1 Sample preparation for western blot 45

2.2.7.2 Immunoprecipitation and kinase activity assay 46

2.2.7.3 GST-Pulldown 48

2.2.7.4 Western blot 49

2.2.7.5 2D Blue Native PAGE (BN PAGE) 51

2.2.7.6 Gel filtration (size-exclusion chromatography) 53

2.2.8 Molecular Biology 54

2.2.8.1 Directional cloning into plasmid vectors 54

2.2.8.2 Bacterial manipulation 55

2.2.8.2.1 Bacterial cell culture 55

2.2.8.2.2 Transformation by electroporation 56

2.2.8.3 Preparation of plasmid DNA (miniprep) 56

2.2.8.4 Agarose gel electrophoresis 57

2.2.8.5 Preparation of plasmid DNA 57

2.2.9 Immunocytochemistry and imaging 58

2.2.9.1 Immunocytochemistry 58

2.2.9.2 2D random migration assay for T cells 59

2.2.9.3 Lentibrite infection protocol 59

2.2.9.4 Raji-T cell conjugation 59

2.2.9.5 Image acquisition and analysis 60

2.2.10 Statistics 61

3. RESULTS **62**

3.1 Characterization of *Arhgef6*$^{-/-}$ T cell motility in a 2D migration model 63

3.2 Characterization of PIX/GIT complex and its constituents in *Arhgef6*$^{-/-}$ thymocytes 67

3.3 Increased ARHGEF7 levels and Rac1 activation in *Arhgef6*$^{-/-}$ CD4^{+} T cells 72

3.4 PIX effector kinases PAK1 and PAK2 in *Arhgef6* deficient cells 77

3.5 The role of ARHGEF6 in LIMK activation 80

3.6 The role of ARHGEF6 in cofilin deactivation 82

3.7 Actin remodeling/turnover in *Arhgef6*$^{-/-}$ CD4^{+} T cells 86

3.8 Reduction of GIT2 in *Arhgef6*$^{-/-}$ CD4^{+} T cells 89

3.9 Paxillin and phospho-paxillin in *Arhgef6*$^{-/-}$ CD4^{+} T cells 90

3.10 Vinculin in *Arhgef6*$^{-/-}$ CD4^{+} T cells 93

3.11 Altered lamellipodia morphology in *Arhgef6*$^{-/-}$ CD4^{+} T cells 95

3.12 Role of LIMK on cellular motility of CD4^{+} T cells 98

3.13 Supplementary figures and movies 101

4. DISCUSSION **104**

4.1 ARHGEF6 controls PAK2 signaling in T cell migration 105

4.2 ARHGEF6 regulates ARHGEF7 signaling in T cell migration 110

4.3 Possible role of ARHGEF6 in adhesion formation 112

4.4 Conclusion and future outlook 116

5. ABBREVIATIONS **119**

6. REFERENCES **122**

Ehrenerklärung **136**

List of tables and figures

Table 1. Materials for Western Blot 28
Table 2. Sterile plastic ware for cell culture 28
Table 3. Other materials 28
Table 4. Machines 29
Table 5. Software 29
Table 6. Kits 29
Table 7. Chemicals and reagents for cell culture 30
Table 8. Cell lines and bacteria 31
Table 9. Vectors 31
Table 10. Primers 31
Table 11. Oligos for shRNA cloning 32
Table 12. Primary antibodies for Western blot 32
Table 13. Secondary antibodies for Western blot 33
Table 14. Primary antibodies for immunocytochemistry 33
Table 15. Secondary antibodies and labelling kits for immunocytochemistry 35
Table 16. Antibodies for stimulation 35
Table 17. Antibodies for flow cytometry 36
Table 18. Cell lines and cultivation media 39
Table 19. J558 Il-7 cultivation medium 40
Table 20. Proliferation medium 42
Table 21. Migration medium 44
Table 22. Lysis buffer composition 45
Table 23. 4xSDS loading buffer 46
Table 24. Immunoprecipitation buffer 46
Table 25. Pulldown buffer 48
Table 26a. Laemmli system: gradient gels for 10 gels (1 mm) 49
Table 26b. Laemmli system: homogels for 8 gels (1 mm) 50
Table 27. Solutions for Coommassie staining 50
Table 28. Blotting and washing buffers 50
Table 29. Materials and solutions for BN PAGE 52
Table 30. Buffers used for size-exclusion chromatography 54
Table 31. Annealing buffer 54
Table 32. LB medium 1 liter 56

Table 33. Miniprep buffers 57
Table 34. Solutions for agarose gel electrophoresis 57
Table 35. Buffers for $CD4^+$ T cell imaging 58
Table 36. Buffers and chemicals for Raji-T cell conjugation 60

Figure 1. T lymphocytes activation 2
Figure 2. Amoeboid cell migration models 11
Figure 3. Rho GTPases activation/inactivation cycle 12
Figure 4. Rho GTPases influence cell polarity and protrusion 12
Figure 5. Rho GTPases influence cell migration 13
Figure 6. Protein interaction domains of the PIX and GIT proteins 15
Figure 7. Route of migration during the different stages of thymocytes development 18
Figure 8. The mechanism of PAK activation 19
Figure 9. The role and cycling of cofilin 21
Figure 10. The role of Rho GTPases and FA proteins in adhesion maturation 26
Figure 11. Increased motility of *Arhgef6*$^{-/-}$ thymocytes in vitro 62
Figure 12. Increased motility of T cell lines upon *Arhgef6* knockdown 64
Figure 13. Velocity and directionality of wt and *Arhgef6*$^{-/-}$ $CD4^+$ T cells on 2D substrates 66
Figure 14. ARHGEF6 interacts with GIT1 and PAK2 in murine thymocytes 68
Figure 15. The PIX/GIT complex is altered in the absence of ARHGEF6 69
Figure 16. Without ARHGEF6 PIX/GIT complex members are enriched in larger complexes 71
Figure 17. Increased ARHGEF7 level in *Arhgef6*$^{-/-}$ $CD4^+$ T cells 73
Figure 18. Increased Rac1 activity in migrating *Arhgef6*$^{-/-}$ $CD4^+$ T cells 76
Figure 19. Increased PAK2 level in *Arhgef6*$^{-/-}$ $CD4^+$ T cells 78
Figure 20. Reduced PAK catalytic activity in *Arhgef6*$^{-/-}$ thymocytes 79
Figure 21. Reduced LIMK1 phosphorylation in *Arhgef6*$^{-/-}$ $CD4^+$ T cells 81
Figure 22. Less pLIMK1 localization in lamellipodia of *Arhgef6*$^{-/-}$ cells 82
Figure 23. Decreased cofilin phosphorylation in *Arhgef6*$^{-/-}$ $CD4^+$ T cells 84
Figure 24. Actin expression is not impaired in *Arhgef6*$^{-/-}$ $CD4^+$ T cells 86
Figure 25. Increased Actin expression at surface contact area of *Arhgef6*$^{-/-}$ $CD4^+$ T cells 88

Figure 26. Reduced GIT1 and GIT2 expression levels
in *Arhgef6*$^{-/-}$ CD4^{+} T cells 90
Figure 27. Reduced phospho-paxillin level in *Arhgef6*$^{-/-}$ CD4^{+} T cells 91
Figure 28. Reduction of paxillin and phospho-paxillin at surface contact area of
Arhgef6$^{-/-}$ CD4^{+} T cells 92
Figure 29. Higher paxillin turnover in lamellipodia of *Arhgef6*$^{-/-}$ CD4^{+} T cells 93
Figure 30. Vinculin expression level in the whole cell
and at surface contact area 94
Figure 31. Lamellipodia defects in *Arhgef6*$^{-/-}$ T cells 95
Figure 32. Morphological differences of lamellipodia between wt and *Arhgef6*$^{-/-}$
CD4^{+} T cells 96
Figure 33. Lamellipodia size parameters in wt and *Arhgef6*$^{-/-}$ T cells
with or without LIMKi3 97
Figure 34. Directionality and velocity of wt and *Arhgef6*$^{-/-}$ CD4^{+} T cells
with or without LIMKi3 inhibitor at 100x 99
Figure 35. Migration parameters of wt and *Arhgef6*$^{-/-}$ CD4^{+} T cells
with or without LIMKi3 inhibitor at 10x 100
Figure 36. Model showing the role of ARHGEF6 in balancing distinct
signaling pathways regulating lymphocyte morphology and migration 117

Supplementary figure 1. Distribution of PIX/GIT complex members
in the presence and absence of ARHGEF6 101
Supplementary figure 2. Unaltered integrin expression level in *Arhgef6*$^{-/-}$
compared to wt CD4^{+} T cells 102
Supplementary figure 3. Recruitment of PIX/GIT proteins in immune synapse 103

Summary

RhoGEF proteins are multi-domain activators of Rho GTPases that mediate signaling from cell surface receptors to the cytoskeleton, thereby regulating variety of cellular processes including cell migration. The PIX family of RhoGEFs, ARHGEF6 and ARHGEF7, constitutively associate with the GIT family of ArfGAPs (GIT1 and GIT2) and together these four proteins form a core complex (PIX/GIT complex) that interacts with other proteins composing a large, multiprotein assembly. ARHGEF6 is an activator of Rho GTPases and its expression is restricted to few cell types including immune cells. In contrast, ARHGEF7 has a much broader expression and its deletion is lethal. Our group generated *Arhgef6*$^{-/-}$ mice, which are viable but showed impaired thymocyte development and altered migratory behaviour of both thymocytes and T cells. Namely, *Arhgef6* deletion results in cells that show increased chemokinesis and chemotaxis, which is a relatively rare phenotype. The aim of the present study was to decipher which signaling pathways are affected by loss of ARHGEF6. We corroborated that activated CD4^{+} T cells from *Arhgef6*$^{-/-}$ mice migrate significantly faster than wild-type cells, and in addition, showed 'twist-and-turn' migration pattern characterized by frequent changing the direction thus resulting in reduced directionality. We identified several molecular mechanisms underlying this phenotype. *Arhgef6*$^{-/-}$ T cells exhibited increased ARHGEF7 level and consequently increased Rac1 activity, suggesting that, at least in some cellular aspects, ARHGEF7 may compensate for ARHGEF6 deficiency. However, although ARHGEF7 interacts with PAK2, the activity of PAK2 was greatly reduced indicating indispensable presence of ARHGEF6 for its function. Compromised PAK2 activity altered the activity of its downstream kinase, LIMK1, which resulted in over-activation of cofilin, leading to increased actin turnover and abnormal lamellipodia morphology. Due to ARHGEF6 deficiency, the level of ARHGEF6 binding partner GIT2 was reduced and GIT1/2-associated protein, paxillin, was mislocalized. Paxillin, together with another FA protein, vinculin, plays important role in formation and maturation of focal contacts. Their reduction in *Arhgef6*$^{-/-}$ CD4^{+} T cells may result in reduced anchoring and adhesion of these cells. Taken together, obtained data suggest an important role of ARHGEF6 in regulating directional migration of lymphocytes.

Zusammenfassung

RhoGEFs sind Multidomänen-Proteine, die als Aktivatoren von RhoGTPasen Signalwege zwischen Zelloberflächenrezeptoren und dem Cytoskelett steuern. Auf diese Weise regulieren RhoGEFs neben einer Vielzahl anderer zellulärer Prozesse auch die Zellmigration. RhoGEFs der PIX-Proteinfamilie, ARHGEF6 und ARHGEF7, regulieren die Aktivität der kleinen RhoGTPasen Rac und Cdc42. Beide PIX-Proteine sind konstitutiv mit den ArfGAP-Proteinen GIT1 und GIT2 assoziiert. Diese vier Proteine bilden zusammen einen zentralen Proteinkomplex, den sogenannten PIX/GIT-Komplex, der sich durch Bindung weiterer Proteine zu sehr großen Multiproteinaggregaten formieren kann. Während ARHGEF7 in vielen Geweben exprimiert wird und das Fehlen dieses Proteins embryonal letal ist, ist die Expression von ARHGEF6 auf wenige Zelltypen, insbesondere Immunzellen, beschränkt. Unsere Arbeitsgruppe hat *Arhgef6*$^{-/-}$ Mäuse hergestellt, die lebensfähig sind, jedoch ein verändertes Migrationsverhalten von Lymphozyten und eine gestörte Thymozytenentwicklung aufweisen. Überraschenderweise führte die Deletion von *Arhgef6* in den untersuchten Zellen zu einer generell erhöhten Motilität mit verstärkter Chemokinese und Chemotaxis. Ziel der vorliegenden Arbeit war die Beschreibung ARHGEF6-regulierter Signalwege in T-Zellen. Wir konnten zeigen, dass CD4^{+} T-Zellen von *Arhgef6*$^{-/-}$ Mäusen schneller migrieren, dabei aber nicht so wie wildtypische Zellen die Migrationsrichtung aufrechterhalten konnten. Wir identifizierten folgende Mechanismen, die diesen Phänotype erklären: *Arhgef6*$^{-/-}$ T-Zellen zeigten (i) verstärkte ARHGEF7 Expression, die folgerichtig auch mit einer stärkeren Aktivität von Rac1 assoziiert war. ARHGEF7 kann daher vermutlich den Verlust von ARHGEF6 teilweise kompensieren. Obwohl jedoch ARHGEF7 mit PAK2 interagieren kann, war (ii) die Aktivität dieser Kinase in Abwesenheit von ARHGEF6 stark reduziert, was die Bedeutung von ARHGEF6 für die Aktivierung von PAK2 unterstreicht. Als direkte Folge der gestörten PAK2 Aktivität war auch die Aktivität der PAK2-Zielkinase LIMK1 reduziert. Dies führte durch Überaktivierung des Aktin-Depolymerisierungsfaktors Cofilin zu einem gesteigerten Umbau von Aktin und, als Folge davon, zu einer unregelmäßigen Morphologie der Lamellipodien migrierender Zellen. Aufgrund der ARHGEF6-Defizienz war (iii) auch die Proteinkonzentration des Bindungspartners GIT2 reduziert. Zusätzlich beobachteten wir eine veränderte Lokalisation des GIT1/2-assoziierten fokalen Adhäsionsprotein Paxillin, sowie von Vinculin, das ebenfalls an der Bildung und Reifung fokaler Zellkontakte beteiligt ist.

Diese Veränderungen in *Arhgef6*$^{-/-}$ CD4^{+} T-Zellen könnten möglicherweise zu einer schwächeren Zell-Verankerung und Adhäsion beitragen. Insgesamt zeigen unsere Daten, dass ARHGEF6 eine wichtige Rolle in der gerichteten Migration von Lymphozyten spielt.

1. INTRODUCTION

1.1 The principle of T cell immunity

The principal role of the immune system is defending an organism against infection and eliminating the pathogen. Critical step in this process is discrimination between self and foreign antigens thus developing tolerance to the first and eliciting a productive immune response to the latter. Higher vertebrates evolved several mechanisms to sense an infection. The innate or unspecific immune system is the first line of defense, which includes physical barriers, such as the skin and mucosa, specialized phagocytic cells, antimicrobial and proinflammatory molecules. Innate immune cells, such as macrophages, dendritic cells (DCs) and neutrophils recognize general molecular patterns, which are present on pathogens but not on host cells by using so-called pattern recognition receptors (PRR) (Klein et al., 2014). A prominent example is Toll-like receptor (TLR) 4 expressed on phagocytes, which binds to lipopolysaccharides (LPS) on bacterial surfaces. Other PRRs, such as complement factors opsonize the pathogen's surface as soluble (humoral) molecules. Binding of PRRs to a respective motive can trigger immediate lysis by the complement system, secretion of toxic oxygen radicals by neutrophils or phagocytosis followed by intracellular killing of the pathogen.

Although the innate immune system can efficiently clear most microbial infections, the adaptive immune system evolved in order to improve pathogen clearance. Adaptive immunity provides very sensitive and specific pathogen recognition and immunological memory, which copes with reinfection by an accelerated and reinforced response. The adaptive immune system recognizes foreign antigens by the use of a large pool of specific antigen receptors expressed by B or T lymphocytes (short B and T cells). This antigen receptor repertoire is established by individual somatic recombination in the gene loci of T cell receptor (TCR) and B cell receptor (BCR) during development of T and B cells, respectively. While antigen-specific B cells upon antigen contact mature to antibody secreting plasma cells and thereby contribute to the humoral immune response, T cells recognize cognate peptide antigen only in the context of antigen presentation on major histocompatibility complex (MHC) molecules. There are two classes of MHC molecules, which present peptide antigens to T cells that either express the co-receptor CD8 or CD4, respectively (Figure 1). MHC molecules class I (present on the surface of all cells)

display peptides derived by proteasomal digestion from intracellularly synthesized proteins e.g. after viral infection. Peptide-MHC (pMHC) class I complexes interact with $CD8^+$ T cells (York and Rock, 1996), also referred to as cytotoxic T cells, which kill infected target cells by the release of lytic granules. MHC class II molecules are expressed on the surface of professional antigen presenting cells (APCs), such as DCs, macrophages and B cells and display peptide antigens derived from material captured by phagocytosis and processed in lysosomes. pMHC class II complexes interact with $CD4^+$ or T helper (Th) cells (Germain, 1994). The main function of $CD4^+$ T cells is intercellular co-operation and activation of macrophages or B cells by the release of cytokines. pMHC-TCR interaction facilitates a very close cell-cell contact between the T cell and the APC by activation of the integrin LFA-1. Binding of LFA-1 to the intercellular adhesion molecule (ICAM) -1 on the APC reinforces the formation of a stable intercellular structure called the immune synapse. Besides the cognate pMHC-TCR interaction, the immune synapse allows for the transmission of 2 additional signals required for full activation of T cells. The second signal is provided by interaction of costimulatory receptors expressed on T cells, such as CD28 with ligands expressed on APCs. Combined signaling via the TCR and costimulatory molecules selectively induces the clonal expansion of antigen-specific T cells.

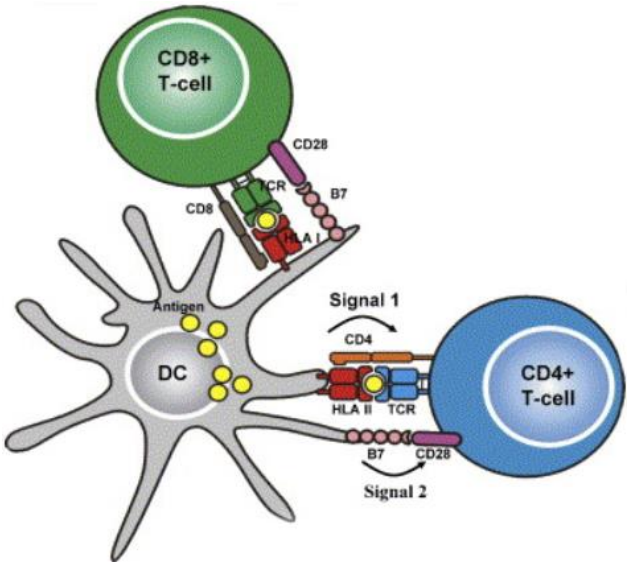

Figure 1. T lymphocytes activation (source: http://knowledge-forlife.com/cd4-t-cell-activate-cd8-t-cell/)

Finally, paracrine and autocrine release of cytokines from the APC and the T cell itself, respectively, provide a third signal, which is required for terminal differentiation of activated T cells. Particularly, $CD4^+$ T cells may differentiate into different type of T

helper cells depending on the type of APC, type of the captured pathogen as well as the proinflammatory milieu present at the site of infection. Th1 cells produce IL-2 and IFN-γ, proinflammatory cytokines, which activate macrophages and cytotoxic T cells and are therefore involved in the processes of intracellular pathogens elimination. Th2 cells produce anti-inflammatory cytokines, such as IL-4, IL-5, IL-10 and IL-13, which support IgE secretion by plasma cells. Th2 cells are therefore part of immune response coping with extracellular parasites but also being a possible cause of allergy and asthma (Ngoc et al., 2005). Th17 cells have a proinflammatory role and produce IL-17 and other cytokines, which play an important role in the activation of neutrophils thereby promoting immune response against extracellular bacteria and fungi. Th17 immune responses are also often associated with autoimmunity. Regulatory T cell (Tregs) produce TGFβ and IL-10, and thus have an anti-inflammatory role, which is required for immune tolerance, lymphocyte homeostasis and regulation of immune responses (Zhu and Paul, 2008).

One major achievement of adaptive immunity is the establishment of immunological memory. While most antigen-specific effector cells die after clearance of the pathogen, few of these effectors survive as long-lived but quiescent memory T or B cells, respectively. However, upon re-exposure to the same cognate antigen, memory cells mount a much faster and stronger immune response than that achieved after the first antigen contact.

The adaptive immune system allows for thorough pathogen clearance, particularly upon reinfection with the same pathogen with very limited collateral damage. However, the danger of producing autoreactive antigen receptors, the difficulty to identify and expand rare antigen specific cells among the large pool of naïve T and B cells and the task to find the pathogen at site of infection require a tight spatio-temporal regulation of development and differentiation. The recent progress of in vitro and in vivo live cell imaging techniques revealed that T and B cells have to be accurately navigated by environmental as well as cell-intrinsic guidance cues.

1.2 T cell development

Like all leukocytes, T lymphocytes originate from multipotent hematopoietic stem cells, located in the bone marrow (BM). Precursors of T cells migrate from the BM via the blood to the thymus, where they mature. Hence, the etymology thymus-dependent (T) lymphocytes, or T cells. The thymus is composed of two zones, the

outer zone–cortex, and the inner zone–medulla. Both of these zones are populated by distinct subsets of thymic resident cells, which interact with developing T cells in a highly ordered sequence (see also Figure 7). Particularly, specialized cortical thymic epithelial cells (cTECs) guide thymocytes through the cortex and are required for T lineage commitment, positive selection and survival of thymocytes with a functional TCR. Medullary thymic epithelial cells (mTECs) on the other hand, which are specialized in processing and presenting tissue-restricted autoantigens, together with thymic medullary DCs, are required for negative selection and apoptosis of autoreactive thymocytes resulting in maturation and emigration into the blood stream of surviving selected thymocytes (Klein et al., 2014).

Thymus settling by the rare lymphoid progenitors (Schwarz et al., 2007) is a highly regulated process which involves cell adhesion molecules and migration in an environment of chemokine gradients. Subsequent arrest and strong adhesion of the cells to the endothelium are mediated by binding of integrins, such as α4β1 (VLA-4) and αLβ2 (LFA-1) to the vascular or intercellular adhesion molecules VCAM-1 and ICAM-1 expressed on thymic endothelial cells (Scimone et al., 2006). Interaction of thymic chemokines, such as CCL21 and CCL25 with their receptors CCR7 and CCR9, respectively, increases integrin affinity via inside-out-signaling (Krueger et al., 2010; Zlotoff et al., 2010), and thereby promotes entry into the thymus at the cortico-medullary junction.

After entry into thymus, progenitor cells become early thymocyte progenitors (ETP), which do not yet express CD4 or CD8 co-receptors and are therefore referred to as double negative thymocytes (Lammermann et al.). At the earliest stage they also do not express the TCR. The migration of DN cells towards the thymic cortex is dependent on interaction of integrins expressed on DN cells and surface-expressed integrin counter receptor VCAM-1 present on cTECs. It has been shown that in vivo administration of an anti-VCAM-1 antibody resulted in decreased thymic size and altered distribution of early precursors within the thymic cortex (Prockop et al., 2002). And it was suggested that DN migration is governed by interaction of chemokines CXCL12 and CCL25 expressed by cTECs and corresponding chemokine receptors CXCR4 and CCR9 expressed by DN cells (Kurd and Robey, 2016; Ladi et al., 2006).

In the cortex DN thymocytes massively proliferate and further migrate to the subcapsular zone. During that stage they also rearrange the TCRβ gene segments in order to first form a pre-TCR consisting of the rearranged β chain and an invariant

pre-Tα chain. DN thymocytes that are able to transmit (MHC independent) signaling by the pre-TCR in the presence of a productive β chain continue to proliferate whereas cells, which do not pass this β-selection checkpoint, die by apoptosis. Some data suggest that CXCR4 is more involved in survival and proliferation of DN cells during β-selection than in outward cortical migration (Trampont et al., 2010; Wurbel et al., 2006).

Following β-selection, thymocytes successively upregulate CD8 and CD4 surface expression to become double-positive (DP) thymocytes that initiate TCRα gene rearrangements and express a mature αβ TCR. In the next step, DP thymocytes are tested if their TCRs can interact with pMHC complexes presented on the cortical epithelium. Only cells with a fully functional TCR are positively selected and survive, whereas cells, which are incapable to receive signals upon encounter with pMHC die by neglect. During positive selection, thymocytes move randomly across the cortex in order to scan APCs for pMHC. However, DP thymocytes have to stop migration transiently in order to form multiple contacts with cTECs and collect positively selecting signals. It has been shown that proteins which modulate motility of DP thymocytes may impact positive selection (see also chapter 1.6).

Positively selected $CD69^+$ DP thymocytes upregulate chemokine receptors CCR4 and CCR7, which results in rapid and highly directed migration towards the thymic medulla mediated by chemokines released from medullary DCs (Hu et al., 2015; Kozai et al., 2017). This switch from random to chemotactic migration facilitates ending of positive selection signals and assures proper beginning of the negative selection process in the medulla (Ladi et al., 2006). It has been shown that CCR7 and CCR4 are essential for central tolerance and avoidance of autoimmune disease (Hu et al., 2015; Kozai et al., 2017). In parallel, post-selection DP thymocytes further upregulate TCR and, depending on the optimal signals received either from MHC class I or II complexes, downregulate either CD4 or CD8 to become immature CD4 or CD8 single-positive (SP) cells, respectively. In contrast to the relatively weak positively selecting signals in the cortex, recognition of cognate pMHC on medullary TECs and DCs medulla induces strong signaling, which results in apoptosis and negative selection of auto-reactive SP thymocytes.

Only a minor proportion of SP thymocytes that do not interact with self-pMHC or are agonistically selected by only weak signals survive. These cells finally become either mature $CD4^+$ or $CD8^+$ SP thymocytes or regulatory T cells (Tregs), respectively,

which finally can exit the thymus (Lancaster et al., 2018; Shah and Zuniga-Pflucker, 2014). Sphingosine receptor (S1PR1) plays the central role in thymocyte egress by binding of its ligand sphingosine 1-phosphate, which is highly present in blood. S1PR1 receptor knockout mice showed altered chemotactic responses of thymocytes to sphingosine 1-phosphate and a block in the egress of mature T-cells (Allende et al., 2004). More recent work by White et al. (2017) provide evidence that IL-4Rα influences thymic egress via a mechanism distinct from the S1P–S1PR1. They showed that in the absence of IL-4Rα mature thymocytes accumulate within thymic medulla and fail to emigrate.

Understanding how changes in thymocyte migration patterns are regulated therefore helped a lot to learn about development of T cell immunity and establishment of central tolerance as well as possible causes of immune deficiencies and autoimmune diseases.

1.3 T cell activation and motility

Naïve T cell migration

Upon emigrating the thymus, SP thymocytes express adhesion molecules, such as L-selectin, integrins α4β7 and LFA-1 and chemokine receptor CCR7. Expression of the corresponding ligands, such as glycoproteins (addressin) and ICAM-1 on high endothelial venules and CCL21 secreted by lymph node DCs mediate T cell rolling, adhesion and directed migration, respectively (von Andrian and Mempel, 2003). These interactions thereby ensure proper homing of lymphocytes to the right secondary lymphoid organ (lymph nodes, spleen, Peyer's patches, and mucosal tissues, such as the nasal-associated lymphoid tissue, adenoids, and tonsils) (Pals et al., 2007). Recent thymic emigrants that arrive in the secondary lymphoid organs (except Tregs) have never encountered the cognate antigen and are therefore known as naïve T cells. They recirculate between blood and the lymphatic system where they await activation by interaction with the specific, cognate antigens presented on APCs.

T cell priming by DCs is characterized by three distinct phases of motility (Mempel et al., 2004). Naïve T cells are not able to immediately sense the location of their cognate antigen, whose frequency within lymph node is extremely low (if it is present at all). Therefore they constantly alternate between exploration and exploitation mode in order to search and scan each APC (Krummel et al., 2016). Naïve T cells in lymph

nodes migrate in a random walk mode, which maximizes the chance to find rare antigens (Cahalan and Parker, 2008; Harris et al., 2012). However, upon contact with the cognate antigen, T cells stop migrating to form stable contacts with the APC in order to receive signals required for effector cell differentiation (Bousso and Robey, 2003). Upon activation T cells begin to proliferate and resume rapid migration (Mempel et al., 2004).

T cell motility in lymphoid tissue is therefore highly dynamic and very well coordinated and balanced process with an average speed of 8-11 µm per minute (Miller et al., 2002). Secondary lymphoid organs have a complex microarchitecture supported by networks of endothelial and mesenchymal stromal cells. Studies demonstrated that the reticular network of stromal cells form a substrate for T cell migration into and within lymph nodes and spleen (Bajenoff et al., 2006; Bajenoff et al., 2008). Both DCs and macrophages are found in close proximity to the stromal cell network in the T cell zone, thereby providing a specific microenvironment that assists the priming of an immune response.

Chemokines, such as CCL19 and CCL21 and adhesion molecules, such as ICAM-1 expressed by the stromal cells are important for promoting T-lymphocyte migration (Luther et al., 2000). CCL19 and CCL21 activate continuous CCR7 chemokine receptor signaling that drive T cell motility (Britschgi et al., 2008). However, studies on CCR7 deficient mice showed that CCR7 is required for T cell velocity but not for their directionality (Worbs et al., 2007), thus promoting chemokinesis rather than chemotaxis. In addition, other soluble mediators, such as lysophosphatidic acid (LPA) promote naïve T cell motility in lymph nodes (Katakai et al., 2014).

Integrins, in general, are not essential for T cell migration within confined 3-D tissues, such as lymphoid organs (Woolf et al., 2007), but speed fluctuations are linked to integrins. Studies on LFA-1 or ICAM-1 deficient mice revealed that high speed T cell migration in lymph nodes is mediated by the interaction of LFA1 with ICAM-1 on DCs and stromal cells, thereby facilitating the antigen scanning process (Hons et al., 2018; Katakai et al., 2013).

A particular role in controlling T cell motility in secondary lymphoid organs is mediated by the contact of T cells with pMHC expressing APCs, which can evoke different responses depending on the affinity of the antigen. A very recent study demonstrates that interaction of naïve T cells with non-cognate self-pMHC facilitates spontaneous Ca^{2+} transients through Orai1 Ca^{2+} channels, which facilitates pausing

and changing of direction required for optimal immune surveillance (Dong et al., 2017). Others showed that presence of low-affinity antigens decelerates T cell migration and increases the frequency of turning, thereby attaining more local exploration (Moreau et al., 2015). However, antigens that strongly activate TCR signaling and prolonged Ca^{2+} signaling cause a full arrest on the APC (Moreau et al., 2015) allowing for effector cell differentiation.

Activated T cell migration

As a consequence of naïve $CD4^+$ T helper cell priming, stromal cells and APCs downregulate secretion of CCR7 ligands CCL19 and CCL21 (Mueller et al., 2007) and upregulate secretion of other chemokines, such as CCL3 and CCL4 (Castellino et al., 2006), respectively. In parallel, T cells decrease CCR7 ligand responsiveness and upregulate chemokine receptors, such as CCR5, CXCR3 and CXCR5 (Mueller et al., 2007). These changes in chemokine and chemokine receptor expression result in a switch from the overall random motility mode required for antigen scanning to more directional migration (Krummel et al., 2016; Mueller and Germain, 2009). In such a differentiating environment, for example, naïve $CD8^+$ T cells are attracted to sites of $CD4^+$ T cell-APC interaction for cross priming (Castellino et al., 2006). Activated $CD4^+$ T cells may also be directed towards the B cell zone in order to support B cell differentiation (Kim et al., 2001).

During the initial phase of T cell activation the responsiveness to S1P present in blood is downregulated in order to retain T cells in the lymphoid organ (Matloubian et al., 2004). However, S1P receptor S1P-R1 is re-expressed on recently divided T cells, which mediates egress via lymphatic vessels and recirculation of activated T cells similar to the mechanism by which mature SP thymocytes are released from the thymus (Matloubian et al., 2004). Interestingly, it was shown that LFA-1 binding to ICAM-1 within the lymph nodes was required to prolong the dwell time in lymph nodes before egress and thereby increases the effectiveness of the T cell antigen response (Reichardt et al., 2013). Particularly, T cells deficient for LFA-1 were less adherent and more motile in contact with medullary lymphatic vessels, and emigrated more rapidly than wild-type T cells, although the average migration speed of wild-type T cells in the T cell zone was much faster than that of LFA-1 deficient T cells.

Finally, the entry of activated T cells from the circulation into inflamed tissues starts with initial rolling on lectin ligands followed by low affinity binding of LFA-1 to ICAM-1

expressed on the luminal side of the endothelium. In this situation, the shear force mediated by the blood flow transmits tensile forces on LFA-1, which by out-side-in signaling induces a high affinity conformation of the integrin. This shear force mediated activation of LFA-1 is required for leukocyte adhesion and active migration on the 2D surface of the inner vessel wall and transendothelial migration (Hogg et al., 2011; Ley et al., 2007). Intra endothelial vesicle stores of chemokines help T cells to sense the site of extravasation (Shulman et al., 2011). A recent exciting finding was that T cells within the inflamed tissue follow the tracks of previously entered neutrophils (Lim et al., 2015). On their path, neutrophils leave behind traces of membrane material, which serves as haptotactic cues guiding T cells to the exact site of infection.

T cell motility is regulated by the presence of chemokines, adhesion molecules and peptide-MHC complexes. However, the sensitivity of T cells to respond to these external cues and fine tune their migrational behavior is intrinsically determined by signaling pathways that control the dynamics of T cell cytoskeleton.

1.4 Mechanism of leukocytes migration

The locomotion of leukocytes is different in comparison to e.g. more stationary, adhesive cells, such as fibroblast, as they constantly shuttle between different tissue compartments and have to quickly adapt to geometry and molecular composition of the new environment (Renkawitz and Sixt, 2010). One of the major differences in the migration strategy between highly adhesive cells and leukocytes is that adhesive cells are dependent on binding to a substrate (ECM) through adhesion receptors, particularly integrins. This form of migration is termed haptokinesis and removal of the signal transmitted by ligand-engaged integrins leads to anoikis- programmed cells death (Chiarugi and Giannoni, 2008). Leukocytes switch between adhesion–dependent and adhesion-independent locomotion. They require integrins and signals from the tissue when entering or when migrating within lymphoid organs (Bajenoff et al., 2006) but their locomotion and survival in the interstitial space does not depend on adhesion. In addition, leukocytes constantly change their shape during migration - so called amoeboid migration, which is mostly independent of neighboring tissue (Lammermann and Sixt, 2009), whereas the shape of adherent cells is predominantly determined by their adhesiveness (Yang and Jiang, 2017).

In order to move, cells can extend four different types of plasma membrane protrusions at the leading edge: fan-shaped lamellipodia, short filopodia, blebs or elongated invadopodia (Ridley, 2011). Locomotion is driven by forces generated by actin polymerization and branching at the leading edge, myosin II mediated contractility and force transmission between the cell and the substrate through adhesion sites and rear retraction (Figure 2A). In the moving cell, actin concentration is high near the leading edge, whereas myosin acts behind the leading edge and pulls the actin cortex backward, thereby supporting polymerization driven retrograde actin movement relative to the cell body. Forward movement of the cell results from coupling of actin to adhesion receptors, thereby pulling the cell body forward (Renkawitz and Sixt, 2010). This coupling is mediated by the interactions of vinculin and talin with actin filaments on the one hand and intergrins on the other hand, forming a 'molecular clutch' (Hu et al., 2007; Swaminathan and Waterman, 2016), a model, which has already been proposed by Mitchison and Kirschner (1988). This model is mostly applicable to 2D surfaces.

An alternative model of locomotion that is also dependent on actin cytoskeleton is termed as blebbing, applicable to 2D (adhesion based) and 3D environments (Figure 2B, C). Bleb driven migration is independent of leading edge extension and actin polymerization but relies on pressure induced by myosin II motor activity that contracts the cortical actin network (Paluch and Raz, 2013).

An additional third model is locomotion by polymerization-driven deformation. As proposed by Haston et al., (1982), similar to 2D migration, the moving of cells in 3D environment results from deformations caused by actin polymerization. Most recently, Hons et al. (2018) demonstrated that in confined 3D tissues, such as lymphoid organs, tight adhesion is not required for T cell locomotion. They showed that CCR7 ligands induce increased actin polymerization and elongation of the cell but not inside-out signaling to integrin activation. Instead, low affinity interaction of LFA-1 with ICAM-1 on stromal cells is sufficient to provide tangential friction forces. As a consequence, chemokine induced actin polymerization and integrin mediated friction forces cooperate independently in moving the cell forward, which is still in line with the above mentioned clutch model. The speed of T cells, particularly in confined tissues, thus exclusively correlates with (chemokine-induced) actin polymerization and (integrin-mediated) tangential friction force but not adhesion. However, leukocytes combine all of these adhesion-dependent and deformation-based models

while migrating and switch between them when changing areas of different adhesiveness (Renkawitz and Sixt, 2010).

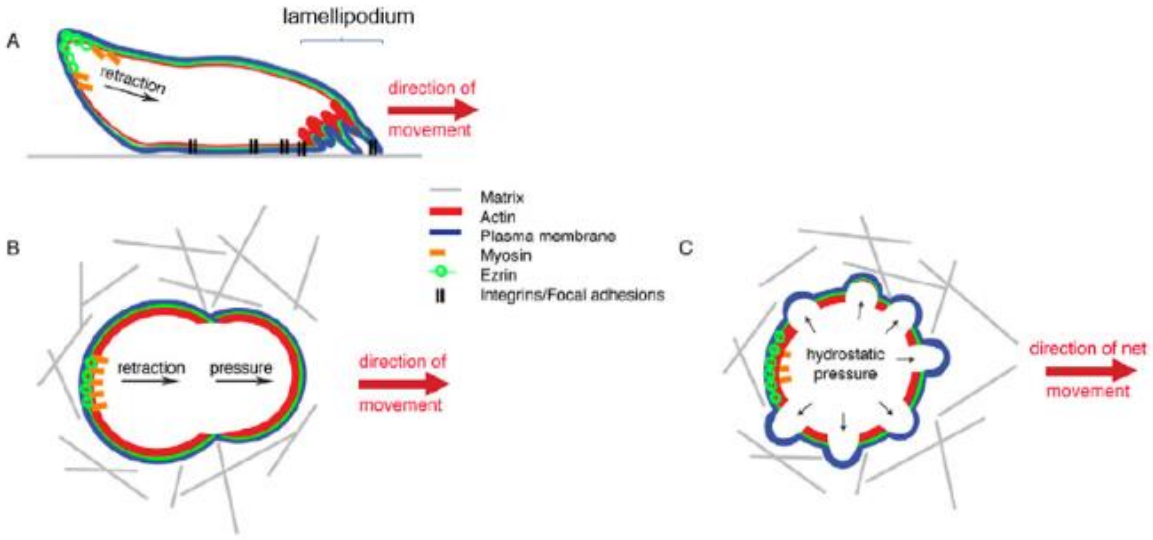

Figure 2. Amoeboid cell migration models
A) 2D surface crawling, lamellipodium defines the direction of movement; B) Sqeezing through pores, the bleb defines the direction of movement; C) Formation of multiple blebs, each bleb contributes to pulling the cell toward bleb augmentation (Lorentzen et al., 2011)

The cell migration is highly controlled and coordinated by numerous protein-protein interactions and signaling pathways regulating the dynamics of the actin cytoskeleton and Rho GTPases play a central role in the regulation of these processes.

1.5 The role of Rho GTPases and RhoGEFs in T cell migration

Rho GTPases are molecular switches that cycle between an inactive and an active confirmation and hence control a wide variety of cellular functions. The activation of Rho proteins is mediated by cell type specific guanine exchange factors, RhoGEFs, which catalyze the exchange of GDP to GTP. In contrast to RhoGEFs, GTPase activating proteins (RhoGAPs) catalyze the inactivation of Rho GTPases by hydrolyzing GTP into GDP. Active Rho GTPases interact with various downstream effectors, whereas inactive Rho GTPases preferentially bind to a guanosine nucleotide dissociation inhibitor (RhoGDI), which prevents their reactivation and binding to effectors (Cherfils and Zeghouf, 2013; Ory and Gasman, 2011; Schmidt and Hall, 2002) (Figure 3).

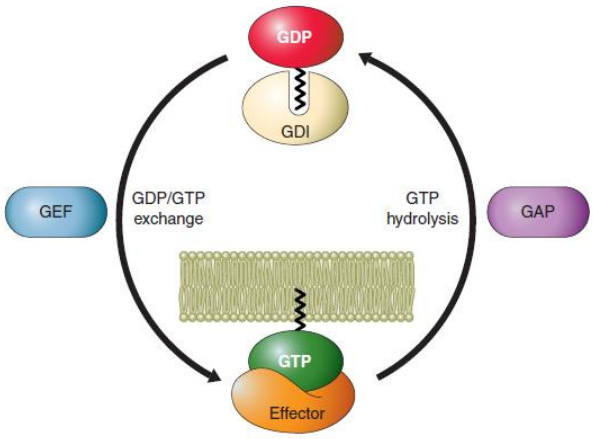

Figure 3. Rho GTPases activation/inactivation cycle (adopted from Jacqueline Cherfils and Mahel Zeghouf)

The Rho family of small G proteins includes more than 20 members, which are highly conserved in plants and yeast and mammals. The best characterized members of small Rho GTPase family include RhoA, Rac1 and Cdc42, which are involved in regulation of cell polarity and cytoskeleton dynamics (Mayor and Carmona-Fontaine, 2010) thereby controlling cell adhesion and migration (Heasman and Ridley, 2008; Raftopoulou and Hall, 2004). Data obtained from tissue culture studies have shown that Rho preferentially regulates the assembly of contractile actin and myosin filaments (stress fibers), while Rac1 and Cdc42 regulate the polymerization of actin to form peripheral lamellipodial and filopodial protrusions, respectively (Mayor and Carmona-Fontaine, 2010) (Figure 4).

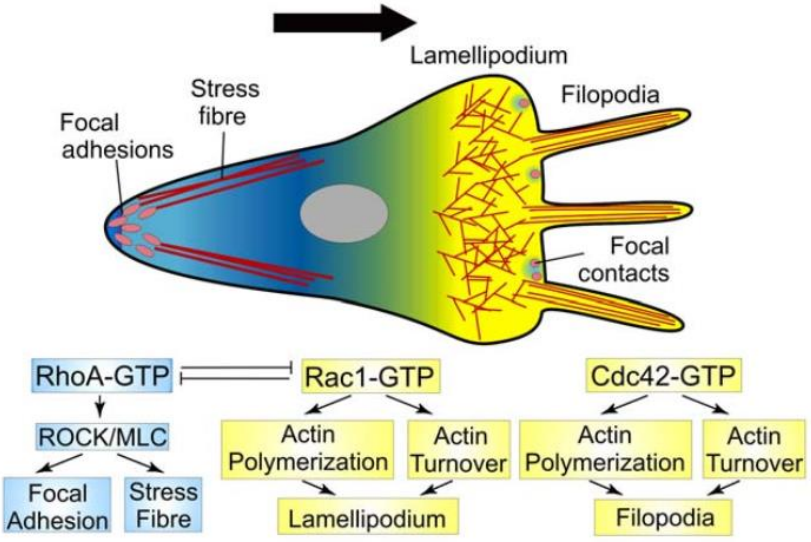

Figure 4. Rho GTPases influence cell polarity and protrusion (adopted from Roberto Mayor and Carlos Carmona-Fontaine)

Rac1 and Cdc42 are active at the leading edge of polarized cells, whereas RhoA is active at the rear. During these processes Rac1 and RhoA inhibit each other, thereby establishing cell polarity. However, Rac1 and RhoA also cooperate in the assembly of focal adhesion complexes. These structures are found in lamellipodia of most migrating cells with the main function to attach the lamellipodium to the extracellular matrix. RhoA may promote their maturation into focal adhesions (FA), particularly at the front of large adhesive cells, which facilitates attachment of the protrusions to the ECM. RhoA-dependent actomyosin contraction at the rear further results in moving the cell body forward (Millar et al., 2017) (Figure 5). A particular role of a RhoA in these processes is activation of its effector kinase ROCK leading to phosphorylation of myosin light chain (MLC) and enabling myosin to interact with actin filaments (Kaibuchi et al., 1999; Millar et al., 2017). Myosin IIA and IIB form the cell rear by inducing localized actinomyosin bundling and creating large stable adhesions, which finally lack Rac signaling and show loss of Rac GEFs including ARHGEF7 (Vicente-Manzanares et al., 2011). On the other hand, RhoA also promotes the disassembly of focal complexes required for the retraction of the rear end of the cell.

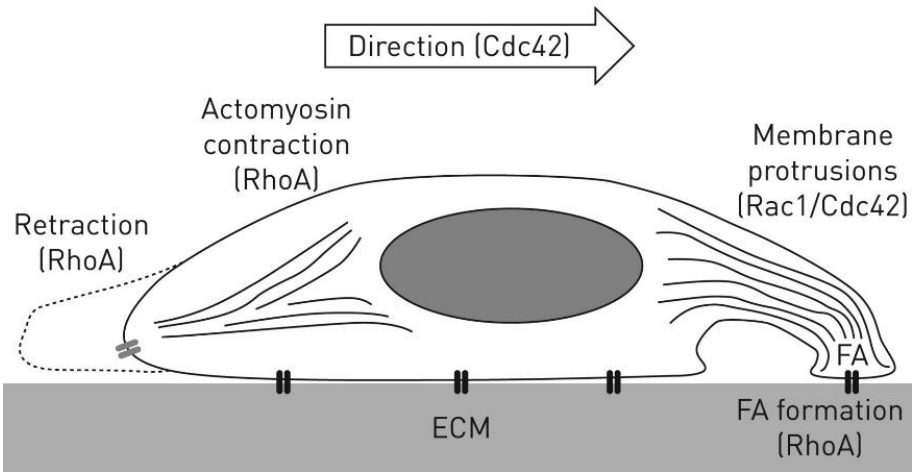

Figure 5. Rho GTPases influence cell migration (adopted from Millar et al., 2017)

1.6 PIX/GIT complex, effectors and implicated signaling pathways

The PIX (PAK-interacting exchange factor) family of proteins, including ARHGEF6 (Cool2/αPIX) and ARHGEF7 (Cool1/βPIX), are RhoGEFs for the Rho GTPases Rac and Cdc42. In addition, PIX proteins have several protein interaction domains and thereby link diverse signaling pathways with cytoskeletal dynamics (Rosenberger and

Kutsche, 2006). ARHGEF7 is expressed in a broad variety of cell types, whereas the expression of ARHGEF6 is mainly restricted to immune and neuronal cells (Missy et al., 2008; Totaro et al., 2012). The deletion of *Arhgef7* in mice is documented to be embryonically lethal (Missy et al., 2008). *Arhgef6* deficiency and mutations are associated with intellectual disability and certain forms of X-linked mental retardation in humans (Baird et al., 2005; Kutsche et al., 2000; Ramakers et al., 2012).

ARHGEF6 may exist as a dimer and as a monomer. In the dimeric form, it appears to function as a Rac-specific GEF, whereas in the monomeric form it may acts as a GEF for both Rac and Cdc42 (Baird et al., 2005). Dimerization of ARHGEF6 is partly regulated via p21-activated kinase (PAK) in response to extracellular signaling (Feng et al., 2004). Binding of Cdc42 to ARHGEF6 increases the Rac GEF activity of the dimer. Activated Rac negatively regulates this process and inhibits dimeric ARHGEF6 Rac GEF activity (Baird et al., 2005).

Arhgef7 has two splice variants, β1PIX and β2PIX. β1PIX is longer, homodimerizes, locates to the cell periphery and locally activates Cdc42 and Rac1, thereby promoting membrane ruffles and protrusion. β2PIX is shorter, does not drive formation of membrane ruffles and represents the main form in the brain (Koh et al., 2001).

ARHGEF6 and ARHGEF7 share high structural similarity (Figure 6). Both ARHGEF6 and ARHGEF7 contain a SH3 domain that binds to a wide range of signaling molecules including PAKs (Mott et al., 2005), the E3 ubiquitin ligase c-Cbl (Flanders et al., 2003; Jozic et al., 2005), and the adaptor protein SAP (Gu et al., 2006). PIX proteins also contain a Dbl homology (DH aka RhoGEF) domain, a pleckstrin homology (PH) domain, which mediates membrane localization (Hart et al., 1994; Whitehead et al., 1997; Zheng et al., 1996) (e.g. via binding of phosphatidylinositol (3,4,5) triphosphate (PIP3) (Li et al., 2003; Yoshii et al., 1999), a coiled-coiled domain implicated in dimerization and a GIT-binding domain (Rosenberger and Kutsche, 2006). In addition, ARHGEF6 contains an N-terminal calponin homology (CH) domain, which is also present in some splice variants of *Arhgef7* (Rhee et al., 2004). The CH domain is found in proteins interacting with the actin cytoskeleton (Rozenblum and Gimona, 2008). ARHGEF6 binds via this domain to the integrin-linked kinase binding protein β-parvin (affixin) (Rosenberger et al., 2003). Integrin-linked kinase (ILK) binding to β-parvin enables it to activate ARHGEF6 leading to Rac/Cdc42 activation affecting the actin cytoskeleton and cell spreading (Filipenko et al., 2005). Furthermore, ARHGEF6 binds to Calpain 4, the small regulatory subunit of

μ-Calpain and colocalizes with ILK during integrin dependent cell spreading (Rosenberger et al., 2005). On the other hand, ARHGEF7, but not ARHGEF6, contains a PDZ-binding domain, which allows for binding of PDZ domain-containing proteins, such as the neuronal post-synaptic density protein Shank (Park et al., 2003), the cell polarity regulator hScrib (Audebert et al., 2004) and the Sorting nexin 27 (SNX27) (Valdes et al., 2011).

PIX proteins bind constitutively to GIT1 and GIT2 (G protein–coupled receptor kinase–interacting protein-1 and 2), which are ArfGAPs (negative regulators of Arf1 and Arf6 GTPases). GIT1/2 are involved in the regulation of vesicle transport and membrane trafficking of internalized receptors between the plasma membrane and endosomes (Hoefen and Berk, 2006). GIT proteins have an ArfGAP domain, an N-terminal paxillin binding sequence, ankyrin repeats involved in intramolecular folding of GIT1, a Spa2 homology domain (SHD) which interacts with PIX, focal adhesion kinase (FAK) and phospholipase C γ (PLC-γ), a coiled-coil region mediating homo- and hetero-dimerization, and a FAT homology domain Rennefahrt et al. (2007) comprising a C-terminal paxillin binding sequence (Frank and Hansen, 2008) (Figure 6). Reduced GIT1 expression in humans and the loss of GIT1 in mice are linked to attention deficit hyperactivity disorder (ADHD) in humans and ADHD-like phenotypes in mice (Won et al., 2011).

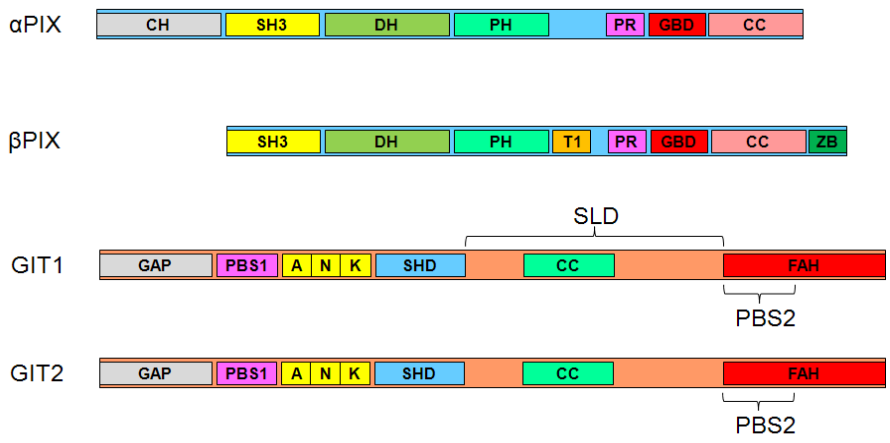

Figure 6. Protein interaction domains of the PIX and GIT proteins.
PIX domains include: CH- Calponin homology domain; SH3- Src homology 3 domain; DH- Dbl homology domain, catalytic domain; PH- Pleckstrin homology domain; T1- insert which inhibits GEF activity; PR- Proline rich region; GBD- GIT binding domain; CC- coiled-coiled region; ZB- PDZ domain binding motif. GIT domains include: GAP- GAP catalytic domain; PBS1- Paxillin binding sequence 1; ANK- Ankyrin repeats; SHD- Spa2 homology domain; CC- coiled-coiled region; FAH- Focal adhesion targeting (FAT) homology domain; PBS2- Paxillin binding sequence 2; SLD- Synaptic localization domain. Possible presented ARHGEF7 isoform is depicted without CH domain (Modified from Frank & Hansen)

Although they control separate signaling pathways, PIX and GIT members are found in the same multimeric complex (Premont et al., 2004). Dimeric GIT1 and trimeric ARHGEF7 constitute a heteropentameric complex as scaffold and signaling module (Schlenker and Rittinger, 2009). The PIX/GIT complex has been implicated downstream of diverse surface receptors, such as integrins, G-protein-coupled receptors (GPCR) and antigen receptors in signaling to actin polymerization, formation of protrusions, cell polarization, adhesion and migration (Frank and Hansen, 2008; Nayal et al., 2006). The different expression profile of PIX proteins together with the individual binding capabilities of the PIX/GIT members may reflect cell type-specific functions of the PIX/GIT complex.

The recruitment of the PIX/GIT complex from the cytosol to cell adhesion sites at the plasma membrane in a highly coordinated spatio-temporal manner has been demonstrated for various cell types, especially in strongly adherent mesenchymal cells, such as fibroblasts or in neurons (Rosenberger and Kutsche, 2006). The mechanism for PIX recruitment to the membrane seems to start with GIT binding to paxillin, which brings the PIX/GIT complex to focal complexes, thus enabling PIX-mediated localized Rac and PAK activation, which in turn triggers actin reorganization, protrusion formation and focal adhesion maturation.

ARHGEF7 drives maturation of nascent adhesions to focal complexes (Yu et al., 2015). It was also shown that ARHGEF7 maintains FAs in an immature state, increases Rac1 activity and promotes actin treadmiling in lamellipodial protrusion where myosin II is inhibited. Thereby, ARHGEF7 accelerates focal adhesion turnover in order to initiate cell migration in adherent cells (Kuo et al., 2011). In neurons, several different interaction partners were shown to be required for ARHGEF7 recruitment to sites of action: GIT1-mediated ARHGEF7 mobilization is required for spine morphogenesis (Zhang et al., 2003), Shank is required for recruitment of ARHGEF7 to spines for the regulation of the postsynaptic structure, and hScrib is required for ARHGEF7 localization to presynaptic vesicles. Interestingly, a complex of ARHGEF6 and GIT2 but not ARHGEF7 and GIT1 was shown to be required for dendritic and axonal branching during hippocampal neuron differentiation (Totaro et al., 2012).

Despite numerous publications on PIX/GIT proteins in fibroblasts, neurons and a range of cell lines, relatively little is known about PIX/GIT function in immune cells, which are highly dynamic and motile. In primary human macrophages, ARHGEF6

together with PAK4, has a central role in podosome formation (Gringel et al., 2006). In a study using *Arhgef6* deficient mice, it was shown in neutrophils that ARHGEF6 recruits PAK1 to the Gβγ subunit of G-protein in response to chemokine-induced GPCR signaling. In turn, ARHGEF6 activates Cdc42 and PAK1 at the leading edge, thereby regulating directional sensing and chemotaxis without affecting the overall speed of migration (Li et al., 2003). Similar results were also obtained with GIT2 deficient mice (Mazaki et al., 2006).

In lymphocytes, it was shown that T cell receptor (TCR) signaling activates a PIX/GIT/PAK1 complex. PIX recruits PAK1 to the T cell - APC contact site where PAK1 activation takes place leading to PLC-γ1 activation and TCR-dependent transcription (Phee et al., 2005). In Jurkat cells it was shown that PIX/GIT complex is activated upon TCR stimulation of Lck, ZAP-70 and Syk signaling but independently from Nck, LAT and Slp-76 (Ku et al., 2001).

Studies by our own group on *Arhgef6* deficient mice revealed reduced numbers of mature lymphocytes and reduced immune responses in the absence of ARHGEF6 due to defective TCR and BCR-induced signaling to PAK activation and to proliferation. *Arhgef6* deficiency impairs formation of T-cell–B-cell conjugates and recruitment of PAK and Lfa-1 integrin to the immune synapse (Missy et al., 2008). Therefore it seems that ARHGEF6 is involved in the inside-out signaling from the TCR to activation of Lfa-1, which promotes adhesion of T cells to antigen presenting cells (APCs) (Burbach et al., 2007; Kinashi, 2005).

Furthermore, ARHGEF6 has an inhibitory effect on basal as well as chemokine induced lymphocyte migration, since T and B cells lacking ARHGEF6 show enhanced migration in vitro (Missy et al., 2008). 2-photon microscopy of the thymic cortex further demonstrated that migration speed of developing *Arhgef6* deficient thymocytes is increased also in vivo (Korthals et al., 2014). Positive selection and production of mature T cells in the absence of ARHGEF6 is impaired due to increased motility of DP thymocytes, which is accompanied by decreased pausing on cortical thymic epithelial cells in vivo. TCR-induced signalling appears to be generally functional in thymocytes while basal Rac activity in freshly isolated thymocytes is even increased (Korthals et al., 2014). Thus, ARHGEF6 seems to restrain thymocyte migration, which is required for efficient positive selection (Figure 7).

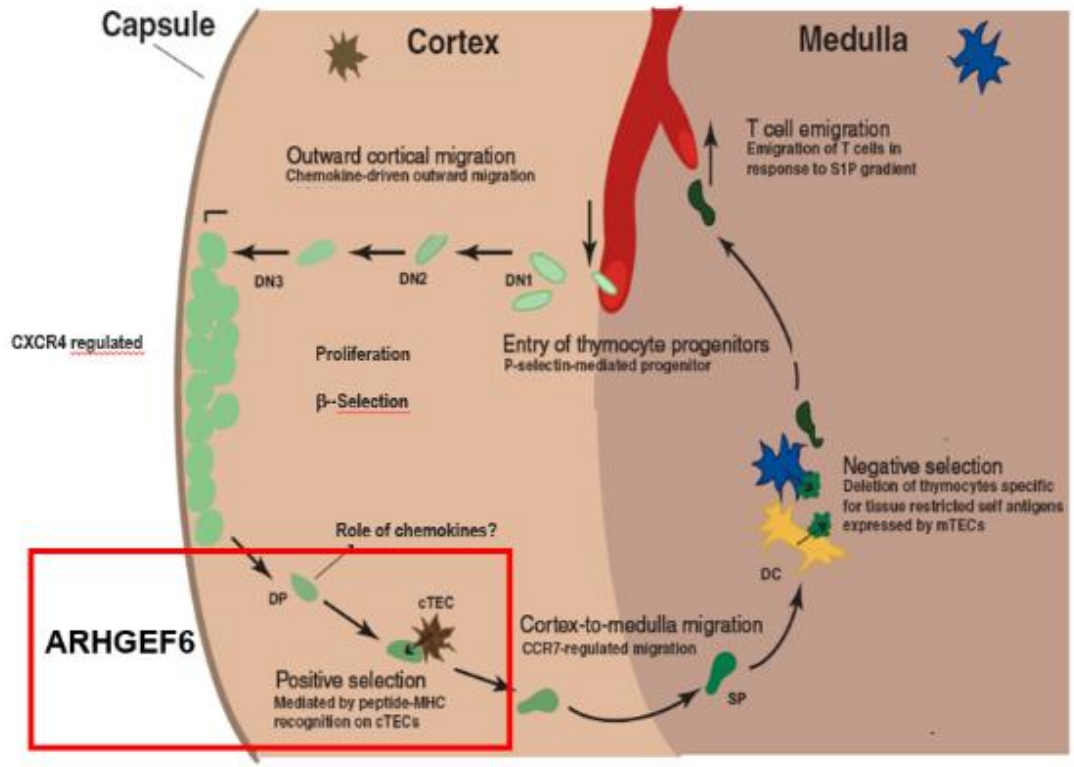

Figure 7. Route of migration during the different stages of thymocytes development
Proposed role of ARHGEF6 in positive selection as marked by red box. See the text for details. Modified from Ladi et al. (2006)

Interestingly, this phenotype is different from *Git2*$^{-/-}$ DP thymocytes, observed by 2-photon live cell imaging of murine explanted thymic lobes. *Git2*$^{-/-}$ thymocytes show increased motility in vitro but decreased motility in vivo, while accumulating near blood vessels due to a hyper responsiveness to CXCL12, which at the end impairs positive selection (Phee et al., 2010). This discrepancy demonstrates that different PIX/GIT members may confer specific functions to the complex rather than being mere links of a linear signaling cascade.

1.7 PAK activation by Rac/Cdc42

The major effectors controlled by Rac/Cdc42 are the PAK kinases, which are required for cytoskeleton dynamics, promoting migration, cell cycle regulation and apoptosis (Chong et al., 2001; Pirruccello et al., 2006). There are six mammalian PAK proteins, which can be classified, based on their structure, into group I, which includes PAK1, PAK2, PAK3 and group II, which includes PAK4, PAK5 and PAK6. The two groups have both similar and different functions, being controlled by special autoinhibitory mechanisms (Radu et al., 2014). The major PAK isoforms expressed in T cells are PAK1 and, at a high level, PAK2 (Chu et al., 2004). In mice, depletion of

PAK2 is embryonic lethal (Hofmann et al., 2004; Kelly and Chernoff, 2012). However, in conditional mouse models with specific depletion of PAK2 in the T cell lineage revealed impaired thymocyte selection and maturation leading to T cell lymphopenia (Phee et al., 2014).

Group I PAK activation is based on multiple phosphorylation events, which regulate interactions between the C-terminal catalytic domain and the N-terminal CRIB/KID domain including a Cdc42/Rac1 interaction/binding (CRIB) region and a kinase inhibitory (KID) region (Figure 8) (Chong et al., 2001; Pirruccello et al., 2006). In the inactive state, PAK exists as a homodimer while the KID domain interacts with the catalytic domain thereby negatively regulating it. Activation of PAK1 and PAK2 occurs in 2 steps (Figure 8). First, binding of Cdc42/Rac1 to the CRIB/KID domain of PAK, results in autophosphorylation of Ser144/141 in the CRIB/KID domain of PAK1 and PAK2, respectively, enabling the KID domain moving away from the catalytic domain. In the second step, opening of the catalytic domain allows transphosphorylation of Thr423/402 in the catalytic domain by the second PAK molecule. Transphosphorylation of Thr423/402 precludes rebinding of the inhibitory domain to the catalytic domain, and promotes dissociation of the homodimer (Lei et al., 2000; Radu et al., 2014). Both Ser144/Ser141 autophosphorylation and Thr423/402 transphosphorylation are required for efficient activation of PAK1 and PAK2, respectively.

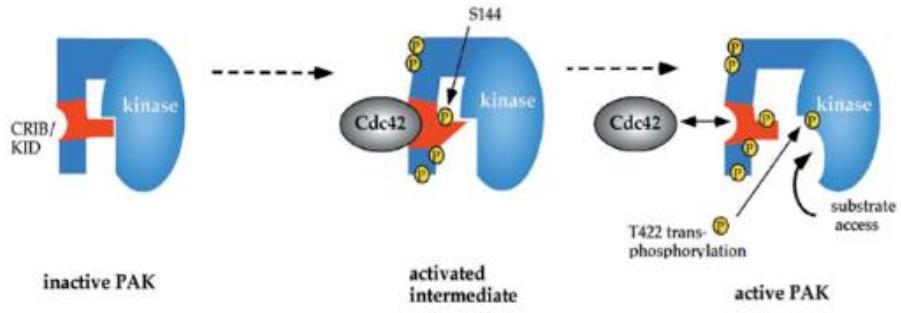

Figure 8. The mechanism of PAK activation
Serine residues Ser144/Ser141 (PAK1/PAK2), situated in kinase inhibitory domain, are first phosphorylated. This PAK2 Ser141 (analogous to PAK1 Ser144) is part of the kinase inhibitory domain (KID) accessible upon Cdc42-GTP binding. KID phosphorylation prevents its acting against the kinase domain. Activation loop threonine phosphorylation follows N-terminal autophosphorylation. When Thr423/402 (PAK1/PAK2) is subsequently transphosphorylated, this precludes interaction of catalytic domain with the KID. Only Cdc42 is presented in the model but the interaction with Rac1 is analogous (Modified from Chong et al., 2001)

In addition, three other phosphorylation sites (Ser21, Ser198 and Ser203) regulate interaction with SH3 domains of PIX and adaptor protein Nck, thereby linking PAK

with focal complexes (Chong et al., 2001). Active state Rac1/Cdc42 triggers and recruits PAK to the complex, which targets FA where PAK performs its effector function (Hoefen and Berk, 2006). Several target proteins for PAK2 mediated phosphorylation are known, including LIM kinases (Dan et al., 2001; Edwards et al., 1999), ARHGEF6 and ARHGEF7 (Koh et al., 2001; Rennefahrt et al., 2007; Shin et al., 2002) and regulatory myosin light chain (Chew et al., 1998; Ramos et al., 1997).

1.8 Downstream regulation of actin dynamics

It's well established that the Rac/PIX/PAK module controls actin dynamics during adhesion and migration in many cell types. However, how ARHGEF6 specifically regulates motility of fast moving cells, such as lymphocytes is unclear. In general, speed and directionality of migrating cells is intrinsically regulated by the rate of actin polymerization at the leading edge, the rate of actin depolymerization in the back, and the degree of actin linkage to adhesion structures.

Actin polymerization

Actin polymerization is initiated by the activation of the actin related proteins 2 and 3 (Arp2/3) complex. Arp2/3 binds both actin monomers and pre-existing filaments, where it creates barbed ends available for the addition of monomers during polymerisation. ATP bound active actin monomers are provided by the actin monomer binding protein profilin, which catalyzes the exchange of ADP to ATP (Pollard and Borisy, 2003).

Arp2/3 first starts actin polymerization perpendicular to actin filaments paralleling the plasma membrane, thereby forming filopodia-like protrusions. Arp2/3 may also nucleate further actin polymerization on newly formed filaments, which broadens the extensions to form sheet-like membrane ruffles and the lamellipodium (Bompard and Caron, 2004). The activity of Arp2/3 is tightly controlled by proteins of the WAVE regulatory complex and the Wiskott-Aldrich syndrome protein (WASp), which are activated by GTP-bound Rac and Cdc42, respectively. While Cdc42 promotes filopodia formation, Rac is particularly critical for lamellipodia formation (Stradal and Scita, 2006). Local restriction of Rac activity by RhoA, however, limits the width of the lamellipodium and thereby supports a clear front to back polarization and promotes directional migration (Sander et al., 1999). In addition, Arp2/3 can be inactivated by

the negative regulator Arpin, which promotes transient stopping from migration and reorientation of protrusions, thereby steering the cell's direction (Dang et al., 2013). Active Rac promotes cell extension at the front, while actin polymerization results in a continuous retrograde actin flow. However, actin polymerization required for migration is limited by the availability of barbed end and actin monomers. In order to sustain actin polymerization at the front, depolymerization further back is required for recycling of monomeric actin (Pollard and Borisy, 2003).

Actin depolymerization

The major player in actin depolymerization is cofilin. Cofilin is a 19 kDa protein that belongs to cofilin/actin-depolymerizing factor (ADF) family of actin-binding proteins. It exists in two isoforms cofilin 1 (ubiquitously expressed) and cofilin 2, which is a muscle specific isoform of cofilin. Cofilin inhibition results in increased stability of polymerized actin (Tybulewicz and Henderson, 2009) (Figure 9). Knockout studies in mice have shown that cofilin 1 is essential for embryogenesis (Gurniak et al., 2005).

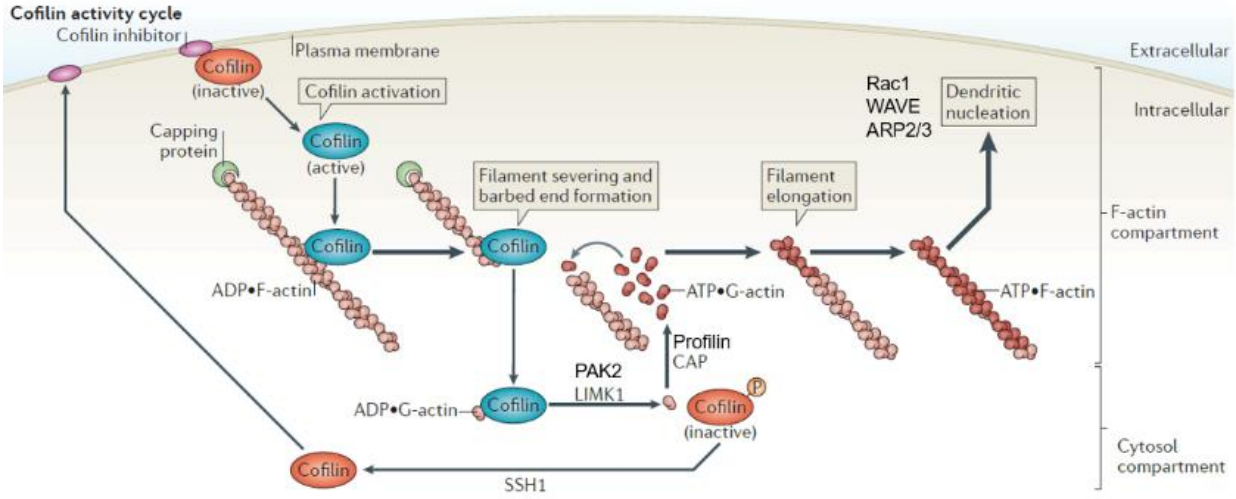

Figure 9. The role and cycling of cofilin
Activated cofilin severs actin filaments creating barbed ends, which further facilitate actin polymerization. LIMK1 and cyclase-associated protein promote ADP/G-actin/cofilin complex disassembly increasing the ATP/G-actin monomer concentration used for filament elongation at barbed ends. LIMK1 phosphorylates and inactivates cofilin thereby releasing G-actin while slingshot 1 (SSH1) dephosphorylates cofilin, which is then driven back to the inhibitory area (modified from Bravo-Cordero et al., 2013)

Cofilin causes actin depolymerization by two mechanisms. First, cofilin may cut off actin monomers from the minus end, which can then be recycled by profilin. Second, cofilin can sever actin fragments from longer filaments, thereby creating new barbed

ends, which are readily available for further extension (Bravo-Cordero et al., 2013). Thereby, cofilin and Rac work together in promoting actin treadmilling (Figure 9). In neurons, active cofilin is necessary for extension of the dendrites and axons. It has been shown that in neurons the reduction of ARHGEF6 results in decrease of phosphorylated cofilin where hyperactive cofilin results in excessive actin filament disassembly thereby negatively altering axonal and dendritic branching (Totaro et al., 2012).

There are several mechanisms regulating the activity of cofilin. Among other phosphorylation sites, Ser3 is the major one that controls its activity (Sakuma et al., 2012; Yoo et al., 2010). Non-phosphorylated active cofilin is present in lamellipodia in epithelial cells and invadopodia in carcinoma cells, whereas under physiological conditions inactive phosphorylated cofilin is equally distributed in cytoplasm excluding the leading edge (Bravo-Cordero et al., 2013). The amount and location of activated cofilin in migrating cells is highly dependent on the balance of activity between kinases and phosphatases targeting cofilin. LIM kinases phosphorylate ADF/cofilin at Ser3, thereby inhibiting its actin-binding, severing, and disassembling activities (Arber et al., 1998; Moriyama et al., 1996). Besides LIMKs there are also TES family of kinases (TESK1 and TESK2), which phosphorylate cofilin at Ser3 (Toshima et al., 2001b). On the other hand, the phosphatases that activate cofilin include slingshot, chronofin and general phosphatases PP1, PP2A and PP2B (Gohla et al., 2005; Nagata-Ohashi et al., 2004). LIM kinases belong to a tyrosine kinase-like family of proteins containing two N-terminal LIM domains, an internal PDZ-like domain and a protein kinase domain at the C terminus (Manning et al., 2002). A number of kinases including ROCK, PAK1, PAK2, PAK4, MRCKα and MAPK-activated protein kinase 2 are involved in phosphorylation and activation of both LIMK1 and LIMK2 (Amano et al., 2001; Edwards et al., 1999; Ohashi et al., 2000; Scott and Olson, 2007). It has been shown that LIMK1 is activated after cell stimulation with growth factors or chemokines. Deficiency of LIMK1 inhibits cell migration and tumor cell invasion and metastasis (Nishita et al., 2002; Yoshioka et al., 2003). Slingshot-1 (SSH1L) activity is significantly increased by its binding to actin filaments thus activating cofilin-mediated actin turnover in lamellipodia (Kurita et al., 2008).

In addition, binding of cofilin to PtdIns(4,5)P2 at the plasma membrane, cortactin and G-actin inhibits cofilin severing activity, while its release from PtdIns(4,5)P2 or cortactin, or binding to F-actin are required for its activation. Phospholipase C (PLC)

leads to the hydrolysis of PtdIns(4,5)P2 creating inositol-1,4,5-triphosphate (IP3) and diacylglycerol (DAG) simultaneously releasing cofilin from its inhibitory interaction with the lipids, which locally activates severing of F-actin filaments, resulting in protrusions and cell polarity in migrating cells (van Rheenen et al., 2007). In T cells, activation of cofilin is induced by TCR stimulation in the presence of costimulation or by chemokines, probably via a Ras/MEK/PI3K pathway, leading to LIMK inhibition or activation of phosphatases, which promotes directional migration (Klemke et al., 2010; Wabnitz et al., 2006). A further way of cofilin inactivation is oxidation, which leads to T cell hyporesponsiveness. However, inactive PtdIns(4,5)P2 bound cofilin, becomes active in a reducing environment resulting in actin dynamics within membrane region (Klemke et al., 2008).

Linkeage of actin filaments to focal contacts

The Arp2/3 complex and cofilin work together to reorganize the actin filaments in lamellipodial morphology dynamics. However, the resulting retrograde actin flow can only be translated into forward movement of the cell by coupling actin filaments to adhesion structures and myosin that provide traction forces to pull the cell body forward as well as friction forces applied to the cell's extracellular environment (Wu et al., 2012).

As previously written, the molecular clutch model emerged as plausible explanation for cell motility. Adaptor proteins forming a clutch module, including talin and vinculin, provide dynamic connection between actin filaments and integrins. The module assumes that these connections can be described as no coupling, transient and strong coupling, respectively. Strong coupling slows down the rearward flow of actin filaments changing actin flow direction to forward, resulting in protrusion and cell spreading (Giannone et al., 2009). Cell locomotion is finally achieved by uncoupling of integrins from actin in the back to allow retraction of the uropod. Adhesions in migrating cells therefore cycle between assembly, maturation and disassembly (Figure 10).

Integrins in this model, including LFA-1, are not static elements of the module but rather mobile. Adhesions in cells expressing LFA-1 integrins on ICAM-1 substrate, show fast integrin retrograde flux (Hons et al., 2018). Adhesion strength on the substrate in protrusion regions of immune cells migrating on ICAM-1 is lower, compared to more adhesive cells, e.g. expressing α5β1 integrins (Chen et al., 2012).

Active adhesion in migrating immune cells is only present in a central region behind the lamellipodium, which enables high speed immune cell migration and rapid change of direction (Smith et al., 2005; Smith et al., 2007; Stanley et al., 2008). High-affinity conformations of LFA-1 and VLA-4 integrins are also involved in tight cell-cell interactions required for immune synapse formation and the arrest on endothelial cells under flow.

Focal contacts or focal adhesions represent elongated structures comprising actin- and myosin- filament bundles (Heath and Dunn, 1978; Zamir et al., 2000), which are required for adhesion and migration of large cells. Assembly, maturation and turnover of focal contacts at the leading edge is required for directional cell migration (Zaidel-Bar et al., 2003). Migrating lymphocytes use only transient adhesion-dots (Smith et al., 2005; Smith et al., 2007), whereas the tight cell-cell adhesion of the immunological synapse is mediated by a stable focal micro-adhesion ring surrounding the TCR (Hashimoto-Tane et al., 2016).

Integrin activation is a multistep process, which is initiated by receptor-triggered inside-out signaling via activation of the small GTPase Rap1 and associated GEFs and adaptor proteins leading to intermediate active integrin (Hogg et al., 2011). Retrograde mechanical outside-in signaling via the integrin may in turn promote full integrin activation and adhesion stabilization. In addition, full adhesion via LFA-1 is achieved by actin-dependent integrin clustering, which increases integrin avidity (Romanova and Mushinski, 2011).

One important ubiquitous regulator for both stabilization and turnover of adhesions is the scaffold protein paxillin (Deakin and Turner, 2008). As a multidomain protein, paxillin can bind integrins, either directly to the β-chain, or indirectly via talin. It also binds the actin binding protein vinculin and recruits the PIX/GIT complex and other signaling molecules to the site of adhesion (Turner, 2000). These interactions are highly dynamic and largely regulated via multiple Tyrosin and Serin/Threonin phosphorylation sites, which are targeted by several kinases (and phosphatases) (Lopez-Colome et al., 2017).

An important event in the initiation of focal complex assembly is paxillin phosphorylation at tyrosine 118 (Zaidel-Bar et al., 2003; Zaidel-Bar et al., 2007), which is mediated by focal adhesion kinase (FAK) (Bellis et al., 1995; Lim et al., 2008). In T cells, FAK is activated by Src kinase-dependent TCR inside-out signaling, which is further promoted by CD28 costimulation and LFA-1 and VLA-4 mediated

outside-in signaling (Chapman and Houtman, 2014; Rodriguez-Fernandez et al., 1999). FAK activity and paxillin Tyr118 phosphorylation both may in turn also regulate actin-dependent clustering of LFA-1 (Giannoni et al., 2003; Romanova and Mushinski, 2011).

PIX/GIT complex localization to focal contacts is mediated by interaction of GIT1 and GIT2 with paxillin (Mazaki et al., 2001; Schmalzigaug et al., 2007). This interaction is controlled by Src/FAK-dependent phosphorylation of PKL (Yu et al., 2010). In addition, PAK mediated phosphorylation of paxillin at Ser273 increases the interaction between paxillin and GIT1 and promotes GIT1-PIX-PAK complex recruitment to the leading edge.

It has been reported that phosphorylation of paxillin at Tyr31 and Tyr118 promotes Rac1 activation and actin polymerization resulting in polarized, migratory cell phenotype (Romanova and Mushinski, 2011). The local activation of Rac by the PIX/GIT complex may also result in local protrusion formation, FA turnover and migration (Nayal et al., 2006). However, nascent adhesions must interact with actomyosin in the lamellum in order to become larger and mature (Parsons et al., 2010). This process is mainly regulated by locally activated Rho, which in turn inhibits Rac and activates myosin II regulatory light chain (RLC) via its effector kinase ROCK. In addition, also PAK (activated by the PIX/GIT complex) activates myosin II by phosphorylation of RLC. As a result, Myosin II produces tension and by crosslinking various adhesion proteins maintains adhesion maturation (Figure 10). This switch from Rac-mediated protrusion formation to Rho-mediated contraction and stabilization of adhesion or disassembly at the rear probably involves paxillin recruitment of many other signaling molecules to the adhesion sites, but how this is regulated is still not well understood.

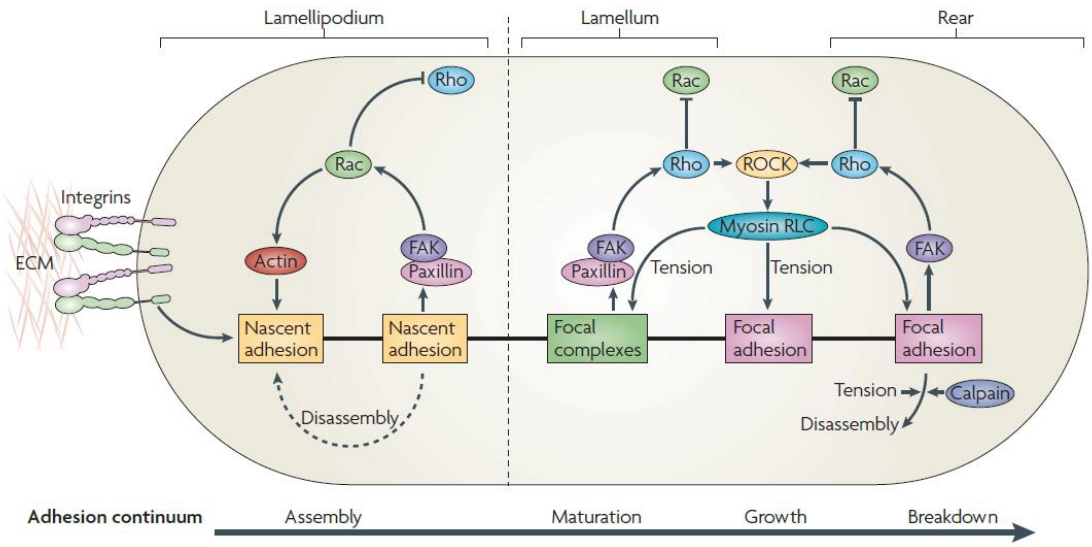

Figure 10. The role of Rho GTPases and FA proteins in adhesion maturation
(Modified from Parsons et al. 2010)

1.9 Immune phenotype of *Arhgef6*$^{-/-}$ mice

Arhgef6$^{-/-}$ mice were generated by creating a null mutation of the mouse *Arhgef6* locus, which is located on the X chromosome. A part of wild-type PH domain was replaced with the neomycin resistance cassette. Male embryonic stem cells were used for homologous recombination with wild-type allele being absent in targeted clones. *Arhgef6* mutant mice were null for *Arhgef6* in males and heterozygous/homozygous for *Arhgef6* mutation in females (Missy et al., 2008). As described previously, deletion of *Arhgef6* results in greatly increased migration of tymocytes, T and B cells without alterations in general TCR-induced signaling, suggesting that ARHGEF6 may act as an inhibitor of limphocyte migration (Korthals et al., 2014; Missy et al., 2008). Taken together, ARHGEF6 deficient PIX/GIT complex may reflect a variation of the PIX/GIT complex otherwise present in highly adhesive cells (fibroblasts) that require stronger activation of migration, where ARHGEF6 is probably not expressed. Detailed analysis of the ARHGEF6 deficient PIX/GIT complex in T cells may therefore shed light on the role of ARHGEF6 in T cell coping with their pro-adhesive versus pro-migratory requirements.

1.10 Aims of the study

Our group's interest in RhoGEFs PIX isoforms (ARHGEF6 and ARHGEF7) revealed the critical role of ARHGEF6 in the maturation of both T cells and B cells and maintaining proper immune response (Missy et al., 2008). Additionally, the study of ARHGEF6 on thymocyte development demonstrated that this PIX isoform has an important role in restricting migration in order to support positive selection (Korthals et al., 2014). However, signaling pathway where ARHGEF6 exerts its role affecting cell motility and morphology is not known.

The aim of my study was to further elucidate the mechanism by which ARHGEF6 affects cellular dynamics and migration. To achieve this aim, we addressed the following questions:

1) Determine how deletion of ARHGEF6 from PIX/GIT complex affects the complex stability and expression/localization of other complex constituents. To this end protein composition of thymocytes from wt and *Arhgef6*$^{-/-}$ mice were analyzed by BN-PAGE and size exclusion chromatography (FPLC).

2) Define the cytoskeletal pathways affected by loss of *Arhgef6* in CD4^{+} T cells. Our line of investigation comprised ARHGEF6, ARHGEF7, Rac1, PAK1/2, LIMK1/2, cofilin and actin. Each segment was explored by using a combination of biochemical methods, immunostaining and live imaging.

3) Determine the molecular mechanisms of PIX regulation of migration. To tackle this question the focus was on cofilin activation, paxillin turnover and subsequent cytoskeleton changes.

2. MATERIALS AND METHODS

2.1 Materials

The chemicals and compounds used in this study were of analytical grade and provided by the following companies.

2.1.1 Membranes and plastic ware

Table 1. Materials for Western Blot

	Cat. #	**Company**
ECL Western Blotting Detection Reagent	RPN2106	Amersham
Hyperfilm ECL (18 x 24cm)	28906836	Amersham
Immobilon-FL Membrane, PVDF transfer membrane	IPFL20200	Millipore
Immobilon-P Membrane, PVDF transfer membrane	IPVH00010	Millipore

Table 2. Sterile plastic ware for cell culture

	Cat. #	**Company**
6-well plates	152795	Nunc
24-well plates 5/85	142485	Nunc
96-well plates, U96 round-bottom	163320	Nunc
Tissue Culture Flask T25 Vent Cap Red	690175	Greiner Bio One
Tissue Culture Flask T75 Vent Cap Red	658175	Greiner Bio One
Tissue Culture Flask T175 Vent Cap Red	660175	Greiner Bio One
uncoated 15 µ-Slide Angiogenesis	81501	Ibidi

Table 3. Other materials

	Cat. #	**Company**
Netwell inlays 6 well (74 µm)	3479	Costar
Neubauer improved counting chamber	631-1111	VWR
Pre-Separation Filters 30 µm	130-041-407	Miltenyi Biotec
syringe filters-pore size 0.2 µm	CLS431222-50EA	Corning
Transwell polycarbonate membrane 5 µm	3421	Costar

2.1.2 Equipment and software tools

Table 4. Machines

AutoMACS Pro Separator	Miltenyi Biotec
CURIX 60	AGFA
Leica TCS SP5 confocal microscope	Leica
DMI6000 (TIRF) microscope	Leica
FACS Canto II	Becton Dickinson
Fast Performance Liquid Chromatography (FPLC)	PHARMACIA
Gene pulser electroporator	Bio-Rad
Mini-PROTEAN® 3 Multi-Casting Chamber	Bio-Rad
Mini Trans-Blot® Electrophoretic Transfer Cell	Bio-Rad
Nanodrop	Thermo Fisher Scientific
Odyssey Infrared Scanner	LI-COR
Tecan Infinite 200	Tecan Group

Table 5. Software

ApE	Oligo/primer/plasmid designs
FacsDiva	FACS analysis/acquisition
FlowJo	FACS analysis
ImageJ	Western blot and image analysis
Odyssey software v2.1	LI-COR
GraphPad Prism 6	Statistical analyses

2.1.3 Kits

Table 6. Kits

Plasmid preparation	**Cat. #**	**Company**
NucleoBond® Xtra Midi EF (50)	740420.50	MACHEREY-NAGEL
QIAquick Gel Extraction Kit (50)	28704	Qiagen
Kinase activity assay		
Omnia® Kinase Assays	KNZ1051	Thermo Fisher Scientific
T cell purification kit		

$CD4^+$ T Cell Isolation Kit mouse	130-104-454	Miltenyi Biotec
Measurement of protein content		
BCA™ Protein Assay Kit	23225	Thermo Fisher Scientific

2.1.4 Chemicals and reagents for cell culture

Table 7. Chemicals and reagents for cell culture

	Cat. #	**Company**
Bovine Serum Albumin (BSA)	A4378	Sigma
Di-methyl-sulfoxide (DMSO)	D-8418	Sigma
DMEM, high glucose, GlutaMAX™	31966-021	Thermo Fisher Scientific
Dulbeccos MEM High Glucose	41965-062	Gibco
FCS	P251110	PAN-Biotech
L-Glutamine 200 mM (100 x)	25030-24	Gibco
HBSS w/o Ca2+, Mg2+	L 2045	Biochrom
HBSS with Ca2+, Mg2+	14025092	Gibco
HEPES buffer solution 1 M	15630-056	Gibco
Horse serum		A gift from, LIN Magdeburg
2-Mercaptoethanol 50 mM	31350-010	Gibco
Non Essential Amino Acids (NEAA) (100 x)	11140-035	Gibco
PBS w/o Ca2+, Mg2+	14190-250	Gibco
PBS with Ca2+, Mg2+	17-513F	Lonza
Penicillin-Streptomycin (100 x)	15140-122	Gibco
Polybrene®		Gift from, LIN Magdeburg
RPMI 1640 Medium	31870-025	Gibco
RPMI 1640 liquid medium with stable glutamine	FG 1215	Biochrom
Sodium-pyruvate (100 x)	11360-039	Gibco
Staphylococcal enterotoxin E		Gift from, LIN Magdeburg

2.1.5 Cells

Table 8. Cell lines and bacteria

Cell lines	
HSB2	Human T lymphoblast cell line
J558	murine B lymphoblast cell line
Jurkat E6-1	Human T lymphoblast cell line
Raji	Human B lymphoblast cell line
Bacteria	
E. Coli BL21	
DH5α electro-competent cells	

2.1.6 Vectors, primers and oligos

Table 9. Vectors

Vector	**Origin**
LentiBrite™ Paxillin-GFP Lentiviral Biosensor	Merck Millipore
pCMS4-H1p-EGFP	Dr. Sefanie Kliche (IMKI Magdeburg)
pGEX 4T-3	IBZ Magdeburg
pGEX 5X-1	Dr. Kristina Langnäse (IBZ Magdeburg)

Table 10. Primers

Primer	**sequence 5´ → 3´**
Arhgef6 wt_rv	GTT CAA ATC CCC ATT GCA TCA TAG TCT G
Arhgef6 wt_fv	GTC TTT AAC CGC TGT GCT TCT TTT TGG ATA
Arhgef6$^{-/-}$ _rv	GAT ATG GGT CTG TAA ACT GTTGCT GCT AAT
Arhgef6 NEO_fv	GTT GGC GCT ACC GGT GGA TGT GG
pCMS4 H1P_fv	GAA CGC TGA CGT CAT CAA C

Table 11. Oligos for shRNA cloning

description	**sequence 5´ → 3´**
Arhgef6 shRNA A	GATCCCCCCTTGGAGCCTCCTCAAATTATTCAAGAGATAATTT GAGGAGGCTCCAAGGTTTTTGGAAA
Arhgef6 shRNA C	GATCCCCCCGTGGAGTTTAAGTTGTCTATTCAAGAGATAGAC AACTTAAACTCCACGGTTTTTGGAAA
Scramble ctrl	GATCCGCGCACGAACTATCAACATATTCAAGAGATATGTTGA TAGTTCGTACACGCGTTTTTTGGAAA

2.1.7 Antibodies

2.1.7.1 For Western Blotting

Table 12. Primary antibodies for Western blot

Antibody	**dilution**	**Isotype**	**Cat. #**	**Company**
αPIX (C23D2)	1:1000	rabbit	4573	Cell Signaling
β-actin	1:5000	mouse	A5316	Sigma
βPIX	1:1000	mouse	611648	BD
cofilin	1:500	mouse	612144	BD
p-cofilin (Ser3) (77G2)	1:500	rabbit	3313	Cell Signaling
ERK1 (K23)	1:1000	rabbit	sc-94	Santa Cruz
pERK (E4) (Y 204)	1:500	mouse	sc-7383	Santa Cruz
FAK	1:500	rabbit	3285	Cell Signaling
pFAK (Tyr397)	1:250	rabbit	3283	Cell Signaling
GAPDH	1:1000	mouse	MAB374	Merck Millipore
GFP	1:2000	mouse	MMS-118P	Covance
GIT1/2 (p95PKL)	1:1000	mouse	611388	BD
GIT1 Clone N39B/8	1:500	mouse	75-094	NeuroMab/UC Davis
LIMK1	1:500	mouse	611748	BD
pLIMK1 (pThr508)	1:500	rabbit	SAB4300103	Sigma
LIMK2	1:500	rabbit	SAB4501760	Sigma

PAK1	1:2000	rabbit	2602	Cell Signaling
PAK2	1:2000	rabbit	2608	Cell Signaling
pPAK1 (Ser144)/ pPAK2 (Ser141)	1:1000	rabbit	2606	Cell Signaling
pPAK1 (Thr423)/pPAK2 (Thr402)	1:250	rabbit	2601	Cell Signaling
pPAK2 (Thr402)	1:250	rabbit	PPS058	R&D Systems
paxillin	1:1000	rabbit	2542	Cell Signaling
p-paxillin (Tyr118)	1:500	rabbit	2541	Cell Signaling
Rac1	1:10000	mouse	610651	BD

Table 13. Secondary antibodies for Western blot

Antibody	**dilution**	**Isotype**	**Cat. #**	**Company**
Peroxidase-conjugated AffiniPure Goat Anti-Mouse IgG	1:5000	goat	115-035-146	Dianova
Peroxidase-conjugated AffiniPure Goat Anti-Rabbit IgG	1:5000	goat	111-035-003	Dianova
anti-mouse, -rabbit IgG Alexa 680	1:30.000	goat	A-21058 A-21109	Invitrogen
anti-mouse or -rabbit IgG, IRDye™-800CW	1:30.000	goat	610-731-002 611-745-127	Rockland

2.1.7.2 For Immunocytochemistry

Table 14. Primary antibodies for immunocytochemistry

Antibody	**dilution**	**Isotype**	**Cat. #**	**Company**
αPIX (C23D2)	1:25	rabbit	4573	Cell Signaling
β-actin	1:1000	mouse	A5316	Sigma
βPIX	1:50	mouse	611648	BD
βPIX	1:50	rabbit	4515	Cell Signaling
Mouse Anti-Human CD3_UCHT1	1:1000	mouse	14-0038	eBioscience

CD49d clone R1-2 Rat Anti-Mouse	1:50	rat	553154	BD Pharmingen™
Cdc42	1:50	rabbit	sc-87	Santa Cruz
Cdc42-GTP (active)	1:25	mouse	26905	NewEast Biosciences
cofilin	1:50	mouse	612144	BD
p-cofilin	1:50	rabbit	3313	Cell Signaling
GFP	1:500	mouse	A-11120	Molecular Probes
GIT1/2 (p95PKL)	1:50	mouse	611388	BD
Integrin β2 chain C7116 Rat Anti-Mouse-FITC	1:50	rat	553292	BD Pharmingen™
Integrin β1 chain HMb1-1	1:50	Armenian hamster	14-0291-82	Thermo Fisher Scientific
LFA-1 (CD11a) M17/4 Rat Anti-Mouse	1:50	rat	550528	BD Pharmingen™
LIMK1	1:50	mouse	611748	BD
pLIMK1 (pThr508)	1:100	rabbit	SAB4300103	Sigma
LIMK2	1:50	rabbit	SAB4501760	Sigma
pLIMK1/2 (pThr508/pThr505)	1:100	rabbit	ab131343	Abcam
PAK1	1:50	rabbit	2602	Cell Signaling
PAK2	1:50	rabbit	2608	Cell Signaling
paxillin	1:50	rabbit	2542	Cell Signaling
p-paxillin (Tyr118)	1:50	rabbit	2541	Cell Signaling
Rac1	1:300	mouse	610651	BD
Rac1-GTP (active)	1:25	mouse	26903	NewEast Biosciences
Anti-vinculin antibody	1:100	mouse	ab11194	Abcam

Table 15. Secondary antibodies and labelling kits for immunocytochemistry

Antibody	**dilution**	**Isotype**	**Company**
anti-mouse IgG, Alexa Fluor™ 488 - conjugated	1:500	goat	Invitrogen
anti-mouse IgG, Cy5™-conjugated	1:500	goat	Jackson Immuno Research
anti-rabbit IgG Cy3™-conjugated	1:500	goat	Jackson Immuno Research
Anti-rat IgG, Alexa Fluor™ 488 – conjugated	1:500	donkey	Invitrogen
Zenon® Alexa Fluor® 488 Mouse IgG1 Labeling Kit			Life Technologies
Zenon® Alexa Fluor® 488 Rabbit IgG Labeling Kit			Life Technologies
Zenon® Alexa Fluor® 532 Rabbit IgG Labeling Kit			Life Technologies

2.1.7.3 For Stimulation

Table 16. Antibodies for stimulation

Antibody	**dilution**	**Cat. #**	**Company**
CD28 clone 37.51 (Purified Hamster Anti-Mouse)	1:1000	553295	Becton Dickinson
CD3ε clone 145-2C11 (Purified Hamster Anti-Mouse)	1:200	553058	Becton Dickinson
Biotin-CD4 clone GK1.5 (Rat Anti-Mouse)	1:250	553728	Becton Dickinson
Biotin-CD3ε clone 145-2C11 (Hamster Anti-Mouse)	1:50	553060	Becton Dickinson
FITC anti-human IgG Fc Antibody	1:200	409310	BioLegend

2.1.7.4 For Flow Cytometry

Table 17. Antibodies for flow cytometry

Antibody	**Note**	**Company**
CD4-APC	1:200	BD
CD4-V450	1:100	BD
CD8-FITC	1:300	BD
LFA-1 (CD11a) M17/4 Rat Anti-Mouse	1:300	BD Pharmingen™
CD49d clone R1-2 Rat Anti-Mouse	1:200	BD Pharmingen™
Goat anti-Rat Secondary Antibody, Alexa Fluor 488	1:500	Thermo Fisher Scientific

2.1.8 Other chemicals and reagents (in alphabetical order)

Acetic acid	J.T. Baker
Acetone p. a. 8002	J.T. Baker
Acrylamide/Bis-Solution 37,5:1 (40%; 2,6%C)	Serva
Acrylamide/Bis-Solution 29:1 (30%; 3,3%C)	Serva
Agarose	Applichem
Albumin, Heat-shocked fractionate, >96%	Sigma
Ammoniumpersulfate (APS)	Sigma
Ampicillin	Sigma
Aqua non-pyrogenic	B/BRAUN
Avidin	Sigma
Bovine Serum Albumin pH 7,0	PAA
Bromophenol Blue	Sigma
BSA (Albumine Fraction V)	Roth
Calcium chloride	Sigma
cOmplete™, Mini, Protease Inhibitor Cocktail	Roche
Cytofix/Cytoperm™	BD
DAPI	Sigma

Dimethylsulfoxide (DMSO)	Sigma
Dithiothreitol (DTT)	Sigma
DNA GeneRuler 1 kb DNA Ladder	Thermo Fisher Scientific
DNA Generuler 100bp DNA Ladder Plus	Thermo Fisher Scientific
ECL Western Blotting Detection Reagents	Amersham
Ethidium bromid solution 1% (10 mg/ml)	Roth
Ethylenediaminetetraacetic acid (EDTA)	Sigma
FACSFlow™	BD
FastDigest BglII	Thermo Fisher Scientific
FastDigest EcoRI	Thermo Fisher Scientific
FastDigest HindIII	Thermo Fisher Scientific
Fatty acid free Bovine Serum Albumin	Roth
Formaldehyde 37%	Sigma
GammaBind Plus Sepharose beads	GE Healthcare
Gene Pulser Cuvettes	Bio-Rad
D(+)-Glucose monohydrate	Roth
Glutathione Sepharose™ 4B	GE Healthcare
Glycerol	Merck Millipore
Glycine	Applichem
HEPES	Roth
ICAM-1 (human)	R&D Systems
ICAM-1 (murine)	R&D Systems
Interleukin 2 (murine)	IBZ self-made
Interleukin 7 (murine)	IBZ self-made
IPA3	Tocris
IPTG	Sigma
Isopropanol	Sigma
Isopropyl-β-D-thiogalactopyranoside (IPTG)	Fermentas
Kanamycin sulfate	Sigma
LB Agar (Lennox)	Invitrogen
LB Broth (Lennox)	Invitrogen
L-Glutathione reduced	Sigma
LIMKi3	Tocris
Manganese(II) chloride	Sigma

2-Mercapto-ethanol	Roth
Methanol	J.T. Baker
Mowiol 4-88	Calbiochem
PageRuler™ Prestained Protein Ladder, 10 to 180 kDa	Thermo Fisher Scientific
Paraformaldehyde (PFA)	Roth
Perm/Wash™	BD
Phenylmethanesulphonylfluoride (PMSF)	Sigma
Phorbol 12-myristate 13-acetate	Sigma
PhosSTOP – Phosphatase Inhibitor Cocktail	Roche
Ponceau S fixative dye solution	Sigma
CXCL12 recombinant human	R&D Systems
Skim milk powder	Applichem
Sodium azide	Roth
Sodium chloride	Roth
Sodiumdodecylsulfat (SDS)	Applichem
Sodium fluoride	Roth
Sodium hydrogen carbonate	Roth
Sodium orthovanadate	Sigma
T4 DNA ligase	NEB
T4 DNA ligase buffer	NEB
N,N,N',N'-Tetra-methyl-ethylene-diamine TEMED	Sigma
Tris-base (Tris(hydroxymethyl)-aminomethan)	Applichem
Triton X-100	Roth
Trypan blue Solution (0.4%)	Sigma
Tween®20	Roth
VCAM-1(human)	R&D Systems
VCAM-1(murine)	R&D Systems

2.2 Methods

2.2.1 Cell cultures

Table 18. Cell lines and cultivation media

Cell line	**Medium**
Jurkat E6.1, Raji, HSB2	RPMI 1640 liquid medium with stable glutamine (Biochrom); 10% FBS (PAN, Biotech); 1% penicillin/streptomycin (Gibco)

Thawing

Jurkat and HSB2 cells were taken from aliquots cryopreserved in liquid nitrogen. The cryovial was placed in a 37°C water bath for approximately 2 minutes until cells were thawed and the cells were immediately transferred to a 15 ml tube containing 10 ml of warm culturing medium (Table 18). The cells were centrifuged at 300 g for 7 minutes, resuspended in 1 ml of warm medium and transferred to 10 ml of medium in a 50 ml tissue culture flask. Density was approximately $1x10^5$ cells/ml. Cells were maintained between 1×10^5 and 1×10^6 cells/ml during culture. The cultivation medium was changed every 2 to 3 days (depending on cell density). Cell were not kept longer than 5 passages in culture before usage in experiments or cryopreservation.

Freezing

HSB2 and Jurkat T cells were frozen when they reached a density of 1×10^6 cells/ml (log phase). $10x10^6$ cells were spun down, resuspended in 1 ml of freezing medium (10% DMSO, 90% FBS) and aliquoted to a 2 ml freezing tube. Raji B cells were frozen in 10% DMSO and 90% cultivation medium. The cryotubes were transferred to an isopropanol box, kept in -20° freezer for 45 minutes, then at -80° freezer overnight and finally transferred to liquid nitrogen for long-term storage.

2.2.2 IL-7 production

J558 IL-7 producing cell line was used. The cells were seeded at 2×10^5 cells/ml and maintained between 1×10^5 and 1×10^6 cells/ml. The cultivation medium (Table 19)

was changed every 2 to 3 days (depending on cell density). After three passages, supernatant was harvested, aliquoted, frozen and stored at -80°C.

Table 19. J558 IL-7 cultivation medium

DMEM, high glucose, GlutaMAX™	
horse serum	10%
Penicillin/Streptomycin	1%

2.2.3 Mice

Arhgef6 deficient mice (*Arhgef6*$^{-/-}$) had been generated in our lab previously (Missy et al., 2008) and crossed to wild-type C57BL/6 mice for >10 generations. LifeAct mice were crossed to wt or *Arhgef6*$^{-/-}$ mice. Mice used for experiments were 8-12 weeks old. All animals were bred at the animal facility of the Medical Faculty of the Otto-von-Guericke University. Animal procedures were performed in agreement with the institutional guidelines. All efforts were made to minimize suffering and the number of animals used.

2.2.4 Primary cell preparations

2.2.4.1 Thymocyte and lymphocyte isolation

The mice were euthanized by CO_2 inhalation. The thymus and inguinal, axillary, brachial, superficial cervical, mesenteric, caudal and lumbar lymph nodes were extracted. Thymocytes and lymphocytes were prepared by homogenising the tissue with a syringe plunger and passing single cells through a cell strainer mesh (74 µm) placed in 6 well plate containing 5 ml of PBS + 0.2% BSA on ice. Thereafter cell suspension was centrifuged at 300 g for 10 min at 4°C and supernatant was discarded. The cell pellet was resuspended in 5 ml of PBS + 0.2% BSA, filtered through 30 µm Miltenyi pre-separation filters and the cells were counted by FACS. Organs and cell suspensions were always kept on ice until usage.

2.2.4.2 Counting cells by FACS

For flow cytometric cell count, the cell suspension was diluted 1:6 in FACS buffer and acquired on a FACS Canto II device for 30 s at medium acquisition speed (1 µl/s). Viable cells were gated by forward/sideward scatter characteristics. Viable cell numbers were determined as follows: FACS count x 200 = cell number per ml cell suspension.

2.2.4.3 Purification of $CD4^+$ T cells

$CD4^+$ T cells were purified from lymphocyte preparations by depletion of other cells using the $CD4^+$ T Cell isolation kit according to manufacturer's protocol. Briefly, cells were spun down and resuspended in MACS running buffer (40 µl per 10^7 total cells). 10 µl of Biotin-Antibody Cocktail was added per 10^7 cells, mixed well and incubated for 5 minutes at 4°C. Immediately after incubation 30 µl of MACS running buffer and 20 µl of Anti-Biotin MicroBeads were added per 10^7 cells, mixed well and incubated for additional 10 minutes at 4°C. Labeled cells were washed with MACS buffer (centrifugation for 10 min at 300g and discarding the supernatant), the pellet was resuspended in 1 ml of MACS running buffer. Magnetic separation was performed on an AutoMACS Pro separator using the program "Depletes". $CD4^+$ T cells were collected as the unlabeled fraction. In order to check cell number and purity of $CD4^+$ T cells in parallel, cells were labelled by addition of a V450 anti-CD4 antibody (1:100 in FACS buffer) 10 minutes before acquisition for cell count. Purity was usually > 95%.
Sorted $CD4^+$ T cells were further used for FACS staining and culturing.

2.2.4.4 Culturing of activated $CD4^+$ T cells

The day before starting the T cell culture, the wells of 96-well round bottom or 24-well plates were incubated overnight at 4°C with 40 or 200 µl PBS, respectively, containing 5 µg/ml anti-CD3 (clone 2C11) and 1 µg/ml anti-CD28 (clone 37.51) antibodies. Next day the wells were washed first with PBS and then proliferation medium (Table 20) without interleukins.

Purified $CD4^+$ T cells were spun down, resuspended in proliferation medium containing cytokines (Table 20) and seeded onto precoated plates at the following density: 1 x 10^5 cells in 200 µl for 96 well plate and 6 x 10^5 cells in 600 µl for 24 well plate. Cells were kept in a humidified incubator with 5% CO_2 at 37°C and harvested on day 7 for functional or biochemical analysis. Proliferation medium was changed every 3 days by replacing half of the medium with the fresh proliferation medium. In some experiments the cells were additionally treated by adding inhibitors LIMKi3 (10 µM) or IPA3 (20 µM) 4h or 2h before harvesting cells for analysis, respectively.

Table 20. Proliferation medium

	dilution
RPMI 1640 liquid medium with stable glutamine	
Pen/Strep	1:100
Heat inactivated FCS	10%
beta-mercaptoethanol	1:500
non-essential amino acids	1:100
sodium pyruvate	1:100
IL-2*	2%
IL-7*	2%

*add interleukins fresh each time

2.2.4.5 Flow cytometry

Cell surface staining

5 x 10^5 cells freshly prepared from wt and *Arhgef6*$^{-/-}$ mice were incubated with primary antibodies in 100 µl of PBS/0.2% BSA, for 30 minutes at 4°C. In order to prevent unspecific binding of antibodies to Fc receptors, Fc blocking antibodies (anti-CD16/CD32) was added to the staining mix. Unbound antibodies were removed by washing once with PBS/0.2% BSA. In case of unlabeled primary antibodies, cells were incubated with secondary antibodies for additional 30 minutes at +4°C and washed again. For acquisition, stained cells were resuspended in cold FACSFlow™.

Intracellular staining

5 x 10^5 surface labelled (or unlabeled) cells from wt and *Arhgef6*$^{-/-}$ mice were washed and then fixed/permeabilized for 20 min using the Cytofix/Cytoperm kit according to manufacturer's directions. Thereafter cells were washed by addition of 2 ml 1x Perm/Wash solution and 10 min centrifugation at 450g and 4°C followed by a second washing in 1 ml of 1x perm wash. Cells were resuspended in 100 µl of primary antibody mix in 1x Perm/Wash, gently vortexed and incubated overnight at +4°C. After two washing steps in 1x Perm/Wash, cells were incubated 1 hour at 4°C with 200 µl of secondary antibody in 1x Perm/Wash. Cells were washed again two times in 1x Perm/Wash and resuspended in 200 µl FACSFlow™.

Data acquisition and analysis

Stained cells were acquired on a FACS Canto II flow cytometer at medium flow rate using FACSDiva software. Viable cells were gated according to forward/sideward scatter characteristics. In order to control specificity of fluorescence signals, possible spectral spill-over of fluorescence emission of one dye to the detector of another dye was digitally compensated for each experiment by the use of single colour labelled control samples. Data analysis, statistic evaluation of fluorescence intensities and generation of FACS plots and histograms was performed with FlowJo software (Tree Star).

2.2.4.6 Stimulation of thymocytes for western blot analysis

Thymocytes were prepared as described in 2.2.4.1. and incubated 15 min on ice with primary antibodies diluted in PBS: CD3 (2C11) (1:50) and biotinylated anti-CD4 antibodies in PBS (1:250). After washing with PBS, the cells were resuspended in pure RPMI 1640 medium at a density of 1 x 10^8 per ml, and starved for 1 h at 37°C. Thereafter Avidin was added (15 µg/ml) to initiate TCR stimulation by crosslinking CD3 and CD4 molecules on the cell surface. Cell aliquots were immediately incubated at 37°C in water bath for additional 1, 2 or 5 min, respectively. To stop the stimulation, 3 ml cold PBS was added. An unstimulated aliquot, as control, was taken and processed in the same way. Finally, the cells were centrifuged (300g, 5 min, 4°C), lysed (described in 2.2.7.1) and used in biochemical analysis.

2.2.5 Electroporation of mammalian cells

A day prior to electroporation, the cells were split to a density of 2.5 x 10^5 cells/ml in RPMI/glutamine/10%FCS medium without antibiotics. Before electroporation, the cells were centrifuged at 300g for 10 minutes. Supernatant was collected and additionally centrifuged at 3000g for 5 minutes to remove residual cells and mixed with equal amount of fresh pre-warmed RPMI/glutamine/10%FCS medium without antibiotics. A total of 25 ml medium was pre-filled per medium tissue culture flask. The cell pellet was washed with pre-warmed PBS with Ca^{2+} and Mg^{2+} and resuspended in 350 µl of pre-warmed PBS with Ca^{2+} and Mg^{2+}. Cells were then transferred to an electroporation cuvette and mixed with 10 µg of DNA (prepared as described in 2.2.8.5.). Electroporation was performed at 250V/950 µF using a Gene Pulser electroporator. Immediately after electroporation, 1 ml of warm RPMI/glutamine/10%FCS medium without antibiotics was added to transfected cells. The cell suspension was transferred to the tissue culture flask pre-filled with medium (described above) and the cells were let to recover at 37°C, 5% CO_2. Transfection efficiency (indicated by GFP expression) and viability of the cells was checked at 24, 48, 72, 96 hours by FACS. Analysis was performed at the peak of transfection efficiency (usually within 48-72 hours after transfection).

2.2.6 Transwell migration (HSB2 and Jurkat cells)

Table 21. Migration medium

	dilution
RPMI 1640	
HEPES	1:100
Penicillin/Streptomycin	1:100
L-Glutamine	1:100
fatty acid free BSA	0.25%

The transwell assay was performed by using Costar 5 µm pore size polycarbonate membranes, coated with 10 µg/ml human ICAM-1 and 2 µg/ml human VCAM-1, overnight at 4°. Prior to assay, the transwells were equilibrated by adding 300 µl of RPMI 1640 in both lower and upper chamber in a 24-well plate. HSB2 and Jurkat

cells were washed in pure RPMI 1640 medium, resuspended to 1 x 10^7 cells/ml in migration medium (Table 21.). The cells were left 30 min at 37°C for starvation. The lower transwell chamber was loaded with 450 µl of migration medium supplemented with 200 ng/ml chemokine CXCL12 and 1 x 10^6 cells (100 µl) were added in the upper chamber. 10% input controls (10 µl of the starting cell suspension) were kept on ice. The time for cells to migrate to the lower chamber was 4h at 37°C. After that, migrated cells and input controls were collected and centrifuged for 1 min at 400 g. The supernatant was discarded, the pellet was resuspended in 100 µl of FACS buffer and the cell suspension was transferred to FACS tubes. The cell count was determined by FACS as described above. Input control samples were used to recalculate the percentage of migrating cells. Migration rate was expressed as the % of input (100 x number of migrated cells/10x number of 10% input control).

2.2.7 Biochemistry

2.2.7.1 Sample preparation for western blot

For lysis, cells were resuspended in lysis buffer (Table 22.) and centrifuged at 14.000 g for 5 minutes. Protein concentration in the supernatant was determined by the BCA protein assay (Pierce, Thermo Scientific) according to manufacturer's protocol. Protein concentration was adjusted with additional lysis buffer to 3 mg/ml in all samples. Lysates were mixed 3:1 with 4xSDS loading buffer (Table 23.), heated at 95°C for 5 minutes and briefly spun down at maximum speed. Denatured protein samples were subjected to SDS-PAGE.

Table 22. Lysis buffer composition

Component	Final concentration
Sodium chloride	300 mM
Hepes	20 mM
sodium-fluoride	20 mM
EDTA	5 mM
sodium orthovanadate	2 mM
DTT	1 mM
PMSF	0.5 mM

Triton X-100	1%
cOmplete™*	1x
PhosSTOP*	1x

*add freshly

Table 23. 4xSDS loading buffer

Component	Final concentration
Tris pH=6.8	250 mM
SDS	4%
Glycerol	40%
ß-mercaptoethanol	20%
Bromophenol blue	0.004%
DTT*	100 mM

*add freshly

2.2.7.2 Immunoprecipitation and kinase activity assay

For immunoprecipitation (IP), the cells were lysed as described above but using IP buffer (Table 24.) and protein concentration was adjusted to 1 mg/ml. The lysate was precleared by 1 hour incubation with uncoupled GammaBind Plus Sepharose beads (GE Healthcare) on a rotation wheel at 4°C. 10% of precleared lysate was saved and used as an input control for loading. The rest of the precleared cell lysates was subjected to IP by adding GammaBind Plus Sepharose beads (GE Healthcare) previously coupled with rabbit antibody against ARHGEF6 (C23D2). After 3h incubation at 4°C on a rotation wheel, samples were centrifuged 2 minutes at 1000 g and supernatant was collected and used as the unbound fraction. Immunoprecipitates were washed 3 times with IP buffer by centrifuging 2 minutes at 1000g, resuspended in SDS loading buffer and heated at 95°C for 5 minutes. After 1 min centrifugation at 14000 g the supernatant was collected and used as IP fraction for western blot.

Table 24. Immunoprecipitation buffer

Component	Final concentration
Sodium chloride	150 mM

Tris-HCl (pH 7.4)	10 mM
EDTA	1 mM
cOmplete™*	1x
Triton X-100	1%

*add freshly

Kinase activity assay was performed by doing IP of PAK2 kinase in wild-type and *Arhgef6*$^{-/-}$ thymocytes in both basal conditions and upon TCR stimulation. PAK2 kinase activity was assessed with Omnia® Kinase Assays kit essentially according to manufacturer's instructions. This assay utilizes substrate peptide containing chelation-enhanced fluoropohore which upon phosphorylation by a kinase leads to increased fluorescence.

First PAK2 was immunoprecipitated as mentioned above. Briefly, precleared cell lysates were incubated with GammaBind Plus Sepharose beads (GE Healthcare) previously coupled with rabbit antibody against PAK2 for 3h at 4°C. Thereafter immunoprecipitates were washed 3 times with IP buffer and resuspended in 1x kinase reaction buffer which were further used for making kinase reaction master mix. As a control, a peptide control master mix was made in parallel. Master mixes were incubated for 5 minutes at 30°C. 5 µl of Omnia® Peptide Substrate, final concentration 50 µM, were added in the plate wells containing 15 µl of each master mix. The plate was incubated at 30°C and the fluorescence intensity was measured on Tecan Infinite 200 plate reader (λex 360/λem 485) every 1 minute for 60 minutes. Data for each experiment were normalized to the mean fluorescence intensity of unstimulated wild-type thymocytes and expressed as % of the mean ± SEM. The final graph is representative of 3 independent experiments.

Peptide Control Master Mix:	**Volume per reaction:**
Kinase Reaction Buffer (10X)	2 µl
ATP solution (10X)	2 µl
DTT Solution (10X)	2 µl
Ultrapure deionized H2O	9 µl

Kinase Reaction Master Mix:	
Kinase Reaction Buffer (10X)	2 µl
PAK2 kinase (obtained by IP)	2 µl
ATP Solution (10X)	2 µl
DTT Solution (10X)	2 µl
Ultrapure deionized H2O	7 µl

2.2.7.3 GST-Pulldown

Obtaining the fusion protein

For GST-pull down assay, pGEX 4T-3 containing GST fused with SH3 domain of wild-type ARHGEF6 (the GST-SH3 sequence) or control vector pGEX 5X-1 containing only the GST sequence (GST-free) were used to transform E. Coli BL21 by electroporation. Transformed Bacteria were grown in LB medium at 37ºC until OD = 0.5 was reached. Over-expression of proteins was induced by 1 mM IPTG for 4h at 37°C in LB medium. Thereafter, the cells were centrifuged 5 min 4000 rpm at room temperature (RT) and pellet was resuspended in 5 ml of cold PBS supplemented with protease inhibitors. The samples were sonicated and centrifuged at 8000g for 10 min at 4ºC. 50 µl of Glutathione Sepharose beads were added to supernatant and incubated at RT for 20 min. After 1 min centrifugation at 1000g the pellet with the beads was resuspended in 500 µl of cold PBS, incubated for 10 min at 4ºC and centrifuged again for 1 min at 1000g. This procedure (washing step) was repeated for 3 times and finally the beads were resuspended in 150 µl PBS. Obtained fusion proteins were loaded on gel and tested by Coomassie staining.

The pulldown

$5x10^7$ murine thymocytes were centrifuged for 10 min at 300g at 4°C. The pellet was resuspended in pulldown buffer (Table 25.), incubated 30 min at 4ºC and centrifuged for 1 min at 14000 rpm at 4ºC. The supernatant was incubated for 1h at 4ºC with 30 µl of beads coupled with GST-SH3 and GST-free (as described previously). After 2 min of centrifugation at 1000g at 4ºC supernatant was saved and used as unbound fraction. The beads were washed 3 times with pulldown buffer following incubation for 10 min at 4ºC between each centrifugation step. Finally the elution of bound proteins from the beads was done by adding 20 mM reduced glutathione in 50 mM Tris-Cl (pH 8.0). After centrifugation at maximum speed for 2 min both eluted proteins and the beads were analyzed by SDS-PAGE.

Table 25. Pulldown buffer

Component	Final concentration
Sodium chloride	150 mM
Tris (pH 8)	10 mM

DTT	5 mM
EDTA (pH 8)	1 mM
cOmplete™	1X
Triton X-100	1%

2.2.7.4 Western blot

SDS-PAGE

Proteins were separated using one-dimensional sodium dodecyl sulphate polyacrylamide gel electrophoresis (SDS-PAGE) under fully denaturing and reducing conditions (Laemmli, 1970). The samples were incubated with 4xSDS-loading buffer (Table 23) at 95°C for 5 minutes, centrifuged and equal amounts of proteins were loaded in wells. Gradient gels or homogels (8% or 12.5%) were prepared according to the Laemmli protocol (Tables 26a and 26b, respectively) and run at constant current of 12 mA per gel in Bio-Rad electrophoresis chamber filled with 1x electrophoresis buffer. Subsequently the gels were either stained with Coomassie blue or were subjected to immunoblotting.

Table 26a. Laemmli system: gradient gels for 10 gels (1 mm)

Buffer	**Composition**
Electrophoresis buffer	192 mM glycine; 0.1% (w/v) SDS; 25 mM Tris-base, pH 8.3
4x separating buffer	0.4% (w/v) SDS; 1.5 M Tris/HCl, pH 6.8
Separation gel (20%)	8.25 ml separation buffer; 7.5 ml Glycerol; 16.5 ml 40% Acrylamyde; 330 µl EDTA (0.2 M); 22 µl TEMED; 120 µl 0.5% Bromophenol blue and 75 µl 10% APS
Separation gel (5%)	8.25 ml separation buffer; 17.94 ml dH2O; 1.89 ml Glycerol; 4.12 ml 40% Acrylamide; 330 µl EDTA (0.2 M), 22 µl TEMED and 118 µl APS.
Stacking gel (5%)	6 ml stacking buffer; 7.95 ml dH2O; 5.52 ml Glycerol; 3.90 ml 30% Acrylamyde; 240 µl EDTA (0.2 M); 240 µl 10% SDS; 17.2 µl TEMED; 30 µl Ponceau and 137 µl 10% APS

Table 26b. Laemmli system: homogels for 8 gels (1 mm)

Resolving gel (12.5%)	9 ml separation buffer; 13.8 ml dH2O; 1.8 ml Glycerol; 11.3 ml 40% Acrylamyde; 23.8 µl TEMED and 144.2 µl 10% APS
Resolving gel (8%)	8.9 ml separation buffer; 17.64 ml dH2O; 1.78 ml Glycerol; 7.12 ml 40% Acrylamide; 71.2 µl Bromophenol blue; 23.6 µl TEMED and 142.6 µl 10% APS
Stacking gel (5%)	3.2 ml stacking buffer; 4.3 ml dH2O; 2.8 ml Glycerol; 1.6 ml 30% Acrylamyde; 8.4 µl TEMED; 60 µl Ponceau and 68.5 µl 10% APS

Coomassie staining of SDS-polyacrylamide gels

Polyacrylamide gels were stained with Coomassie solution (Table 27) for 30 minutes at RT with gentle agitation. Proteins were visualized by incubating the gel in destaining solution for several hours by shaking and visualized using Odyssey Infrared Imaging System (LI-COR Bioscience).

Table 27. Solutions for Coommassie staining

Coommassie blue staining solution	1 mg/l Coommassie brilliant blue R-250, 60% (v/v) methanol, 10% (v/v) acetic acid
Destaining solution	7% (v/v) acetic acid, 5% (v/v) methanol

Western blotting (WB)

Proteins were electrotransferred from polyacrylamide gels to Millipore Immobilon-FL or Millipore Immobilon-P transfer membranes (polyvinylidene fluoride membrane, PVDF). The transfer was performed in Bio-Rad chamber in blotting buffer (Table 28) at 4°C for 1.5h by using 200 mA.

Table 28. Blotting and washing buffers

Buffer	Composition
Blotting buffer for TrisGlycin	192 mM Glycine; 0.2% (w/v) SDS; 18% (v/v) methanol, 25 mM Tris-Base, pH 8.3

Tris-buffered saline with Tween 20 (TBS-T) buffer	20 mM Tris, pH 7.5; 150 mM NaCl; 0.1% Tween 20

Immunoblot detection

After transfer, PVDF membranes were blocked in 3% BSA in TBS-T (Table 28) for 30 min at RT with constant agitation. Blots were incubated at 4°C overnight with primary antibody diluted in TBS-T containing 5% of BSA and 0.05% of sodium azide. After three washing steps with TBS-T for 10 minutes each time, peroxidise-coupled secondary antibodies (diluted in 1% of BSA) were applied for 1 hour at RT. Membranes were rinsed again three times with TBS-T and chemo-luminescence signal was revealed by commercial ECL reagent kit (Amersham). Films were developed on Agfa Curix 60 developing machine. Alternatively, membranes were incubated for 1 hour at RT with fluorescently-labelled secondary antibodies diluted in 5% of BSA and 0.01% of SDS in TBS-T. After four washing steps in TBS-T and two in TBS, membranes were scanned by using Odyssey Infrared Imagine System (LI-COR). Quantifications of band intensities were performed either by using ImageJ (for ECL films) or Odyssey software v2.1 (for LI-COR scans). After background subtraction all OD values were normalized to β-actin or GAPDH as a loading control. When using phosho-specific antibodies, antibody recognizing total protein was used as internal loading control. Normalization was done as following: first, it was determined which sample has the highest OD for the loading control and then all the values of the loading control were divided by the highest OD value. In that case all the values were between 0 and 1.00. Thereafter, all the values of the target proteins were divided by the corresponding relative OD value of the loading control. These adjusted values were then used in the calculation of the average. Average OD of the signal obtained from wt cells was taken as 100% and the signal of *Arhgef6*$^{-/-}$ cells (obtained after normalization to corresponding loading control) was expressed as % of wt.

2.2.7.5 2D Blue Native PAGE (BN PAGE)

2D blue native polyacrylamide gel electrophoresis (BN PAGE) was essentially performed under previously published conditions (Swamy and Schamel, 2009; Swamy et al., 2006) using materials and buffers listed in Table 29. Cell lysates were

prepared as described above (2.2.7.1), mixed with 4xBN-PAGE Sample Buffer and 5% G-250 sample additive was added immediately prior to electrophoresis. The samples were centrifuged at 20.000 g at 4°C for 20 min and supernatant was used for loading. Loading volume per well (in 1st dimension) was 30 µl containing maximum 90 µg of proteins in total.

Dark Blue Cathode Buffer was added to the wells and to the middle buffer chamber up to 70% of its total volume. Outer buffer chamber was filled with Anode Running Buffer up to 30% of its volume. Samples and marker were loaded, middle buffer chamber was filled up with Dark Blue Cathode Buffer and the remaining Anode Running Buffer was poured in outer buffer chamber. Electrophoresis was performed on ice, at constant 150 V for 60 minutes and afterwards at constant 250 V for 45 minutes. Thereafter, the gel was incubated in fixation solution at RT for 30 minutes. Fixation solution was changed to water and the marker lane was cut out and scanned. BN PAGE gel was stored at 4°C in water until used for second dimension.

The gel cuts were resolved by SDS-PAGE using either 8% or 12.5% homogels, which were prepared basically as described in 2.2.7.4 using a 1.5 mm spacer plate. The gel cuts were placed in 15 ml falcon tube and incubated in 5 ml SDS/DTT-Buffer at RT for 1 hour with moderate agitation. Comb was removed from SDS-PAGE gel and the space was filled with electrophoresis buffer. 7 µl of protein marker was loaded in the designed well. BN PAGE gel cut was placed on the top of SDS-PAGE gel until it slides in and the remaining space was filled with 0.5% agarose in electrophoresis buffer. Electrophoresis was performed in Bio-Rad system at constant 30 V for 30 minutes until running front runs out of BN PAGE gel layer, then increased to constant 80 V for 30 minutes until running front runs out of stacking gel layer and finally increased to constant 150 V for 45 minutes until running front runs out of resolving gel layer. Afterwards it was proceeded with immunoblotting, which is described in 2.2.7.4.

Table 29. Materials and solutions for BN PAGE

	Company/composition
Blue Native Page running system	Invitrogen
NativePAGE™ Novex® 3-12% Bis-Tris	Invitrogen

Gels 1.0 mm, 10 Well	
NativePAGE™ Sample Buffer (4X)	Invitrogen
Running Buffer Kit: 20×Running Buffer and 20×Cathode additive	Invitrogen
The NativeMark™ Unstained Protein	Invitrogen
G-250 sample additive	5%
Anode Buffer	30 ml 20×Running Buffer and 570 ml MilliQ water
Dark Blue Cathode Buffer	10 ml 20×Running Buffer, 10 ml 20× Cathode additive, 180 ml MilliQ water
Light Blue Cathode Buffer	10 ml 20×Running Buffer, 1 ml 20× Cathode additive, 189 ml MilliQ water
fixation solution	40% Methanol, 10% Acetic Acid
SDS/DTT-Buffer	2% SDS; 0.1M DTT; 50 mM Tris/HCl, pH 6.8

2.2.7.6 Gel filtration (size-exclusion chromatography)

Cell lysates (5 mg of protein in 1 ml) were run on a 120 ml HiPrep 16/60 column (Amersham, GE Healthcare) equilibrated with lysis buffer (Table 30). The column was calibrated by using molecular-mass markers diluted in lysis buffer: Blue dextran 2000, 2,000 kDa; Thyroglobulin 669 kDa; ferritin, 440 kDa; catalase, 232 kDa; aldolase, 158 kDa; ovalbumin, 45 kDa. Flow rate at the FPLC system was 0.2 ml/min. Fractions containing protein complexes of different molecular size were collected in 1.5 ml of separation buffer (the same composition as lysis buffer). For each fraction acetone precipitation was performed by adding 6 ml of -20°C pre-cooled acetone. The tubes were covered with parafilm and left overnight at -20°C. The fractions were centrifuged at 3500 rpm for 30 minutes at 4°C and supernatant was removed. The remaining pellet was resuspended in 4xSDS loading buffer and equal amounts of proteins for each fraction, were subjected to immunoblotting as described in 2.2.7.4. The equal loading was confirmed by Coomassie staining.

Table 30. Buffers used for size-exclusion chromatography

	Company/composition
Lysis buffer	1% TritonX-100, 300 mM NaCl, 20 mM Hepes, 20 mM sodium-fluoride, 5 mM EDTA

2.2.8 Molecular Biology

2.2.8.1 Directional cloning into plasmid vectors

The shRNA cloning procedure was done according to pSUPER protocol (Oligoengine™). Oligonucleotides used in this study were synthesized by Biomers.net and resuspended in nuclease-free H_2O to a concentration of 3 mg/ml. These oligos were synthesized with BamHI and HindIII sticky ends, so no digestion was required prior to cloning. Vector pCMS4-H1p-EGFP (pSUPER) was digested with restriction enzymes HindIII and BglII and gelpurified with the QIAquick Gel Extraction Kit (Qiagen) as described by the manufacturer. Oligos were cloned in the vector whereas BglII and BamHI sites were destroyed. This vector was used for bacteria transformation and amplification by midiprep as described in the following chapter. Finally mammalian cells were transfected with pSUPER vector and EGFP fluorescence was monitored to visualize transfection efficiency as described in chapter 2.2.5.

Anneal Oligos

The annealing reaction was assembled by mixing 1 µl of both forward and reverse oligos with 48 µl annealing buffer (Table 31.). The mixture was incubated at 90°C for 4 min and then 10 minutes at 70°C. The annealed oligos were slowly cooled to 37°C and used immediately in a ligation reaction (see later).

Table 31. Annealing buffer

Sodium chloride	100 mM
HEPES	50 mM, pH 7.4

Linearization of the pSUPER vector with BglII and HindIII

In order to linearize 1 µl of the pSUPER vector, BglII and HindIII restriction enzymes were used in sequential digestion. The vector was digested with HindIII for 60 minutes followed by 2 hours digestion with BglII. The reaction was heat inactivated by raising the temperature to 65°C for 20 minutes. Control digestion after cloning steps, was performed with restriction endonucleses HindIII and EcoRI.

Ligation of the annealed oligos into pSUPER Vector

2 µl of the annealed oligos were mixed with 1 µl of T4 DNA ligase buffer. Thereafter 1 µl pSUPER vector, 5 µl nuclease-free H_2O and 1 µl T4 DNA ligase were added to reaction mix. The ligation reaction was carried out at RT overnight. Simultaneously, a negative control cloning reaction was performed with the linearized vector alone and without insert. Sequencing of the vector containing cloned insert was done by using an appropriate primer designed for this purpose (Table 11.).

2.2.8.2 Bacterial manipulation

2.2.8.2.1 Bacterial cell culture

Liquid culture

In order to grow sufficient amounts of bacteria for subsequent plasmid isolation or protein overexpression, liquid culture was used. To select the clones containing the plasmid of interest, bacteria were cultured in autoclaved LB medium (Table 32) supplemented with antibiotics, 100 µg/ml ampicillin and 50 µg/ml kanamycin, respectively, at 37°C and shaking at 130 rpm.

LB agar plates

Single bacteria clones were separated by using plate culture. Autoclaved liquid LB Agar supplemented with antibiotics was cast into petri dishes. Inoculation of plates was done with liquid bacteria culture followed by incubation of plates at 37°C overnight. The plates were then stored at 4°C until use.

Table 32. LB medium 1 liter

Tryptone/peptone	10 g
Yeast extract	5 g
Sodium chloride	5 g
With or without Agar	15 g

2.2.8.2.2 Transformation by electroporation

50 µl electro-competent bacteria aliquot was incubated with 1 µl plasmid DNA or 5 µl ligation mixture shortly on ice in the cuvette. The bacteria transformation was done by electroporation. 1 ml of antibiotic free LB medium was added to the cells immediately after electroporation, bacteria were resuspended, transferred into 1.5 ml tube and incubated for 1h on the heater at 37°C, 750 rpm. The bacteria were centrifuged at 5000 rpm for 5 min at RT and supernatant was discarded. The pellet was resuspended in 100 µl of antibiotic free LB medium and this suspension was transferred on LB Agar plate supplemented with antibiotics and incubated overnight at 37°C. A single colony was picked and inoculated as described in 2.2.8.3.

2.2.8.3 Preparation of plasmid DNA (miniprep)

The selected colonies were inoculated in 2 ml of LB medium supplemented with 100 µg/ml Ampicillin and incubated at 37°C overnight. The overnight cultures were centrifuged for 5 minutes at 5000g and supernatant was discarded. The pellet was resuspended in 300 µl buffer P1 (Table 33) by vortexing. 300 µl of P2 was added to suspension, inverted a few times and incubated for 5 min at RT. Finally, 300 µl of neutralization buffer-P3 was added and mixture was incubated for additional 5 min on ice. After centrifugation for 10 minutes at maximum speed, 750 µl of supernatant was transferred to the new tube and 510 µl of isopropranol was added. The suspension was inverted several times, incubated for 5 minutes at RT and centrifuged again for 10 minutes at maximum speed. The residual pellet was washed with 1 ml of cold 70% ethanol and centrifuged for 10 minutes. After supernatant was discarded, the pellet was air dried and finally resuspended in 50 µl of pure H_2O. DNA concentration of the sample was measured on Nanodrop and the DNA was stored at -20°C.

Table 33. Miniprep buffers

Buffer P1 - Resuspension Buffer	50 mM Tris-Cl; pH 8.0; 10 mM EDTA; 100 ug/ml RNase A
Buffer P2 - Lysis Buffer	200 mM NaOH; 1% SDS
Buffer P3 - Neutralization Buffer	3.0 M potassium acetate, pH 5.5

2.2.8.4 Agarose gel electrophoresis

Gels containing 1% and 2% agarose in 1x TAE buffer (Table 34) were used for separation of DNA fragments. Ethidium bromide was added to the final concentration of 0.5 µg/ml to visualize DNA bands under UV light. Before the loading, DNA samples were mixed with gel loading buffer. Electrophoresis was performed in 1x TAE buffer at 120 V. Ethidium-bromide DNA complexes were visualized using UV scanner. The clones which were positive after restriction digestion screening, were sent for sequencing. Positive clones after this step were used for midiprep as described in 2.2.8.5.

Table 34. Solutions for agarose gel electrophoresis

1x Tris-Acetate-EDTA (TAE)	Tris-HCl 40 mM; Acetic acid 40 mM; EDTA (pH 8.0) 1 mM;
5 x DNA Gel Loading Buffer	Glycerol 30% (w/v); Bromphenol blue 0.25%; Xylene cyanol 0.25%; EDTA 0.1 M
DNA molecular weight markers, 5 µl per lane	GeneRuler, 1 kb DNA Ladder and Generuler 100bp DNA Ladder Plus

2.2.8.5 Preparation of plasmid DNA (NucleoBond Xtra midiprep)

Plasmid DNA was prepared using NucleoBond Xtra midiprep kit according to the manufacturer's instructions and DNA concentration and purity (the ratio between the absorption at 280 nm and 260 nm) was determined by Nanodrop.

2.2.9 Immunocytochemistry and imaging

2.2.9.1 Immunocytochemistry

Preparation of the slides

Uncoated 15-well µ-slides from Ibidi were incubated with 20 µl per well of PBS containing 10 µg/ml mouse ICAM-1 and 2 µg/ml VCAM-1 or 10 µg/ml mouse ICAM-1 alone as indicated in each experiment, overnight at 4°. After washing two times with 50 µl of washing buffer and once with blocking buffer, the wells were incubated in blocking buffer for 1 hour at RT. Again wells were washed once with washing buffer and once with migration buffer and kept in migration buffer until use (Table 35).

Table 35. Buffers for $CD4^+$ T cell imaging

washing buffer	HBSS w/o Ca^{2+}/Mg^{2+} + 0.2% BSA
blocking buffer	HBSS w/o Ca^{2+}/Mg^{2+} + 2% BSA
migration buffer	HBSS with Ca^{2+}/Mg^{2+} (1 mM each); 10 mM HEPES; 0.2% BSA

Immunostaining

Cultivated $CD4^+$ T cells were adjusted to density of 300.000 cells/ml and 60 µl/well (20.000 cells) were seeded on previously coated Ibidi slides. Cells were incubated 45 min at 37 °C in order to let them adhere and migrate. After one time washing with migration buffer the cells were fixed and permeabilized for 20 min by adding 50 µl of Cytofix/Cytoperm solution. Prior to immunostaining cells were washed 3x with Perm/ Wash. Primary antibodies were applied overnight at +4°C and after two washing steps, the cells were incubated with secondary antibodies for 1 hour at RT. Both primary and secondary antibodies were diluted in Perm/Wash. After antibody labelling the cells were washed once and DAPI staining (1:5000 in Perm/Wash) was applied for 5 min at RT. The cells were washed two times in Perm/Wash and finally kept in 0.2% BSA in PBS for imaging.

2.2.9.2 2D random migration assay for T cells

For live imaging, cultured cells (described in 2.2.4.4) from one well (96 well plate) were harvested to 1 ml of migration buffer (Table 35), centrifuged at 300g for 7 minutes and resuspended in 500 µl migration buffer. 50 µl of cells were seeded per well of coated slides prepared as described in 2.2.9.1. The slide was placed at 37°C / in 5% CO_2 atmosphere in an incubator installed on the stage of the microscope, and cells were let to settle down for 20 minutes. Prior imaging, the wells were carefully washed with pre-warmed migration buffer to remove dead cells.

2.2.9.3 Lentibrite infection protocol

Viral Infection of $CD4^+$ T cells was achieved via spinoculation. $1x10^6$ stimulated T cells (described in 2.2.4.4) were spun down by centrifuging for 4 min at 1200 rpm, resuspended in 1 ml of proliferation medium (Table 20) and mixed with Polybrene (1:1000) and Lentibrite biosensor (3.125 µl per 1 ml). Infected cells were incubated overnight at 37°C in the 24 well plate, harvested and washed with proliferation medium two times by centrifugation at 300g for 7 min. The cell pellet was resuspended in 1 ml of proliferation medium containing IL-2 and IL-7 and the cells were plated again in 96 well plate (200 µl per well) freshly coated with anti-CD3/anti-CD28 as described in 2.2.4.4. Infected cells were imaged after 48h of restimulation. Infection efficacy of ≈90% was assessed by microscopic inspection of GFP fluorescence.

* *Viral infection was performed in laboratory biosafety level S2.*

2.2.9.4 Raji-T cell conjugation

Loading of Raji B cells with superantigen

Raji cells were centrifuged for 3 min at 2000rpm and resuspended in pre-warmed RPMI supplemented with 10% FCS and 1 µg/ml staphylococcal enterotoxin E and incubated overnight at 37°C. After centrifugation cells were resuspended in conjugation medium (CM, Table 36) and let to sit at 37°C for 10 min. After a second centrifugation cells were finally resuspended in CM (0.5×10^6 cells in 200 µl used for 10 coverslips).

Conjugation

Jurkat cells were harvested, washed and resuspended in CM at the same final density as Raji cells. Both Jurkat and SEE loaded Raji cells were kept in CM for at least 1.5h before conjugation step. Both Raji and Jurkat cells were the mixed 1:1 in a tube and 40 µl of the mixture was pipetted per poly-L-lysine coated coverslip and incubated for 15 min at 37°C. After incubation time, the cells were fixed with 2% PFA for 15 min at RT and washed with 1xPBS. Thereafter the cells were permeabilized for 10 min with 0.1% Triton-X100 in PBS, washed two times for 10 min with PBS and blocked for 30 min in 2% horse serum in PBS. The same blocking buffer was used for all antibody incubation steps. Primary antibodies were applied overnight, and after three washing steps, the cells were incubated with secondary antibody for 1h at RT. Finally the cells were washed three times for 10 min with PBS and coverslips were mounted on microscopic slides using Mowiol. Slides were kept at +4°C until microscopic analysis.

Table 36. Buffers and chemicals for Raji-T cell conjugation

conjugation medium, CM	RPMI1640; 1% FCS; 1%Glu; no antibiotics
Permeabilization solution	0.1% Triton-X100 in PBS
Blocking buffer	2% horse serum in PBS

2.2.9.5 Image acquisition and analysis

Images of stainings were acquired using Leica TCS SP5 confocal microscope (LAS AF software, version 2.0.2; 1024x1024 pixel display resolution; 12 bit dynamic range; 63x objective; 4x optical zoom). Live images (brightfield and TIRF) were acquired using Leica DMI6000 microscope (LAS AF software, version 2.0.2; 10x objective for brightfield cell tracking; 100x objective for additional cell tracking, lamellipodia morphology and TIRF imaging).

For quantifications of fluorescence intensities and morphological parameters, all settings of the microscope were identical within one experiment. Per each condition ≥30 cells were acquired and further analyzed using NIH ImageJ (https://imagej.nih.gov/ij/). Brightfield images of single cells were used to identify cells and cellular lamellipodia were defined by manual free-hand bordering of thin sheet-

like processes at the leading edge in bright-field images. The outline of the cell was defined by image thresholding, which enabled measuring of the total immunofluorescence with the cell. Total immunofluorescence (IF) signal intensity of whole single cells or lamellipodia was obtained from maximum projections of Z stack images (20 steps at 500 nm each) after threshold subtraction. Fluorescence intensity at the contact region of a cell with the substrate was obtained from single TIRF images. TIRF penetration depth was 200nm.

Brightfield images were also used for lamellipodia size analysis. Each lamellipodium was characterized by area, depth (the shortest perpendicular distance between lamellipodia front and nuclear membrane), width (distance between the furthermost opposite points of lamelipodia front) and the angle, which is defined as angle between present and newly formed lamellipodia formed by the tips of consecutive dominant lamellipodial filaments at the leading edge and vertex located in the visual centre of the nucleus.

Cell tracking was done manually by using manual tracking plugin for ImageJ at 10x or 100x and at different time resolutions as indicated in the respective text and figure legends. Results were further analyzed by using Ibidi chemotaxis and migration tool version 2.0.

For the presentation, the original images were processed using ImageJ and Adobe Photoshop 7.0.

2.2.10 Statistics

Statistical analyses were performed by GraphPad Prism 6. The normal distribution of the data was assessed by using D'Agostino-Pearson test and parametric (unpaired Student's t-test) or unparametric test (Mann–Whitney test) were applied (as indicated in each experiment). For multiple comparisons when comparing 2 different genotypes under 2 different conditions two way ANOVA with Bonferroni *post hoc* test was used. Data were obtained from at least three independent experiments for each condition. Most data were normalized to the mean of the control group and expressed as the mean ± SEM. Where indicated, the median with interquartile range was shown. The level of statistical significance was set for $p<0.05$.

3. RESULTS

Previous studies of our group revealed altered migratory behavior of thymocytes and peripheral lymphocytes in *Arhgef6*$^{-/-}$ mice, leading to impaired thymocyte development. In particular, our data proved enhanced basal and chemokine-induced transwell migration of *Arhgef6*$^{-/-}$ thymocytes (Figure 11) and lymphocytes, increased velocity of *Arhgef6*$^{-/-}$ thymocytes migrating on 2D ICAM and in the thymus and reduced arrest. These migration phenotypes were associated with irregular cell shapes frequently observed in thymocytes derived from *Arhgef6*$^{-/-}$, increased ARHGEF7 expression, increased basal Rac activity and impaired PAK phosphorylation (Korthals et al., 2014; Missy et al., 2008).

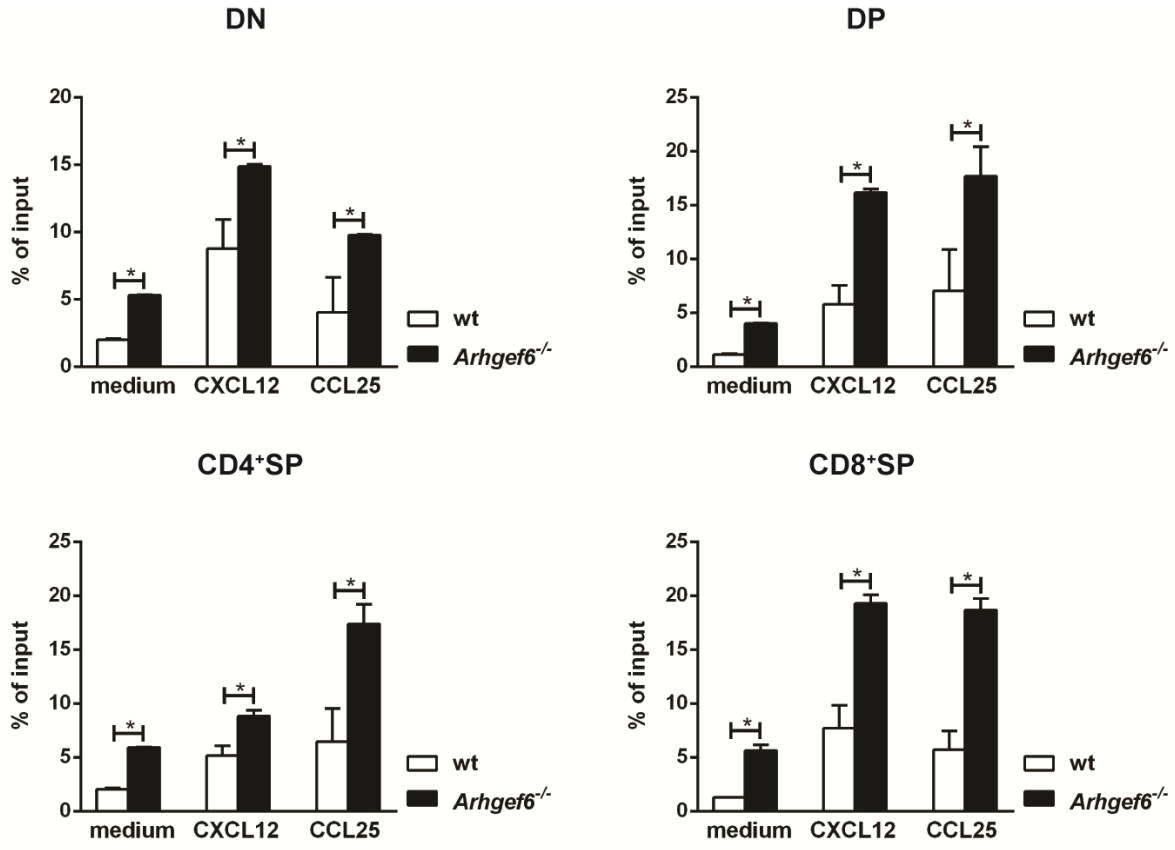

Figure 11. Increased motility of *Arhgef6*$^{-/-}$ thymocytes in vitro
Transwell migration of thymocte subsets (DN, DP, CD4$^+$SP, and CD8$^+$SP) to CXCL12 or CCL25. Results expressed as the mean percentage ± SD of migrated cells to input cells, from one representative of three experiments. Stastistical significance was assessed by using Student's t-test, * $p<0.05$; Adopted from Korthals et al. (2014)

The major goal of my study was to further reveal additional functional roles for ARHGEF6 in thymocytes and CD4$^+$ T cells.

3.1 Characterization of *Arhgef6*$^{-/-}$ T cell motility in a 2D migration model

In initial experiments, we first aimed to confirm that the observed T cell migration phenotypes were direct effects of *Arhgef6* deficiency rather than a result of cellular changes during early T cell development. For that purpose we applied a short hairpin RNA (shRNA) approach to acutely knockdown *Arhgef6* in two different human T cell lines, Jurkat and HSB2, and tested motility of transfected cells in transwell migration assays. In all experiments, data were normalized to the mean of the control group set to 100% and expressed as the mean ± SEM.

Both WB (Figure 12A) and FACS quantification confirmed reduction of ARHGEF6 in transfected cells (22.7±1.2% of control) (Figure 12B). Jurkat cells are not a good model for 2D cell migration, but these cells migrate well through transwells in response to CXCL12. Our data revealed no significant difference between Jurkat control cells and Jurkat *Arhgef6* kd cells, although there was a tendency towards increased motility of *Arhgef6* kd cells (Figure 12C). However, knockdown of *Arhgef6* in HSB2 cells, which are generally more motile than Jurkat cells, resulted in strongly increased basal as well as chemokine induced transwell migration (*Arhgef6* kd without CXCL12 265.5±30.4% of control; *Arhgef6* kd with CXCL12 286.4±24.5% of control) (Figure 12D). Therefore, *Arhgef6* deficiency plays a direct role in the control of T cell migration, leading us to conduct the study using primary murine T cells derived from wild-type and *Arhgef6*$^{-/-}$ mice.

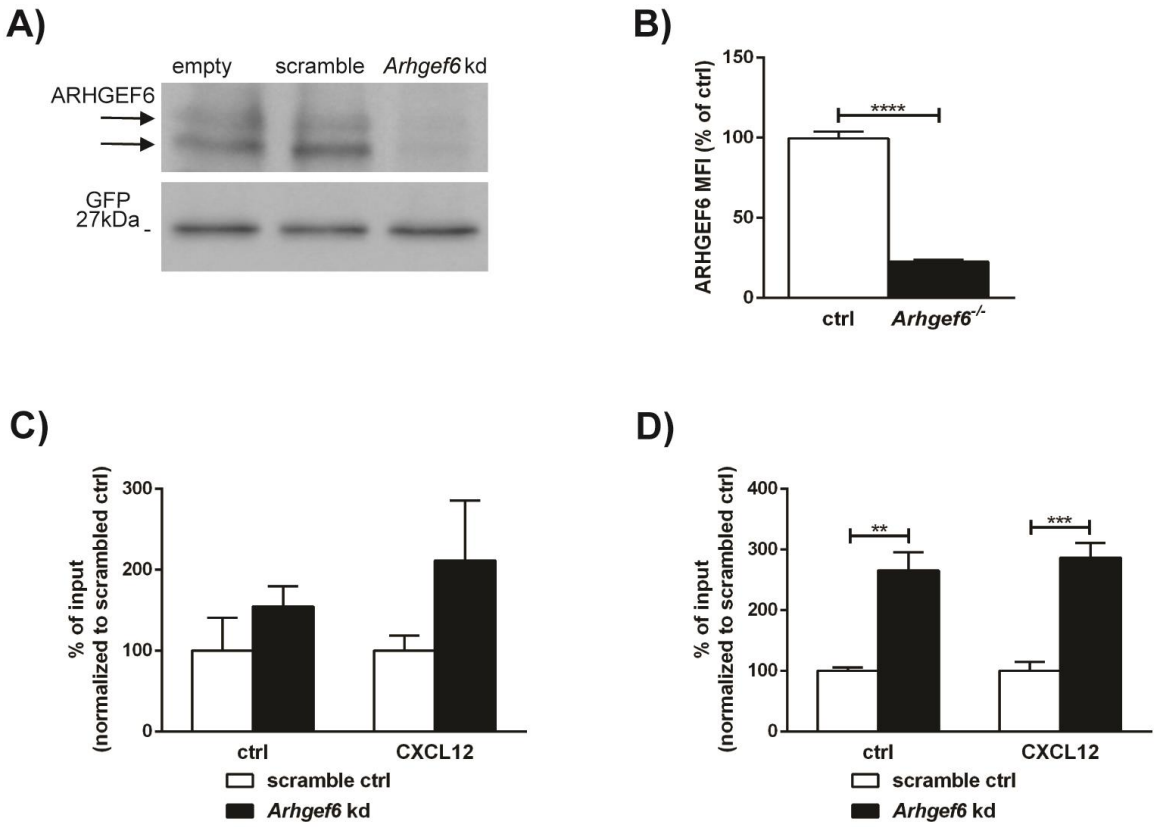

Figure 12. Increased motility of T cell lines upon *Arhgef6* knockdown
A) Expression level of ARHGEF6 obtained by SDS-PAGE/western blotting of cell lysates of Jurkat cells transefected with empty pCMS4 vector, pCMS4 vector harboring scramble sequence and pCMS4 vector harboring *Arhgef6* shRNA sequence. GFP expression level was used as loading control. B) Representative FACS quantification of the expression level of ARHGEF6 in Jurkat cells transefected with pCMS4 vector harboring scramble sequence and pCMS4 vector harboring *Arhgef6* shRNA sequence. Data on the graph represent mean MFI ± SEM obtained from 3 independent cell preparations. Statistics was done by using Student's t-test, **** $p<0.0001$. C)-D) Transwell assay of Jurkat (C) or HSB2 (D) cells transefected with pCMS4 vector harboring scramble sequence and pCMS4 vector harboring *Arhgef6* shRNA sequence, in the presence or absence of CXCL12. Data on both graphs represent mean ± SEM percentage of migrated cells obtained from 3 independent cell preparations. Statistical significance was assessed by using Student's t-test. ** $p<0.01$, *** $p<0.001$.

In search for a simple in vitro model to study the migratory behaviour of primary T cells, we decided to use wt and *Arhgef6*$^{-/-}$ activated CD4^{+} T cell blasts, which after 7 days of cultivation display pronounced morphological polarization and readily migrate on ICAM-1 coated 2D surfaces (Figure 13A; Supplemental movies 1 and 2). This model may represent the in vivo situation of activated T cells exploring the surrounding for antigen or guidance cues along ICAM-1 expressing APC, reticular cells or vessel walls in inflamed tissues. All experiments were performed using cultured peripheral T cells, unless the need for high cell numbers favoured the use of thymocytes, e.g. for biochemical assays, which required large amounts of protein material.

To characterize the migratory phenotype of *Arhgef6* deficient T cells in greater detail,

we performed in vitro live-cell imaging of wt and *Arhgef6*$^{-/-}$ T cells randomly migrating on ICAM-1 or ICAM-1+VCAM-1 substrates in the absence of other chemical or mechanical cues. The combination of VCAM-1 and ICAM-1 was used because it was previously shown that VLA-4/VCAM-1 interaction may promote ICAM-1 mediated migration (Romanova and Mushinski, 2011; Rose et al., 2003).

Time-lapse recordings were done at 10x magnifaction in order to specifically address the speed (velocity), the directional persistance (directionality, or sometimes referred to as straightness or meandering index), and the final distance reached from the starting point (displacement) within a defined time interval of 20 minutes. The representative movies and track plots of single cells (Supplemental movies 1 and 2; Figure 13A) demonstrate strong motility of both wt and *Arhgef6*$^{-/-}$ T cells in this experimental setup. Although analysis of the tracks revealed quite variable single cell behaviour, the median velocity of *Arhgef6*$^{-/-}$ T cells was clearly increased compared to that of wt cells on both substrates (on ICAM-1: wt 9.9 µm/min; *Arhgef6*$^{-/-}$ 12.7 µm/min; on ICAM-1+VCAM-1: wt 10.9 µm/min; *Arhgef6*$^{-/-}$ 13.2 µm/min) (Figure 13B). At the same time, median directionality of *Arhgef6*$^{-/-}$ T cells was significantly reduced as compared to wt (on ICAM-1: wt 0.68; *Arhgef6*$^{-/-}$ 0.62; on ICAM-1+VCAM-1: wt 0.69; *Arhgef6*$^{-/-}$ 0.60) (Figure 13C). The combination of VCAM-1 and ICAM-1 increased velocity and straightness of wt compared to ICAM-1 alone. However, these parameters did not change in *Arhgef6*$^{-/-}$ cells when combination of VCAM-1 and ICAM-1 was used compared to ICAM-1 alone (Figure 13B and C). Since being proportional to the product of velocity and straightness, the median displacement of *Arhgef6*$^{-/-}$ T cells was also increased only on ICAM-1 but not when mix of VCAM-1 and ICAM-1 was used (Figure 13D).

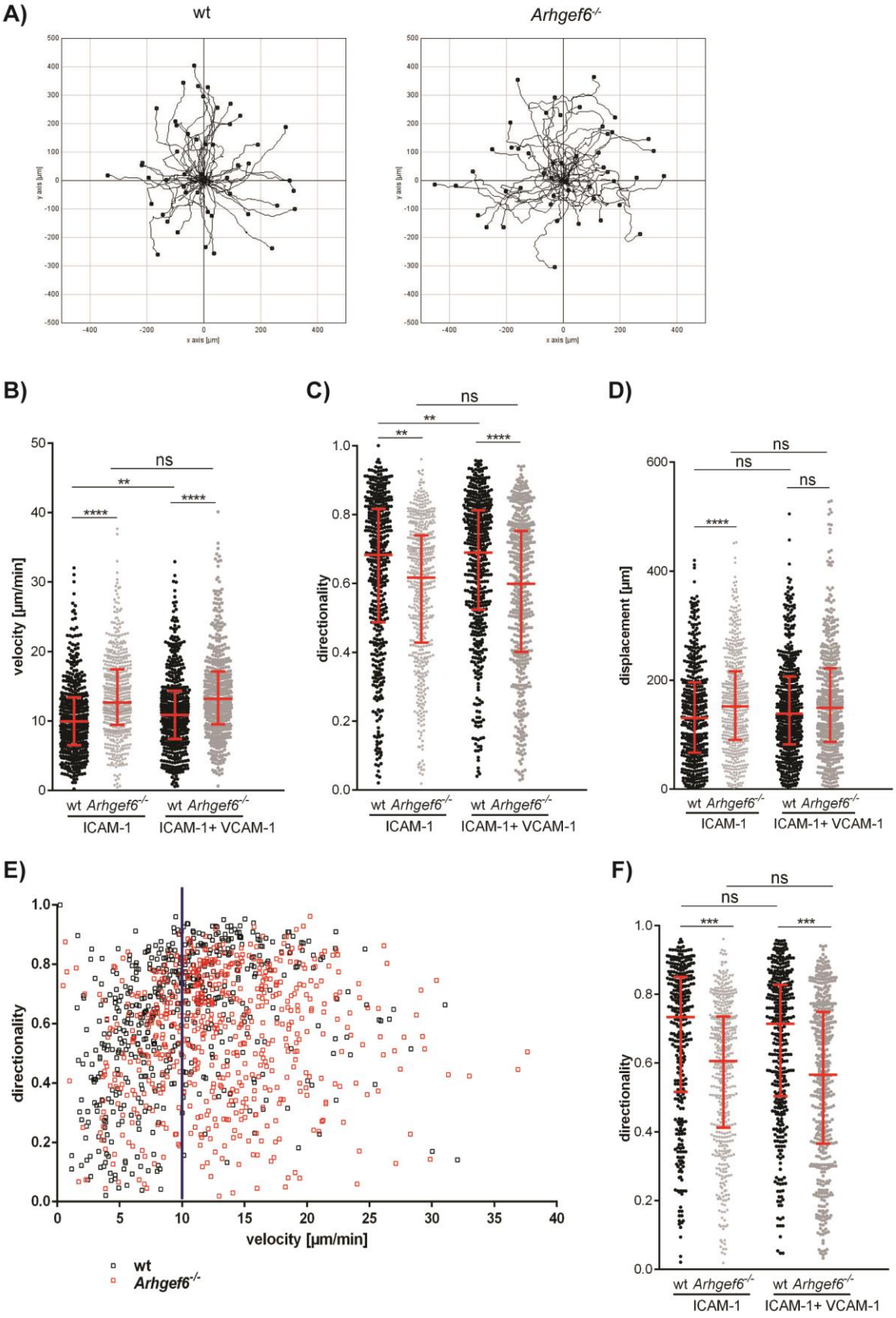

Figure 13. Velocity and directionality of wt and *Arhgef6*$^{-/-}$ CD4^{+} T cells on 2D substrates (data provided by Dr. Mark Korthals)
Wt and *Arhgef6*$^{-/-}$ CD4^{+} T cell migrating on 2D surfaces coated with ICAM-1 alone or ICAM-1+VCAM-1 were recorded at 10X magnification for 20 min and manually tracked. A) Track plots of wt and

Arhgef6$^{-/-}$ T cells on ICAM-1 from one representative experiment. B)-D) Quantification of velocity (B), directionality (C), and displacement (D) of all tracked cells from 5 independent experiments (ICAM-1: 459 wt cells, 510 *Arhgef6*$^{-/-}$ cells; ICAM-1+VCAM-1: 500 wt cells, 495 *Arhgef6*$^{-/-}$ cells. E) Relation between velocity and directionality of all cells tracked on ICAM-1. The blue line marks a velocity threshold of 10 µm/min. F) Quantification of the directionality only of cells from these 5 experiments, which were moving faster than 10 µm/min. Scatter plots show values for all single cells with red lines representing median with interquartile range. Significance was assessed by Mann–Whitney test. ** p<0.01; **** p<0.0001.

We also compared the relation between velocity and directionality of single cells and found that faster wt cells are also straighter than slower cells (Figure 13E). In contrast, *Arhgef6*$^{-/-}$ T cells lack an obvious relation between velocity and directionality. This was further confirmed analyzing cells moving faster than 10 µm/min. In these fast migrating cells, the observed reduction in median directionality of *Arhgef6*$^{-/-}$ cells compared to wt was even more pronounced (on ICAM-1: wt 0.73; *Arhgef6*$^{-/-}$ 0.61; on ICAM-1+VCAM-1: wt 0.71; *Arhgef6*$^{-/-}$ 0.57) (Figure 13F). Because the *Arhgef6*$^{-/-}$ phenotype did not differ on ICAM-1 alone compared to the combination of ICAM-1 and VCAM-1, we only used ICAM-1 coated surfaces in further experiments.

Allover, our study showed that the absence of ARHGEF6 increased the migration speed of CD4^{+} T cells and reduced their directionality, suggesting the important role of ARHGEF6 protein in regulation of migratory parameters in T cells.

3.2 Characterization of PIX/GIT complex and its constituents in *Arhgef6*$^{-/-}$ thymocytes

In order to understand how ARHGEF6 can regulate both velocity and directional persistance of fast moving cells, such as T cells, we continued our study with biochemical analyses of PIX binding proteins in the presence or absence of ARHGEF6. PIX proteins interact with a variety of signaling molecules, including GIT1 and GIT2, Rac1, Cdc42, PAK kinases, paxillin and focal adhesion kinase (FAK) (Bagrodia et al., 1998; Manser et al., 1998; Zhao et al., 2000). All these proteins are constituents of a large multiprotein complex that localize to cellular focal adhesions as shown in transfected HEK293 and COS7 cells (Premont et al., 2004).

In order to characterise proteins of PIX/GIT complex in T cells and to reveal possible alterations in the absence of ARHGEF6, we performed co-IP, Blue-Native and size exclusion chromatography.

First, we tested by co-immunoprecipitation ARHGEF6 binding to GIT1 in wt thymocytes. As shown in Figure 14A, ARHGEF6 was efficiently immunoprecipitated from the lysate of wt thymocytes. Probing the membrane with GIT1 antibody revealed

a positive band in the IP fraction demonstrating the interaction of ARHGEF6 with GIT1 and confirming the existence of the PIX/GIT complex in lymphocytes. We also tested the previously published interaction between PIX proteins and PAK (Manser et al., 1998) by a GST pull down assay using a bacterially expressed fusion protein containing GST and the SH3 domain of wt ARHGEF6 as a bait or GST-free as a control. The beads-coupled GST-SH3 fusion protein efficiently pulled down PAK2 in wt thymocytes (Figure 14B). Therefore, we confirmed that ARHGEF6 can interact with PAK2 also in thymocytes.

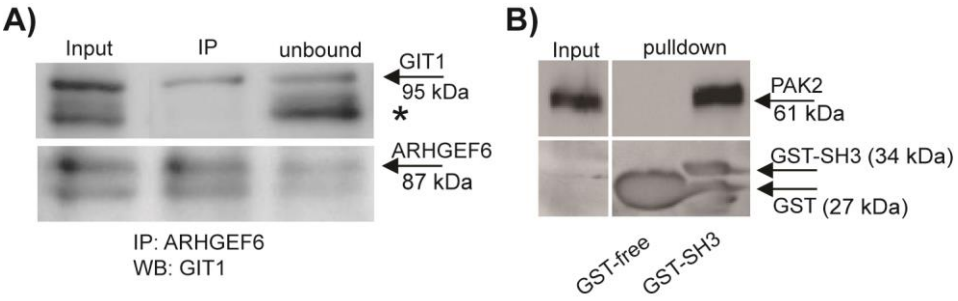

Figure 14. ARHGEF6 interacts with GIT1 and PAK2 in murine thymocytes
A) Immunoprecipitation with an ARHGEF6 antibody performed from the lysates of wt thymocytes. The western blot of the input control, the IP and unbound fractions was probed with GIT1 and ARHGEF6 antibodies. B) GST pull-down assay of PAK2 in wt thymocytes using the recombinant GST-SH3 domain of wt ARHGEF6 fusion protein or GST alone (GST-free) as a control. The Western blot of the input control, unbound and pulldown fractions derived from the beads-coupled GST-SH3 fusion protein or GST alone was probed for PAK2 and GST. * denotes unspecific band.

In order to estimate the size of the PIX/GIT complex in thymocytes we aimed to analyze cell lysates under conditions which preserve native protein-protein interactions. To this end, we performed a Blue Native-PAGE, a technique which is suitable to separate multiprotein complexes in a native conformation, thus allowing to determine complex size and composition.

BN-PAGE of protein complexes in lysates of wt and *Arhgef6*$^{-/-}$ thymocyte was followed by a subsequent second dimension separation of the complex constituents by SDS-PAGE and immunodetection by WB for ARHGEF6, ARHGEF7 and GIT proteins (GIT1/2). As shown in Figure 15, ARHGEF6 and ARHGEF7 in wt cells are mainly found in relatively large macromolecular complexes ranging between 0.4 MDa and more than 1.2 MDa, whereas GIT1/2 exist both complex bound (>0.4 MDa) and as free molecules (<0.4 MDa). The results of this experiment also implied that in the absence of ARHGEF6 the amount and distribution of other complex constituents were altered - ARHGEF7 levels appeared generally increased whereas GIT protein levels seemed to be reduced.

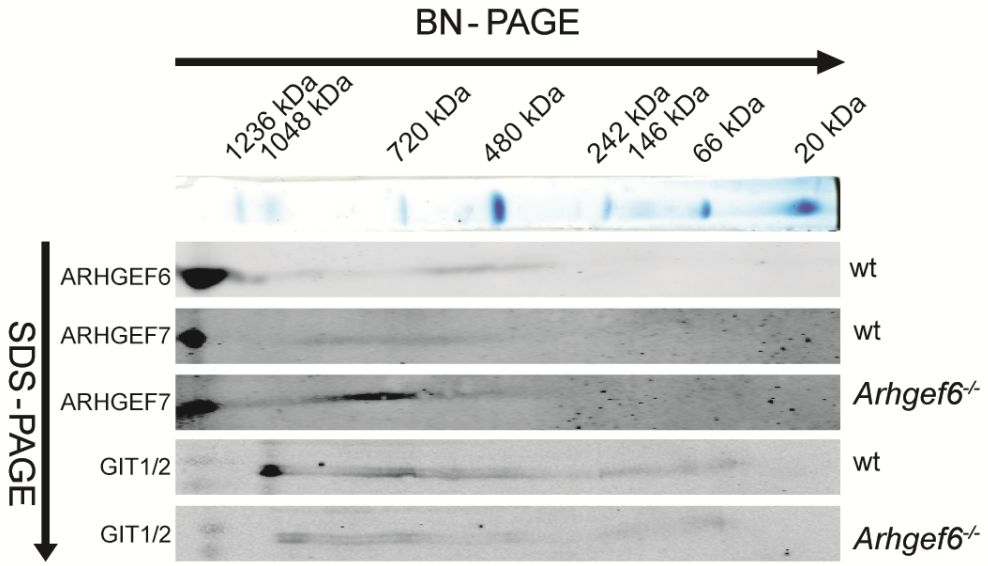

Figure 15. The PIX/GIT complex is altered in the absence of ARHGEF6
Separation of native protein complexes by 2D electrophoresis. Total cell lysates of thymocytes from wt and *Arhgef6*$^{-/-}$ mice were first separated by a complex-preserving Blue Native-PAGE followed by standard SDS-PAGE. Subsequent Western blotting was performed with antibodies indicated to the left. A BN marker lane on top indicates the position of protein complexes with indicated mass.

Because BN-PAGE is not suitable for quantitative comparisons (without modifying it or coupling it to other proteomics methods), and for a more detailed analysis of the complex components, we next performed size exclusion chromatography (FPLC) to separate the complexes by size, followed by WB analysis. With this separation technique, low fraction numbers reflecting faster elution but larger complex size, we found that in wt thymocytes ARHGEF6 was distributed in complexes ranging between 0.5 and 1.3 MDa, consistent with the results of the BN-PAGE analysis. The overlap between complexes containing both ARHGEF6 and ARHGEF7 was ~0.8-1.3 MDa (fractions #32-28) so we focused our attention on this range (Figure 16). The full range of fractions is shown in Supplementary figure 1. Quantification of the WB bands in wt thymocytes revealed peak levels of ARHGEF6 in fraction 31 corresponding to a complex size of ~0.9MDa (Figure 16B). Similarly, in wt thymocytes, peak levels of ARHGEF7, PAK1, PAK2 and GIT1 were also found in the same fraction (Figures 16C,D,F and G), whereas peak level of GIT2 was found in complexes of slightly lower mass (fraction #32, ~0.8MDa) (Figure 16E). Thus, both PIX isoforms together with all major PIX interacting proteins are mainly enriched in wt PIX/GIT complexes of approximately 0.8-0.9MDa.

However, in the absence of ARHGEF6, expression peaks of proteins were slightly shifted to fractions corresponding to larger complexes of ~1.1-1.3 MDa. Namely, expression peaks of ARHGEF7, GIT1 and PAK1 were shifted from fraction 31 in wt to

fraction 29 in *Arhgef6*$^{-/-}$, whereas the peak expression of GIT2 was shifted from fraction 32 in wt to fraction 30 in *Arhgef6*$^{-/-}$. The peak expression of PAK2 was not changed (for both wt and *Arhgef6*$^{-/-}$ in fraction 31) (Figure 16C-G). In detail, as shown in Figure 16C, ARHGEF7 protein levels, although not significantly altered in smaller complexes (fraction #32 and #31), was dramatically increased in large size complexes in the absence of ARHGEF6 (fraction #30, 39.1±2.7 a.u. in wt vs 61.5±3.4 a.u. in *Arhgef6*$^{-/-}$ fraction; fraction #29, 23.8±8.3 a.u. in wt vs 62.8±10.2 a.u. in *Arhgef6*$^{-/-}$; fraction #28, 19.3±3.1 a.u. in wt vs 45.2±8.7 a.u. in *Arhgef6*$^{-/-}$). Similar enrichment in large and very large complexes was also observed for GIT1 (fraction #29, 19.7±5.0 a.u. in wt vs 42.8±3.6 a.u. in *Arhgef6*$^{-/-}$; fraction #28, 16.8±2.8 a.u. in wt vs 37.4±4.4 a.u. in *Arhgef6*$^{-/-}$), GIT2 (fraction #28, 4.5±0.9 a.u. in wt vs 19.9±3.2 a.u. in *Arhgef6*$^{-/-}$) and PAK1 (fraction #29, 25.1±4.0 a.u. in wt vs 55.6±7.0 a.u. in *Arhgef6*$^{-/-}$; fraction #28, 26.3±4.6 a.u. in wt vs 50.9±2.9 a.u. in *Arhgef6*$^{-/-}$). In contrast to ARHGEF7 and PAK isoforms, increased GIT protein levels in large complexes, observed in *Arhgef6*$^{-/-}$ thymocytes, were paralleled by a severe reduction in small size complexes (GIT1, fraction #32, 36.7±7.0 a.u. in wt vs 18.9±1.2 a.u. in *Arhgef6*$^{-/-}$; GIT2, fraction #32, 73.1±9.9 a.u. in wt vs 21.0±4.5 a.u. in *Arhgef6*$^{-/-}$; GIT2, fraction #31, 55.9±6.9 a.u. in wt vs 27.3±4.9 a.u. in *Arhgef6*$^{-/-}$) (Figure 16D and E).

PAK kinases were not limited to protein complexes, but both were present in the non-complex fraction range. Similarly, Rac1, the main target of PIX GEF activity, was also not specifically found in the complex fractions but it was rather distributed throughout all fractions, a large proportion thus being existent as monomers or small oligomers (Supplementary figure 1).

Taken together, the FPLC results revealed that in the absence of ARHGEF6, the PIX/GIT complex is particularly enriched with ARHGEF7 and becomes larger, suggesting that ARHGEF6 is required for maintaining a stoichiometric balance in the complex.

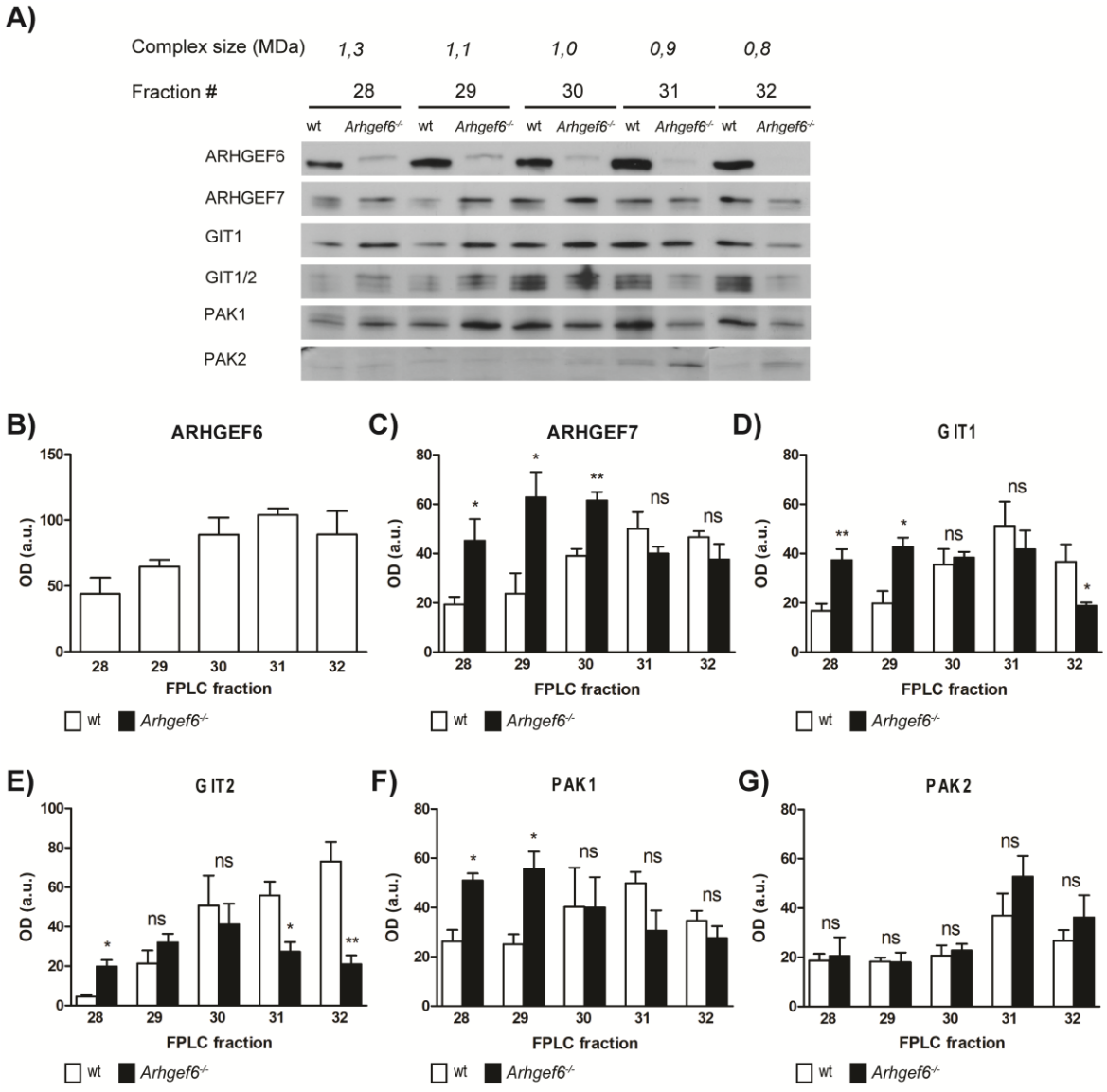

Figure 16. Without ARHGEF6 PIX/GIT complex members are enriched in larger complexes
A) Overview of protein expression levels in complexes of different sizes after separation by gel filtration FPLC with lysates of wt and *Arhgef6*$^{-/-}$ thymocytes. Eluates from FPLC fractions 28-32 were applied to Western blot detection of the indicated proteins B-G) Corresponding densitometric quantification of the expression levels of selected proteins in given fractions. Data originate from ≥3 independent preparations and represent the mean ± SEM. Statistical significance was assessed using Student's t-test, * $p<0.05$; ** $p<0.01$. a.u., arbitrary units.The full range of FPLC fractions is given in Supplementary Figure 1.

3.3 Increased ARHGEF7 levels and Rac1 activation in *Arhgef6*$^{-/-}$ CD4^{+} T cells

Our next question was whether the observed changes in the PIX/GIT complex composition translate into altered signaling downstream of the affected constituents. Most strikingly, the BN-PAGE (Figure 15) and FPLC (Figure 16) data suggest that in the absence of ARHGEF6 the total expression level of ARHGEF7 in thymocytes is increased, indicating that ARHGEF7 may compensate for the loss of ARHGEF6. In order to test if ARHGEF7 upregulation is also visible in migrating cells, we used activated wt and *Arhgef6*$^{-/-}$ CD4^{+} T blasts readily migrating on ICAM-1 coated 2D surface.

Applying quantitative WB of total cell lysates from cultured wt and *Arhgef6*$^{-/-}$ CD4^{+} T lymphocytes, we confirmed upregulation of ARHGEF7 in *Arhgef6* deficient cells (143.1±10.7% of wt) (Figure 17A and B). The same result was obtained applying immunocytochemistry where cells were fixed and stained with ARHGEF7 antibody. Confocal imaging of these cells clearly confirmed the upregulation of total ARHGEF7 in the absence of ARHGEF6 (149.8±5.8% of wt) (Figure 17C and D).

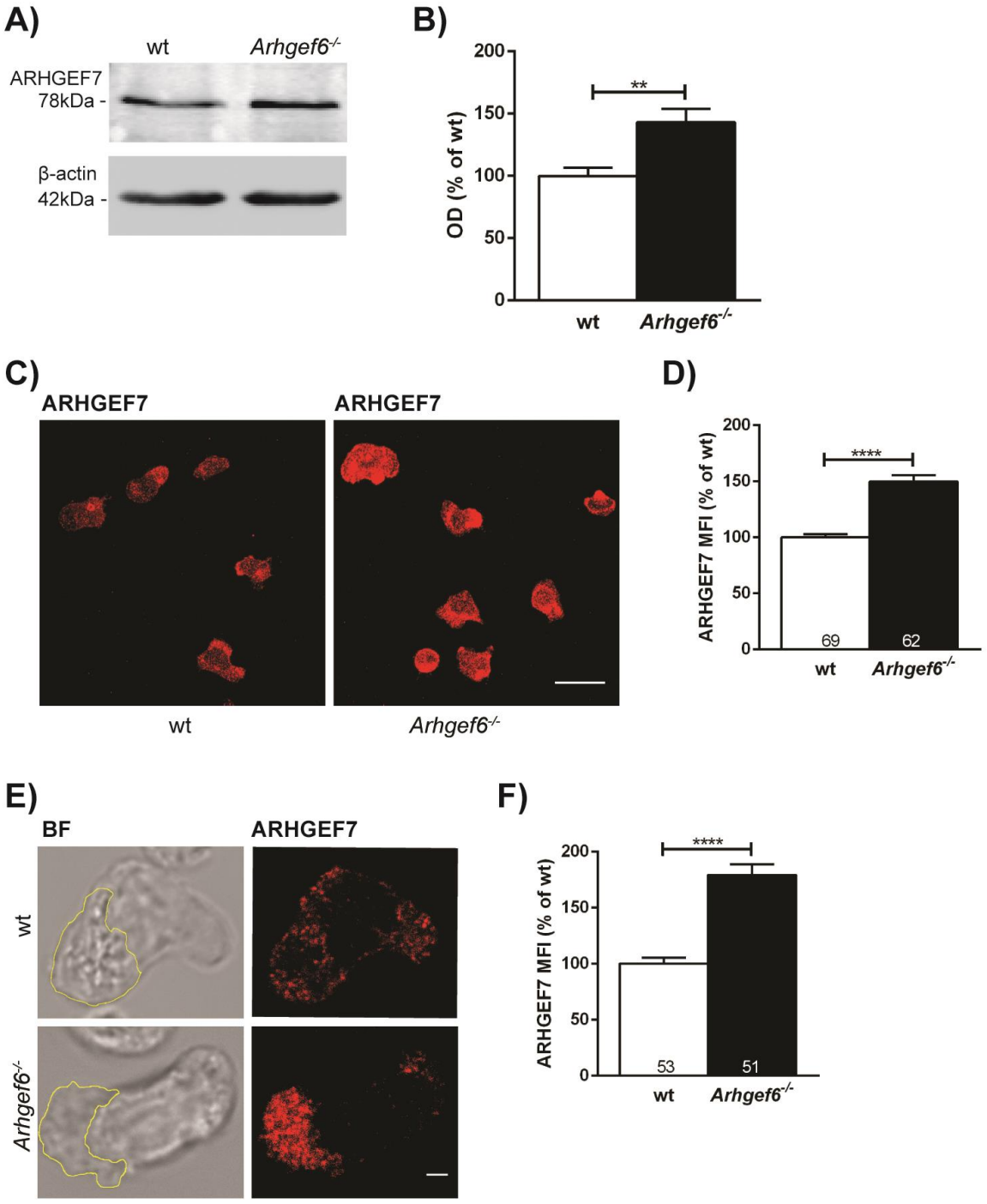

Figure 17. Increased ARHGEF7 level in *Arhgef6*$^{-/-}$ CD4^{+} T cells
A) Representative immunoblot of ARHGEF7 expression level in total cell lysates derived from wt and *Arhgef6*$^{-/-}$ CD4^{+} T cells. β-actin was used as a loading control. B) Quantification of the WB data pooled from 3 independent preparations and expressed as % of the mean ± SEM in wt cells. Within each experiment after appropriate background subtraction, the signal was normalized to β-actin and normalized to the mean of the signal in wt cells. Statistical significance was assessed using Student's t-test, ** p<0.01. C) Representative confocal images of immunofluorescent staining for ARHGEF7 in wt and *Arhgef6*$^{-/-}$ CD4^{+} T cells fixed while migrating on ICAM-1. Scale bar, 20 µm. D) Quantification of ARHGEF7 fluorescence intensity in single wt and *Arhgef6*$^{-/-}$ T cells obtained from 3 independent experiments. Within each experimental setup values were normalized to the mean of wt cells and expressed as % of the mean ± SEM. The numbers within bars represent the total number of analyzed cells. Statistical significance was assessed using Student's t-test. **** p< 0.0001. E) Confocal images showing ARHGEF7 localization in lamellipodia in a single wt or *Arhgef6*$^{-/-}$ CD4^{+} T cell, respectively. Lamellipodia are indicated by yellow overlay in bright field images. Scale bar, 1 µm. F) Quantification of ARHGEF7 fluorescence intensity in lamellipodia of single wt and *Arhgef6*$^{-/-}$ T cells obtained from 3

independent experiments. Values were normalized to the mean of wt cells and expressed as % of the mean ± SEM. The numbers within bars represent the total number of analyzed cells. Statistical significance was assessed by using Mann–Whitney test. **** p< 0.0001.

Increased level of ARHGEF7 in both *Arhgef6*$^{-/-}$ thymocytes (BN-PAGE, FPLC) and *Arhgef6*$^{-/-}$ CD4^{+} T lymphocytes (qWB, qICC), suggests that the compensatory role of PIX isoforms remains constant throughout the life span of T cell. A closer look at single cells suggest that in contrast to wt cells, ARHGEF7 is prominently concentrated in lamellipodia of *Arhgef6*$^{-/-}$ CD4^{+} T cells (Fig 17E). Therefore, in the absence of ARHGEF6, ARHGEF7 is dominating the PIX/GIT complex and its subcellular localization is directed to the lamellipodium. Of note, a similar upregulation of ARHGEF7 could be observed upon *Arhgef6* knockdown in Jurkat T cells and an enrichment of ARHGEF7 at the immune synapse formed between transfected Jurkat T cells and Raji B cells (Supplementary figure 3).

Since both ARHGEF6 and ARHGEF7 can act as GEFs for the small GTPase Rac, our next question was whether *Arhgef6* deficiency would alter Rac activity or whether ARHGEF7 upregulation could compensate for the loss of ARHGEF6. In order to check the expression and activity level of this small GTPase we performed quantitative WB and immunostaining. Our WB data revealed that the total expression level of Rac1 in wt and *Arhgef6*$^{-/-}$ CD4^{+} T cells was not changed (Figure 18A and B). Previously, we reported that the basal level of activated Rac1 (Rac1-GTP) was increased in *Arhgef6*$^{-/-}$ thymocytes (Korthals et al., 2014). Here, we confirmed these data by immunostaining of migrating wt and *Arhgef6*$^{-/-}$ CD4^{+} T cells using antibodies specific for total Rac1 and Rac1-GTP, respectively. Immunoreactivity of Rac1-GTP was significantly increased in *Arhgef6* deficient cells (188.2±13.8% of wt), while the level of total Rac1 remained the same (Figure 18C,D). Thus, ARHGEF7 upregulation was not only sufficient to sustain Rac activation but appears to make the PIX/GIT complex an even more efficient Rac activator in the absence of ARHGEF6. This suggests that ARHGEF6 function in the PIX/GIT complex is to limit Rac1 activity.
In addition to Rac1, PIX proteins may also promote nucleotide exchange for the other small GTPase Cdc42. It was previously shown that ARHGEF6 dimer functions as a specific GEF for Rac1, whereas the ARHGEF6 monomer promotes nucleotide exchange on both Cdc42 and Rac1 (Baird et al., 2005; Feng et al., 2004). Since we showed that the absence of ARHGEF6 increased Rac1 activity in CD4^{+} T cells, we expected the similar result for Cdc42.

However, our preliminary data revealed the opposite result. The data obtained from quantitative immunostaining demonstrated that total Cdc42 was not changed, but active Cdc42 (Cdc42-GTP) was reduced by ~30% in *Arhgef6*$^{-/-}$ CD4^{+} T cells (Figure 18E). It is not clear if this result is also a consequence of increased ARHGEF7 in *Arhgef6*$^{-/-}$ CD4^{+} T cells, or it is a direct consequence of diminished ARHGEF6 expression in these cells. However, we can only speculate that the stoichiometry of ARHGEF6 and ARHGEF7 may balance the activity of Rac1 vs Cdc42.

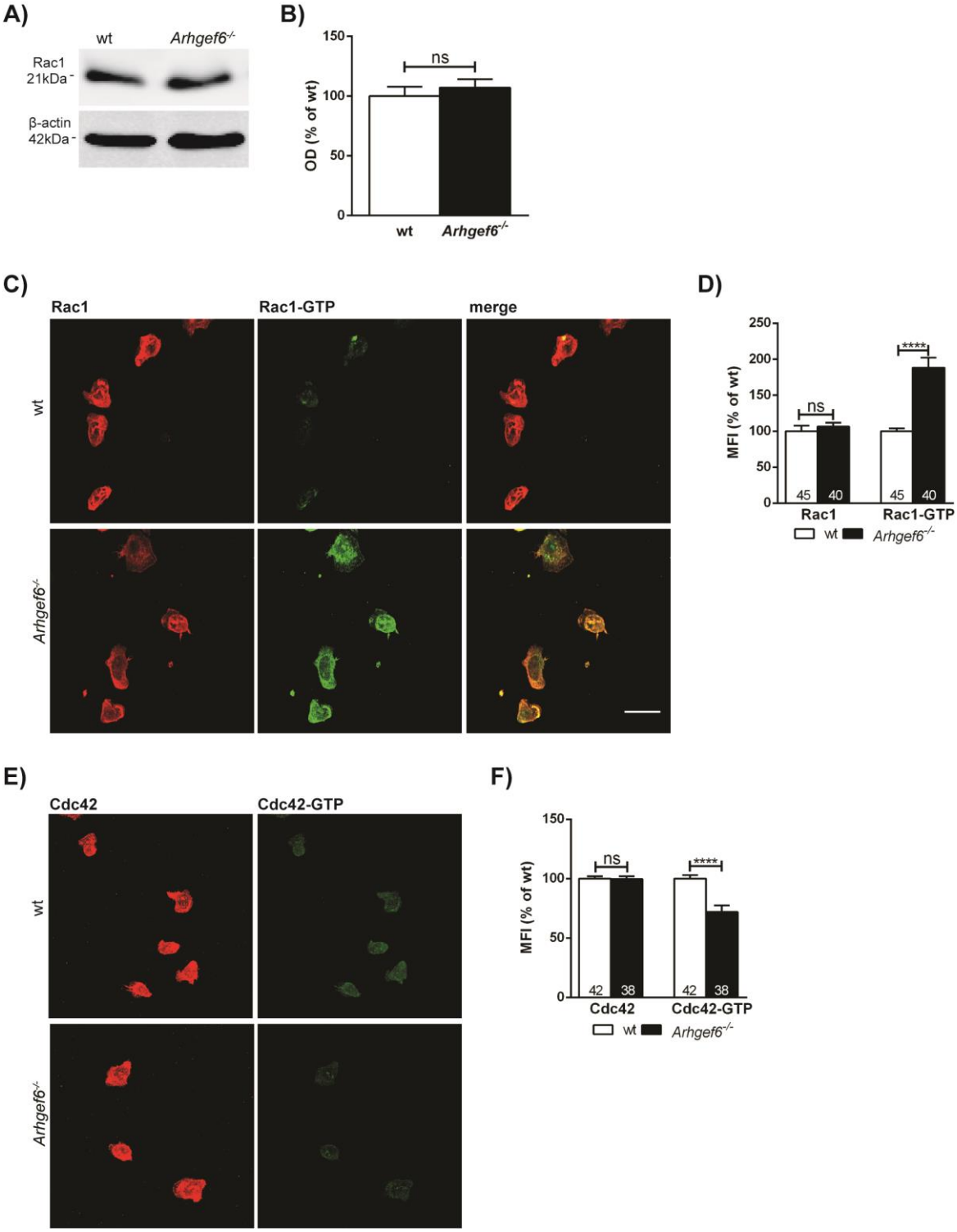

Figure 18. Increased Rac1 activity in migrating *Arhgef6*$^{-/-}$ CD4^{+} T cells
A) Immunoblot of Rac1 expression in cell lysates from wt and *Arhgef6*$^{-/-}$ CD4^{+} T cells. β-actin was used as a loading control. B) Quantification of Rac1 expression level normalized to β-actin and expressed as % of the mean ± SEM in wt cells. Data originate from 3 independent experiments. Statistics were assessed by Student's t-test. C) Representative confocal images of fixed migrating CD4^{+} T cells from wt and *Arhgef6*$^{-/-}$ mice stained with specific antibodies against Rac1 (red), Rac1-GTP (green) and corresponding overlays. Scale bar, 20 µm. D) Quantification of Rac1 and Rac1-GTP immunofluorescence signal normalized to the mean of the signal in wt cells and expressed as a % of the mean ± SEM. The numbers within bars depict the number of analyzed cells derived from 3 independent experiments. Statistic was done by Student's t-test, **** p< 0.0001. E) Representative

confocal images of fixed migrating CD4$^+$ T cells from wt and *Arhgef6*$^{-/-}$ mice stained with specific antibodies against Cdc42 (red) and Cdc42-GTP (green). F) Quantification of Cdc42 and Cdc42-GTP immunofluorescence signal in wt and *Arhgef6*$^{-/-}$ CD4$^+$ T cells. The signal is normalized to the mean of the signal in wt cells and expressed as a % of the mean ± SEM. The numbers within bars depict the number of analyzed cells derived from 2 independent experiments. Statistic was done by Student's t-test, **** p< 0.0001.

3.4 PIX effector kinases PAK1 and PAK2 in *Arhgef6* deficient cells

p21-activated kinases (PAK1 and PAK2) are interaction partners of PIX proteins and major downstream effectors of Rac. Our next question was whether the enrichment of ARHGEF7 together with an increased Rac activity in *Arhgef6*$^{-/-}$ T cells is sufficient for PAK activation or whether the presence of ARHGEF6 is required. Quantitative WB and ICC data showed no significant difference in the expression level of total PAK1 between wt and *Arhgef6*$^{-/-}$ CD4$^+$ T lymphocytes (Figures 19A-D), whereas the total PAK2, which is the major isoform in CD4$^+$ T cells, was slightly increased in *Arhgef6* deficiency (134.9±11.4% of control in WB and 116.6±4.1% of control in ICC) (Figure 19E-G and Figure 20C).

Two major events in PAK1/2 activation are autophosphorylation of Ser144/141 and Thr423/402 (Chong et al., 2001), the latter being a hallmark of a full PAK1/2 catalytic activation (Wu and Wang, 2003). Using phospho-specific antibodies, we measured PAK1/2 phosphorylation in freshly prepared thymocytes as well as upon TCR stimulation of thymocytes by WB (Figure 20A). Both wt and *Arhgef6*$^{-/-}$ thymocytes showed similar baseline levels of Ser144/141 phosphorylation and similar TCR-induced increase of PAK2 Ser141 phosphorylation at all time points measured. However, Thr423/402 phosphorylation of PAK1/2 was strongly induced by the TCR stimulus in wt thymocytes, while *Arhgef6*$^{-/-}$ thymocytes showed only faint (and delayed) Thr423/402 phosphorylation. At the same time, Erk phosphorylation, another prototypical proximal TCR signaling event, was not affected (Figure 20A).

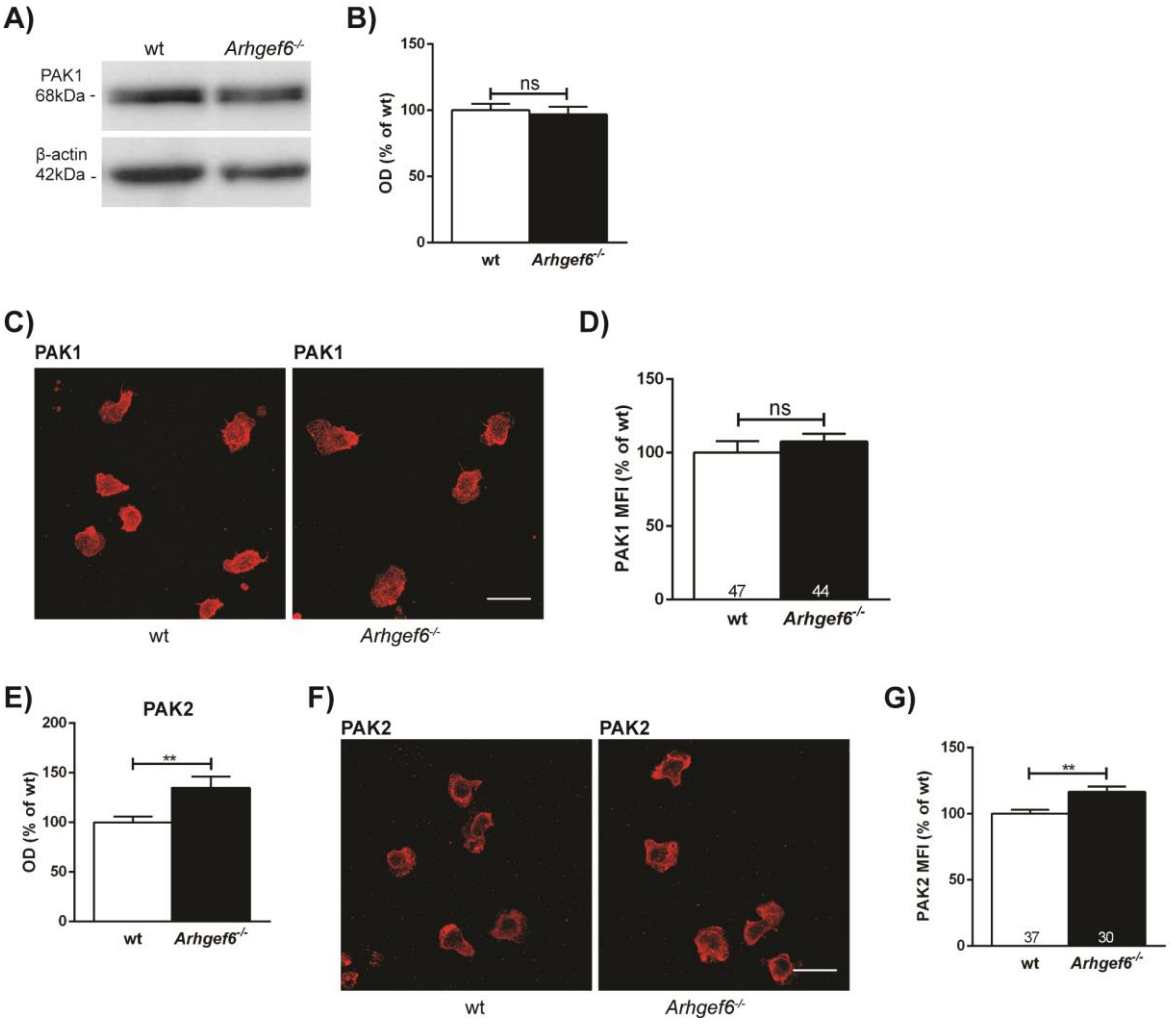

Figure 19. Increased PAK2 level in *Arhgef6*$^{-/-}$ CD4^{+} T cells
A) Immunoblot of cell lysates from wt and *Arhgef6*$^{-/-}$ CD4^{+} T cells showing the expression level of PAK1. β-actin was used as a loading control. B) Quantification of PAK1 expression level normalized to β-actin and expressed as % of the mean ± SEM in wt cells. Data originate from 3 independent experiments. Statistics was done by using Student's t-test. C) Representative confocal images of PAK1 immunofluorescence in wt and *Arhgef6*$^{-/-}$ CD4^{+} T cells and D) quantification. Data on the graph represent mean ± SEM obtained from 3 independent cell preparations. The numbers within bars show the number of cells used for analysis. Statistical significance was assessed by Mann–Whitney test. Scale bar, 20 µm. E) WB quantification of PAK2 expression level normalized to β-actin and expressed as % of the mean ± SEM in wt cells. Data originate from 4 independent experiments. A representative PAK2 WB is shown in Figure 20C. Statistics was done by using Student's t-test. F) Confocal PAK2 immunofluorescence in wt and *Arhgef6*$^{-/-}$ CD4^{+} T cells. G) Quantification of PAK2 immunofluorescence. Graph represents mean ± SEM of relative MFI obtained from 3 independent cell preparations. The numbers within bars denote the number of cells used for statistics. ** p<0.01 using Student's t-test. Scale bar, 20 µm.

This indicates that the catalytic activity of PAK toward the substrate may be specifically reduced in *Arhgef6*$^{-/-}$. Performing PAK kinase activity assay, we showed that PAK2 is indeed less catalytically active in *Arhgef6*$^{-/-}$ thymocytes in both basal conditions and upon TCR stimulation (*Arhgef6*$^{-/-}$ unstimulated 72.5±2.8%; wt stimulated 325.0±7.7%; *Arhgef6*$^{-/-}$ stimulated 240.0±3.9% of unstimulated wt control)

(Figure 20B). We also analyzed PAK phosphorylation in cultured CD4$^+$ blasts by WB using an antibody specifically recognizing PAK2 phosphorylation at Thr402. Quantification revealed an almost 80% reduction of Thr402 phosphorylation in *Arhgef6*$^{-/-}$ CD4$^+$ T cells compared to wt CD4$^+$ T cells (22.5±5.6% of wt) (Fig 20C,D). Furthermore, we analyzed the localization of PAK2 in wt and *Arhgef6*$^{-/-}$ CD4$^+$ T cells. Although PAK2 was much less phosphorylated, our confocal data indicated that in contrast to wt cells, the absence of ARHGEF6 leads to PAK2 accumulation in lamellipodia (Figure 20E), similarly as shown for ARHGEF7 (Fig 17E). This is in line with increased total PAK2 levels observed in WB (Figure 19E) and also implied by results from FPLC fractions (Figure 16A and Supplementary Figure 1).

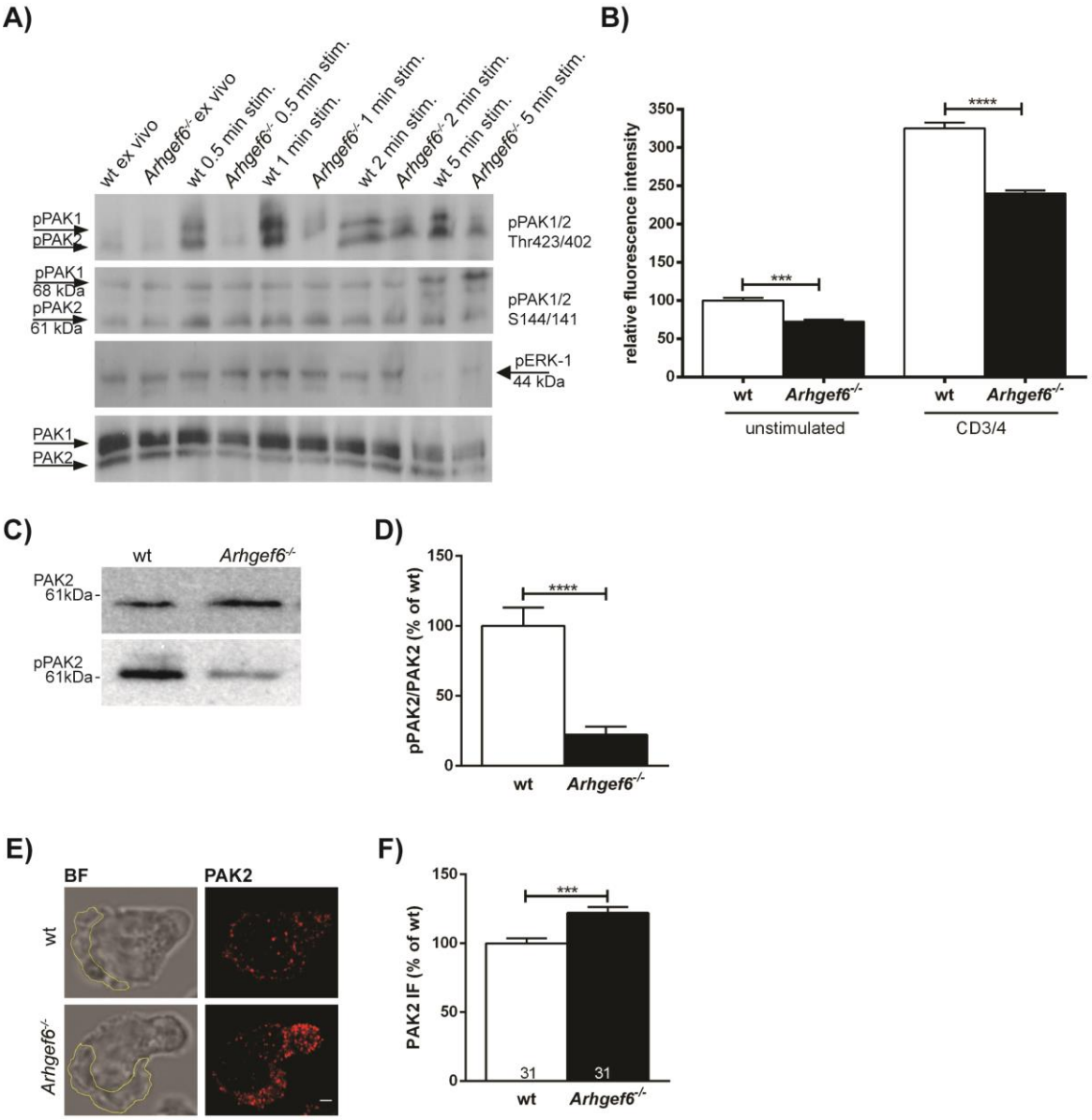

Figure 20. Reduced PAK catalytic activity in *Arhgef6*$^{-/-}$ thymocytes
A) Representative western blot of unstimulated and αCD3/CD4 stimulated wt and *Arhgef6*$^{-/-}$ thymocytes. *Arhgef6*$^{-/-}$ thymocytes demonstrated less PAK1/2 phosphorylation at Thr423/402, while there was no difference in phosphorylation in pPAK1/2 at Ser144/141 upon αCD3/CD4 stimulation. pERK-1 was used as internal stimulation control. Total PAK1 and PAK2 were used as a loading control. Data are representative of 3 independent experiments. B) Quantification of results from PAK2 kinase activity assays. The activity of endogenous PAK2 kinase was reduced in both unstimulated and αCD3/CD4 stimulated *Arhgef6*$^{-/-}$ thymocytes. C) Representative western blot of cell extracts from wt and *Arhgef6*$^{-/-}$ CD4^{+} T cells tested with specific antibodies for PAK2 and pPAK2 Thr402. D) Quantification of (C) showed significant downregulation of pPAK2 Thr402 in *Arhgef6*$^{-/-}$ cells. Data are obtained from 4 independent experiments. The signal of phosphorylated protein was normalized to the level of the total PAK2 in each genotype and expressed as % of the signal in wt cells. Statistical significance was assessed using Mann–Whitney test, **** $p<0.0001$. E) Confocal images of PAK2 localization in lamellipodia (marked in yellow) of wt and *Arhgef6*$^{-/-}$ CD4^{+} T cells. Scale bar, 1 µm. F) Quantification of PAK2 fluorescence intensity in lamellipodia of single wt and *Arhgef6*$^{-/-}$ T cells obtained from 3 independent experiments. Values were normalized to the mean of wt cells and expressed as % of the mean ± SEM. The numbers within bars represent the total number of analyzed cells. Statistical significance was assessed by using Student's t-test. *** $p<0.001$.

3.5 The role of ARHGEF6 in LIMK activation

To further investigate PIX/PAK2 signaling pathway, we resumed with LIM kinases (LIMK) as well characterized substrates of PAK kinase activity. It was shown that LIMK1 is phosphorylated at Thr508 by PAK and ROCK (Ohashi et al., 2000), a molecular event which partially correlates with LIMK activity (Edwards et al., 1999) and downstream signal propagation. The reduced PAK catalytic activity in *Arhgef6*$^{-/-}$ cells (Figure 20), therefore led us to check the phosphorylation status of LIMK1. Unfortunately, due to the lack of specific pLIMK2 antibodies, we were unable to perform the same study on LIMK2.

Using an antibody specifically recognizing LIMK1 phosphorylated at Thr508, we found that the level of pLIMK1 was reduced by almost 50% in *Arhgef6*$^{-/-}$ CD4^{+} T cells as compared to control cells (52.9±9.7% of control) (Figure 21A,B). Due to the lack of an antibody suitable for western blot detection of total LIMK1, the signal for pLIMK1 was normalized to GAPDH, which was used as a loading control. In addition, we estimated the level of total LIMK and pLIMK in T cells by ICC. Quantification of the immunofluorescence intensities confirmed the global reduction of phosphorylated LIMK1 in *Arhgef6*$^{-/-}$ cells (78.6±1.8% of untreated wt control) (Figure 21C,F). Furthermore, using LIMKi3, a specific inhibitor of LIMK kinase activity, we wanted to test if the level of LIMK phosphorylation also depends on its own kinase activity as suggested by Mardilovich et al. (2015). After treatment of cells with LIMKi3, the pLIMK1 level in wt cells was significantly reduced and dropped to the level of that observed in untreated *Arhgef6*$^{-/-}$ cells. At the same time pLIMK1 level in *Arhgef6*$^{-/-}$ cells was not significantly changed upon LIMKi3 treatment in comparison to untreated

Arhgef6 deficient CD4⁺ T cells (treated wt 77.5±5.0%; treated *Arhgef6*$^{-/-}$ 77.8±4.0% of untreated wt control) (Figure 21F).

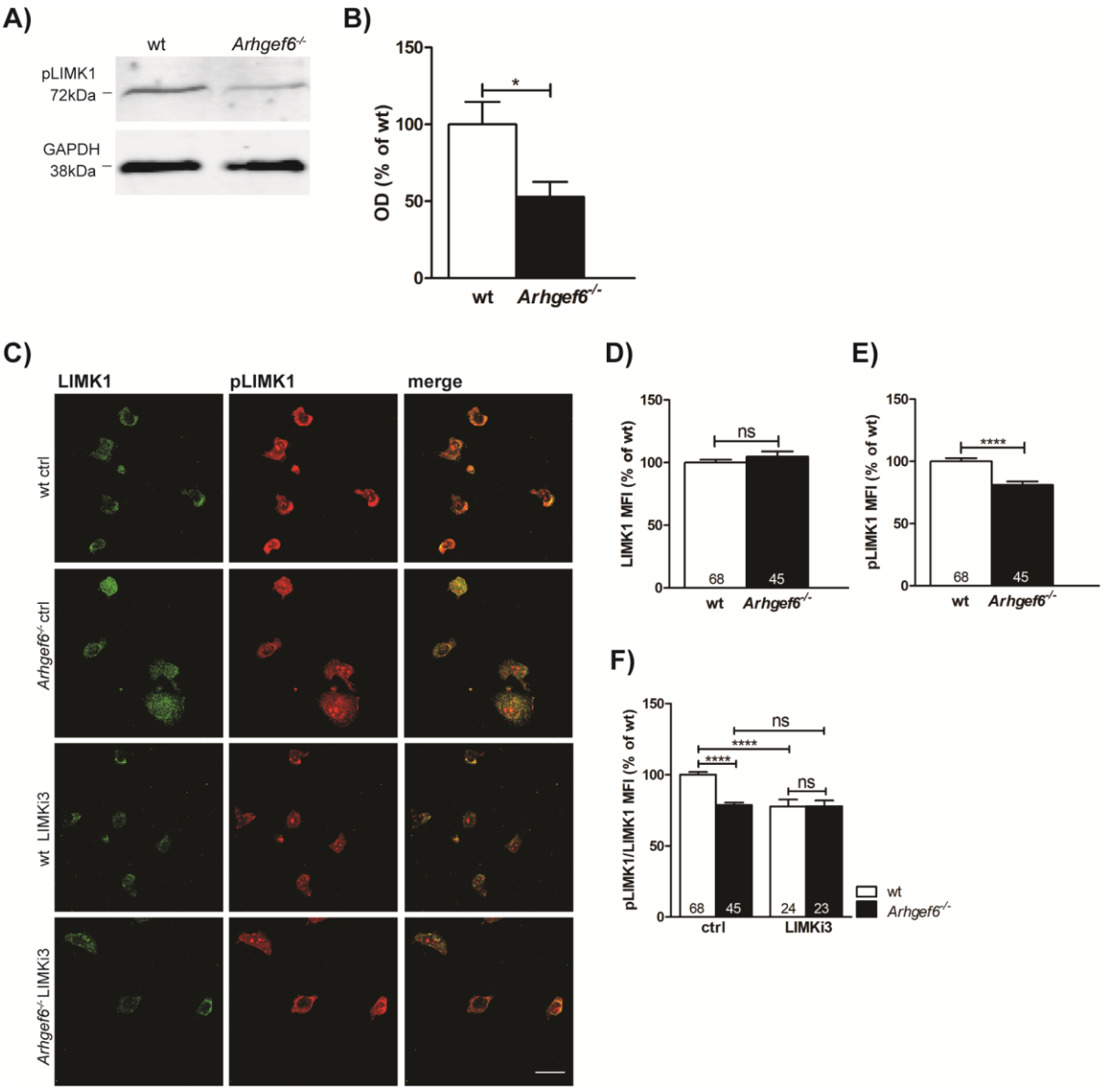

Figure 21. Reduced LIMK1 phosphorylation in *Arhgef6*$^{-/-}$ CD4⁺ T cells
A) Representative western blot and B) quantification of the signal for pLIMK1 in wt and *Arhgef6*$^{-/-}$ CD4⁺ T cells lysates. GAPDH was used as a loading control. The bar graph displays pooled data from 3 independent experiments. Within each experiment data were normalized to the mean of wt cells and expressed as % of the mean ± SEM. Statistics was done by using Student's t-test, * $p<0.05$. C) Representative confocal images of wt and *Arhgef6*$^{-/-}$ CD4⁺ T cells stained for LIMK1 (green), pLIMK1 (red) and overlay in the presence and absence of LIMKi3 (10 µM, 4h). Scale bar, 20 µm. D) Quantification of normalized LIMK1 MFI. E) Quantification of normalized pLIMK1 MFI. F) Quantification of normalized pLIMK1/LIMK1 MFI. Graphs represent the mean ± SEM obtained from 3 independent experiments, normalized and expressed as % of the mean of wt per each experiment. The numbers within bars denote the number of cells used for statistics. **** $p<0.0001$ using Mann–Whitney test (D), Student's t-test (E) and two-way ANOVA followed by Bonferroni's post hoc test (F).

Quantitative ICC of the subcellular distribution of pLIMK1 also revealed strong LIMK1 phosphorylation particularly in the lamellipodia of wt cells but less pLIMK1 localization in lamellipodia of *Arhgef6*$^{-/-}$ cells (72.6±2.0% of control) (Figure 22A,B).

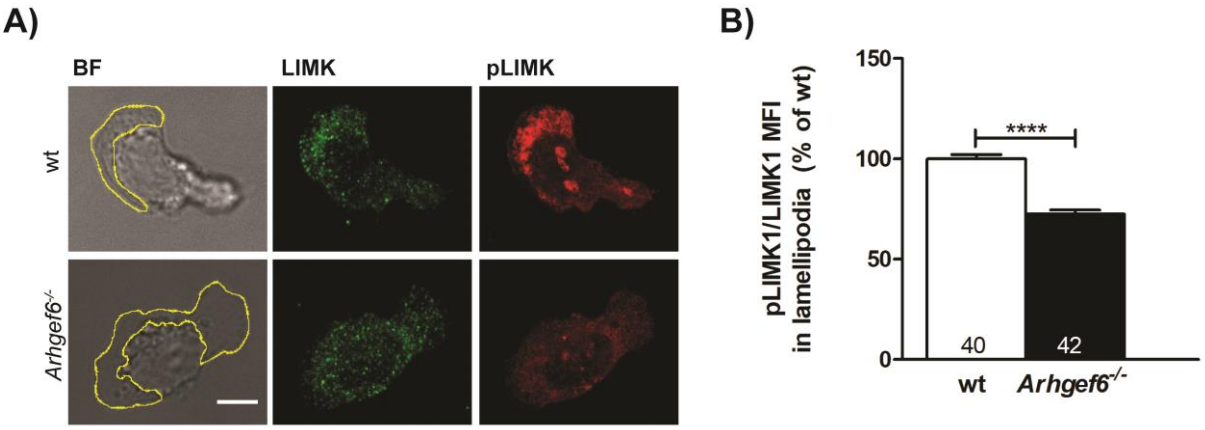

Figure 22. Less pLIMK1 localization in lamellipodia of *Arhgef6*$^{-/-}$ cells
A) Representative bright field images showing a typical lamellipodia shape (marked in yellow) in wt and *Arhgef6*$^{-/-}$ T cells. LIMK staining is shown in green and pLIMK in red. Scale bar, 5 µm. B) Quantification of normalized pLIMK1/LIMK1 IF in lamellipodia of wt and *Arhgef6*$^{-/-}$ cells. Graph represents the mean ± SEM obtained from 3 independent experiments, normalized and expressed as % of the mean of wt per each experiment. The numbers within bars denote the number of cells used for statistics. **** p<0.0001 using Student's t-test.

Taken together, obtained data clearly showed reduced LIMK1 activity in *Arhgef6* deficient cells due to decreased PAK2 activity in these cells. As a consequence, in the absence of ARHGEF6 the signaling pathway PAK2/LIMK1 which leads to cofilin activation may be impaired. Therefore our next task was to investigate cofilin activation in *Arhgef6* deficient cells.

3.6 The role of ARHGEF6 in cofilin deactivation

Reduced phosphorylation of LIMK1 (Figures 21 and 22) suggested that its activity is compromised in *Arhgef6*$^{-/-}$ CD4^{+} T cells. However, the final proof could only be obtained from inspection of the phosphorylation status of its target molecules. Cofilin is one of the best characterized target molecules of LIM kinases (Moriyama et al., 1996; Sumi et al., 1999) therefore, the level of cofilin phosphorylation (pSer3) is a read out of LIMK activity. Using antibodies specific for total cofilin and phospho-cofilin (p-cofilin), respectively, we investigated the level of cofilin phosphorylation by quantitative WB and ICC. Our quantitative WB data revealed that phosphorylation of cofilin is greatly reduced in *Arhgef6* deficient CD4^{+} T cells by almost 70% as

compared to wt T cells (32.8±5.0% of wt) (Figure 23A, B). Quantitative ICC also confirmed the reduction of cofilin phosphorylation in *Arhgef6*$^{-/-}$ T cells to almost half of the level in wt cells. A similar 50% reduction of p-cofilin was also found in the lamellipodia region of *Arhgef6*$^{-/-}$ T cells (56.0±2.8% of wt in the whole cell; 51.0±5.9% of wt in lamelipodia region) (Figure 23C,D).

In order to test if cofilin phosphorylation status can be specifically caused by reduced PAK activity, we treated both wt and *Arhgef6* deficient cells with the PAK inhibitor IPA3. As expected, IPA3 application resulted in the reduction of cofilin phosphorylation in wt cells (by approximately one third) to a level which was not significantly different to that of untreated *Arhgef6*$^{-/-}$ cells. However, the same treatment did not further influence the level of phosphorylated cofilin in *Arhgef6*$^{-/-}$ cells (untreated *Arhgef6*$^{-/-}$ 56.0±2.8%; treated wt 67.6±7.4%; treated *Arhgef6*$^{-/-}$ 52.9±7.3% of control) (Figure 23E). These data further confirmed impaired PAK activity in *Arhgef6* deficient cells and implicate that the decreased PAK activity in *Arhgef6*$^{-/-}$ T cells greatly accounts for the decreased phosphorylation of cofilin, probably via reduced LIMK activation.

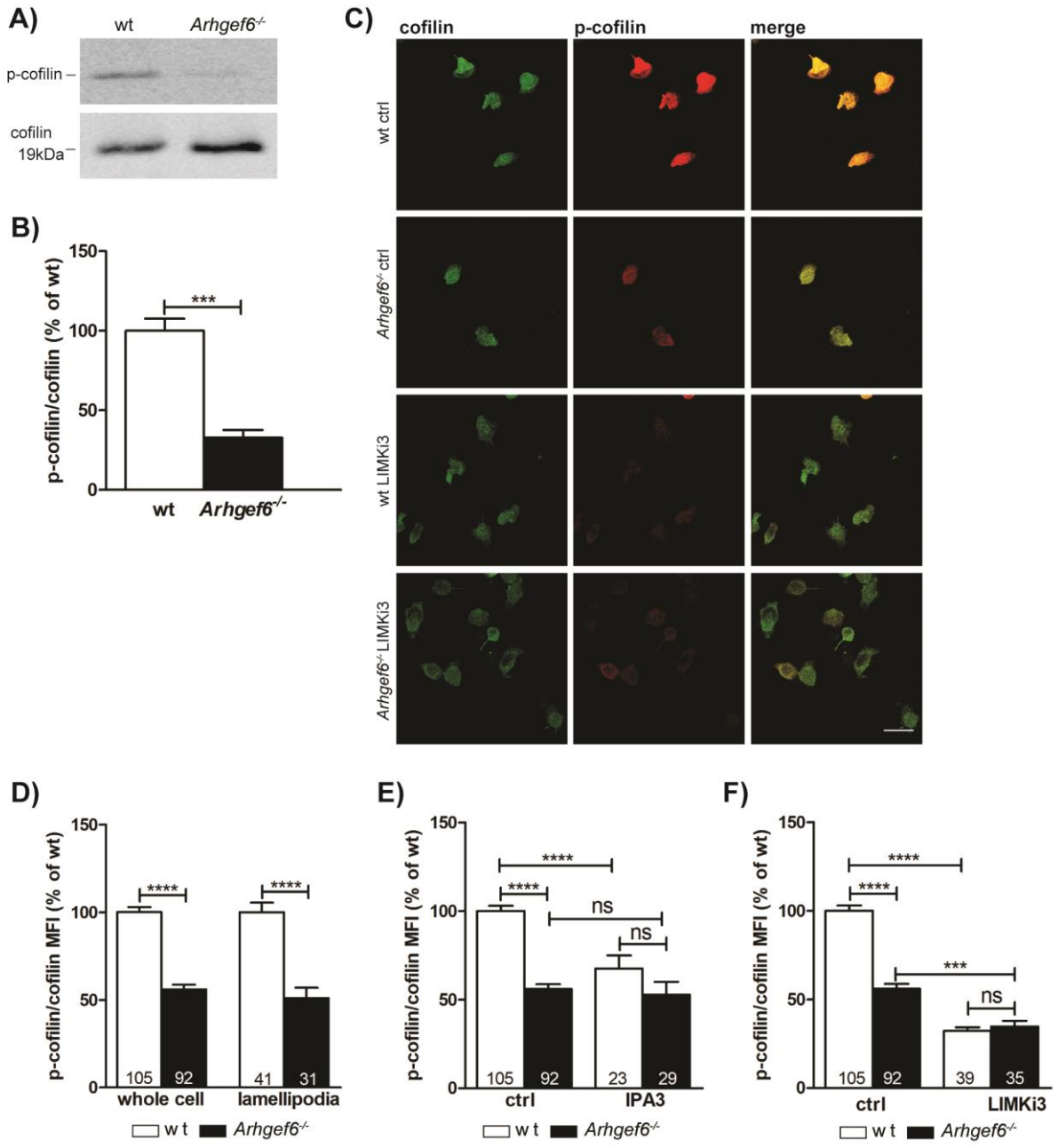

Figure 23. Decreased cofilin phosphorylation in *Arhgef6*$^{-/-}$ CD4^{+} T cells
A) Representative western blot and B) quantification of p-cofilin and cofilin assessed in lysates of wt and *Arhgef6*$^{-/-}$ CD4^{+} T cells. Data are obtained from 4 independent experiments. Per each experiment the signal of phosphorylated cofilin was normalized to the level of the total cofilin in each genotype and expressed as % of the mean of the signal in wt cells. Statistical significance was assessed using Student's t-test, *** p<0.001. C) Representative confocal images of wt and *Arhgef6*$^{-/-}$ CD4^{+} T cells treated with control solution or LIMKi3 (10 µM, 4h). Cells were fixed and stained for cofilin (green), p-cofilin (red). Scale bar, 20 µm. D) Quantification of normalized pLIMK1/LIMK1 IF signal in the whole cell and lamellipodia region of wt and *Arhgef6*$^{-/-}$ CD4^{+} T cells. Graphs represent mean ± SEM obtained from 3 independent experiments for the whole cell and 4 independent experiments for lamellipodia region. In each experiment signal was normalized to the mean of the wt cells and expressed as % of the mean E) Quantification of normalized pLIMK1/LIMK1 IF signal in the presence and absence of IPA3 (20 µM, 2h), in wt and *Arhgef6*$^{-/-}$ CD4^{+} T cells. Graphs represent mean ± SEM obtained from 3 independent experiments, always normalized to the mean of the wt control cells and expressed as % of the mean. F) Quantification of normalized p-cofilin/cofilin IF signal in whole cell volume of wt and *Arhgef6*$^{-/-}$ CD4^{+} T cells in the presence or absence of LIMKi3. Graphs represent mean ± SEM obtained from 5 independent experiments. In each experiment data were normalized to the mean of the wt control cells and expressed as % of the mean. The numbers within bars denote the

number of cells used for statistics. Statistical significance was assessed by using Student's t-test (B) and two-way ANOVA followed by Bonferroni's post hoc test (D-E), respectively. *** $p<0.001$; **** $p<0.0001$.

To further analyze this, we assessed the level of phosphorylated cofilin also in the presence or absence of LIMK inhibitor LIMKi3. As expected, the application of LIMKi3 to migrating wt cells strongly reduced the level of phosphorylated cofilin to approximately one third of that of untreated wt cells. LIMKi3 treatment of *Arhgef6*$^{-/-}$ cells resulted also in a further reduction of phosphorylated cofilin to the same level of treated wt cells (treated wt 32.2±2.0%; treated *Arhgef6*$^{-/-}$ 34.7±3.2% of untreated wt control) (Figure 23C,F).

Taken together, our data showed that the decrease of LIMK activity may account for increased cofilin activation in *Arhgef6*$^{-/-}$ cells. Therefore we strongly believe that ARHGEF6 is the crucial regulator of PAK2/LIMK1 signaling module required for cofilin activation in CD4^{+} T cells.

3.7 Actin remodeling/turnover in *Arhgef6*$^{-/-}$ CD4^{+} T cells

Given that cofilin phosphorylation represses its actin disassembling activity (Sumi et al., 1999) and given that cofilin activity is greatly affected in *Arhgef6* deficient cells (Figure 23), we resumed our experiments in order to test actin dynamics. Applying quantitative WB and confocal microscopy we did not observe any significant difference in overall β-actin expression between wt and *Arhgef6*$^{-/-}$ cells (Figure 24A-D).

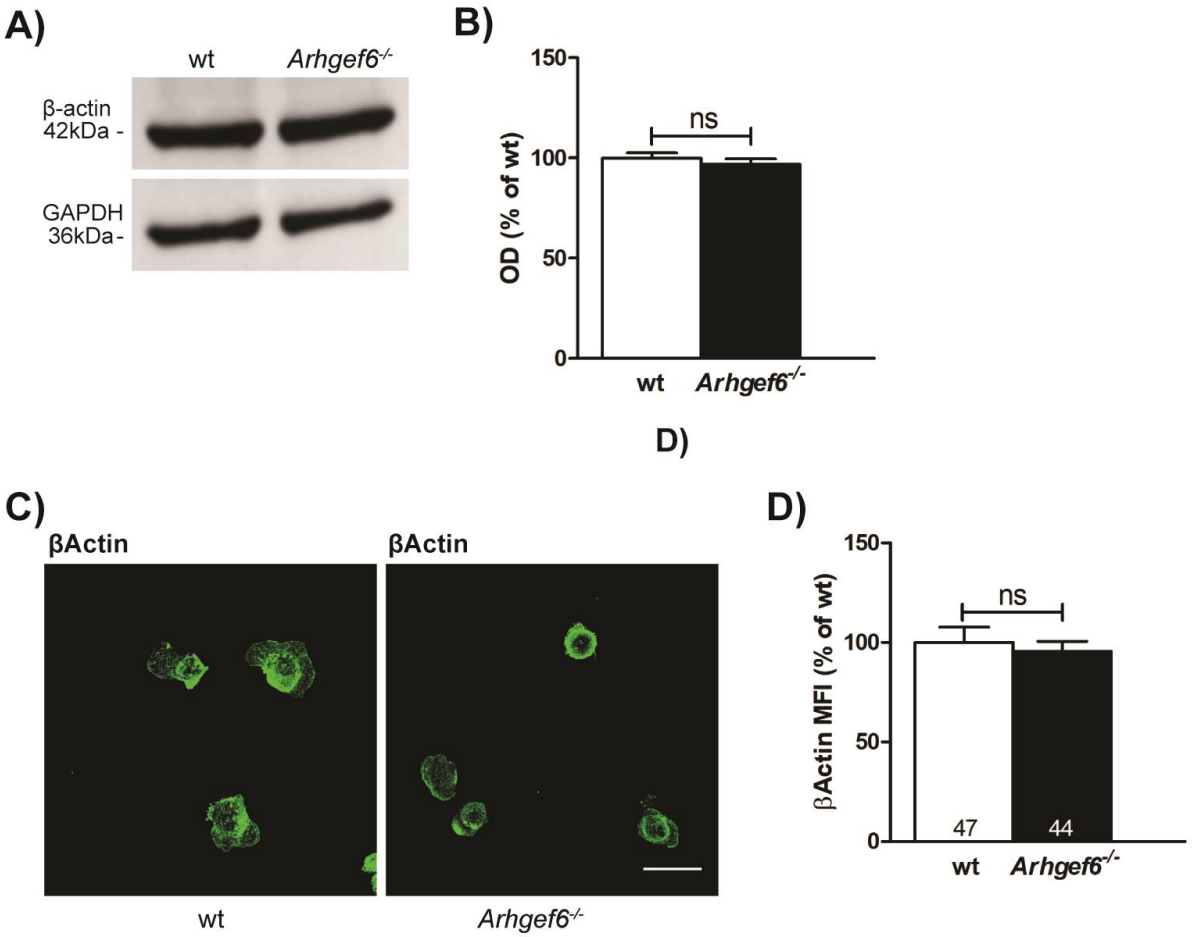

Figure 24. Actin expression is not impaired in *Arhgef6*$^{-/-}$ CD4^{+} T cells
A) Immunoblot of β-actin assessed in lysates of wt and *Arhgef6*$^{-/-}$ CD4^{+} T cells. B) Quantification of band intensities showed no significant difference of protein expression level in two genotypes. Data represent mean ± SEM obtained from 3 independent experiments. Per each experimental setup data were normalized to the mean of wt cell and expressed as % of the mean. Student's t-test was used for statistics. C) Confocal images of wt and *Arhgef6*$^{-/-}$ CD4^{+} T cells stained for β-actin. D) Quantitative analysis showed no difference in immunofluorescence signals. Data on the graph represent mean ± SEM obtained from 3 independent experiments pooled together. Within each experiment signal was normalized to the mean of wt cells and expressed as % of the mean. The numbers within bars show the number of cells used for analysis. Statistical significance was assessed by Mann–Whitney test. Scale bar, 20 µm.

To be able to specifically focus our study on actin dynamics near the site of cell contact to the substrate and in lamellipodia, we used TIRF microscopy. To this end, we either labelled endogenous actin with antibody against β-actin or we used T cells from mice harboring Lifeact-GFP. TIRF images revealed a twofold increase of β-actin along the whole ventral cell body with strong accumulation at the lamellipodia region of *Arhgef6*$^{-/-}$ cells (the whole cell 197.0±10.8% of control; lamellipodia 218.1±11.8% of control) (Figure 25A,B). Similarly, we observed a ~50% increase in Lifeact expression with strongly pronounced expression in the lamellipodia (the whole cell 144.0±12.8% of control; lamellipodia 162.6±16.5% of control) (Figure 25C,D; Supplemental movies 5 and 6). These data are in line with over-activation of both cofilin and Rac1 observed in *Arhgef6*$^{-/-}$ cells, as actin severing by cofilin generates actin bundles therefore promoting actin polymerization by Rac1 (Eden et al., 2002).

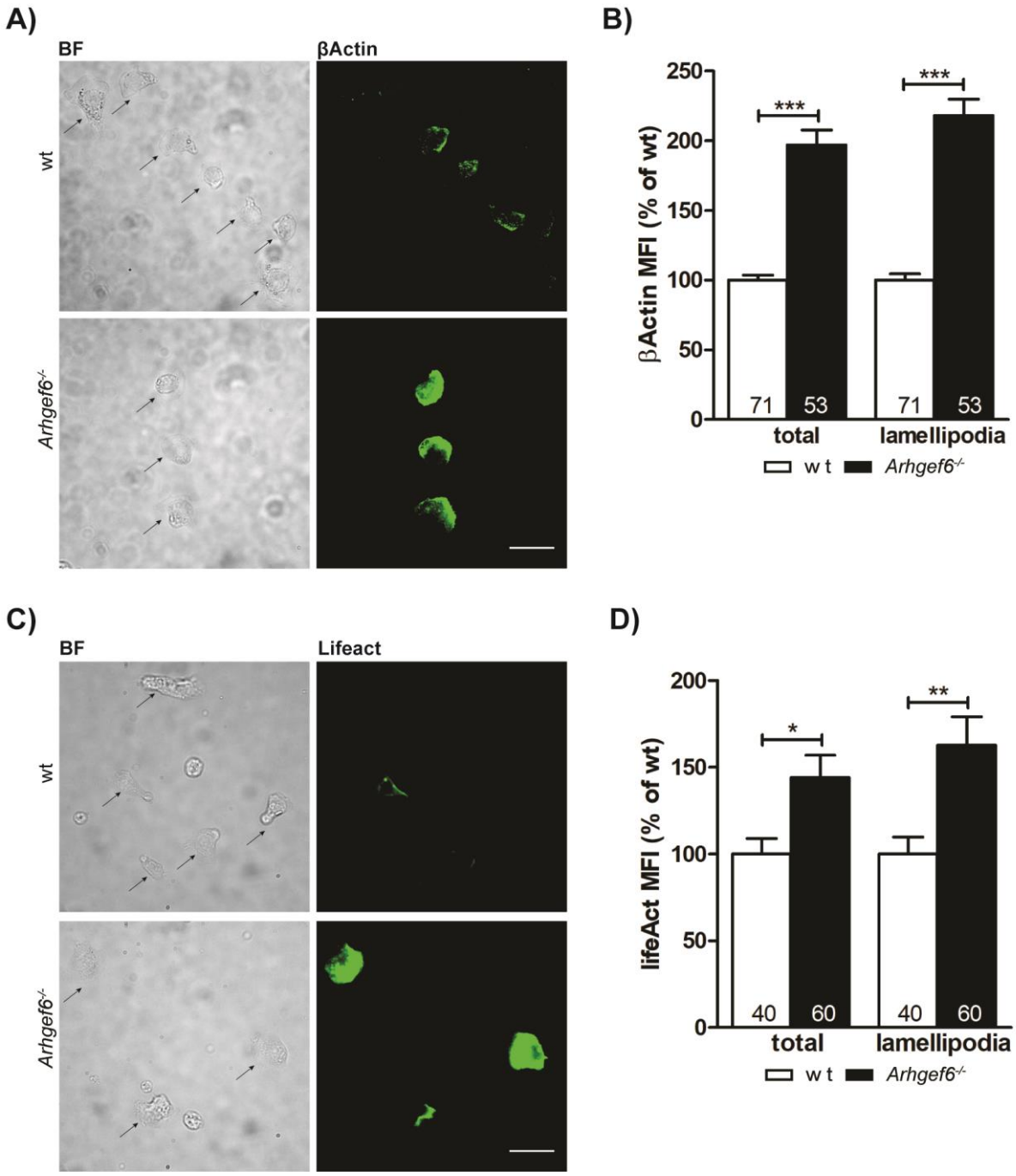

Figure 25. Increased Actin expression at surface contact area of *Arhgef6*$^{-/-}$ CD4^{+} T cells
A) Bright field and TIRF images of wt and *Arhgef6*$^{-/-}$ CD4^{+} T cells stained for β-actin. B) Graphs represent the level of β-actin IF in the whole cell and lamellipodia. Data on the graph represent mean ± SEM obtained from 3 independent experiments. In each experiment signal was normalized to the mean of wt cells and expressed as % of the mean. The numbers within bars show the number of cells used for analysis. Statistical significance was assessed by Mann–Whitney test (the whole cell) and Student's t-test (lamellipodia). *** $p<0.001$. Scale bar, 20 µm. C) Bright field and TIRF images of Lifeact wt and *Arhgef6*$^{-/-}$ CD4^{+} T cells. D) Graph represents the level of Lifeact IF in the whole cell and lamellipodia. Data on the graph represent mean ± SEM from 3 independent experiments pooled together. Within each individual experiment signal was normalized to the mean of wt cells and expressed as % of the mean. The numbers within bars show the number of cells used for analysis. Statistical significance was assessed by Mann–Whitney test (the whole cell) and Student's t-test (lamellipodia). * $p<0.05$; ** $p<0.01$. Scale bar, 20 µm.

3.8 Reduction of GIT2 in *Arhgef6*$^{-/-}$ CD4^{+} T cells

So far, we described a role for ARHGEF6 in regulating actin dynamics in T cell migration by regulating Rac GTPase activity and by promoting PAK signaling to cofilin, which together regulate actin turnover. However, the PIX/GIT complex is also described as a molecular hub, which mobilizes proteins involved in the maturation and turnover of focal contacts to the substrate via integrins (Frank and Hansen, 2008; Nayal et al., 2006; Parsons et al., 2010). Thereby it links actin dynamics to adhesion in order to transmit the force required for spreading and motility. Therefore, our next question was whether the absence of ARHGEF6 and altered PIX/GIT complex in *Arhgef6*$^{-/-}$ CD4^{+} T cells influences the surface expression of integrins. We stained intact wt and *Arhgef6*$^{-/-}$ cells with different antibodies against LFA-1 and VLA-4 integrins and measured the signal by flow cytometry. Obtained data revealed equal surface expression of both LFA-1 and VLA-4 in CD4^{+} T cells in both genotypes (Supplementary figure 2).

Actin turnover and recruitment of proteins to focal contact sites are both required for the formation of focal contacts (Ciobanasu et al., 2012). We therefore assumed that *Arhgef6* deficiency would lead to impaired focal contact formation in migrating T cells. PIX/GIT complex localization to focal contacts and its function in remodeling of focal contacts are both mediated by the interaction of GIT1 and GIT2 with paxillin (Mazaki et al., 2001; Schmalzigaug et al., 2007). Previous data from our group showed that total GIT2 protein level is reduced in lymphocytes lacking *Arhgef6* (Missy et al., 2008). Here, these data were reproduced by quantitative WB of CD4^{+} T cell lysates (64.9±4.6% of control) (Figure 26A,B). Furthermore, immunostaining of migrating T cells also showed global reduction of GIT1/2 in *Arhgef6* deficiency (71.1±1.9% of control) (Figure 26C,D). The results are also in line with the severe reduction of GIT proteins in FPLC fractions from thymocyte lysates containing small size protein complexes (Figure 16). Of note, reduction of GIT1/2 was also found in Jurkat T cells after *Arhgef6* knock down, particularly at the immune synapse of Jurkat-Raji cell pairs (Supplementary figure 3). We therefore wondered if both, the reduction in GIT2 protein and the altered stoichiometry of the PIX/GIT complex had an influence on the maturation and turnover of focal contacts in migrating *Arhgef6*$^{-/-}$ T cells. So we

proceeded with investigation of expression and turnover of selected focal contact constituents.

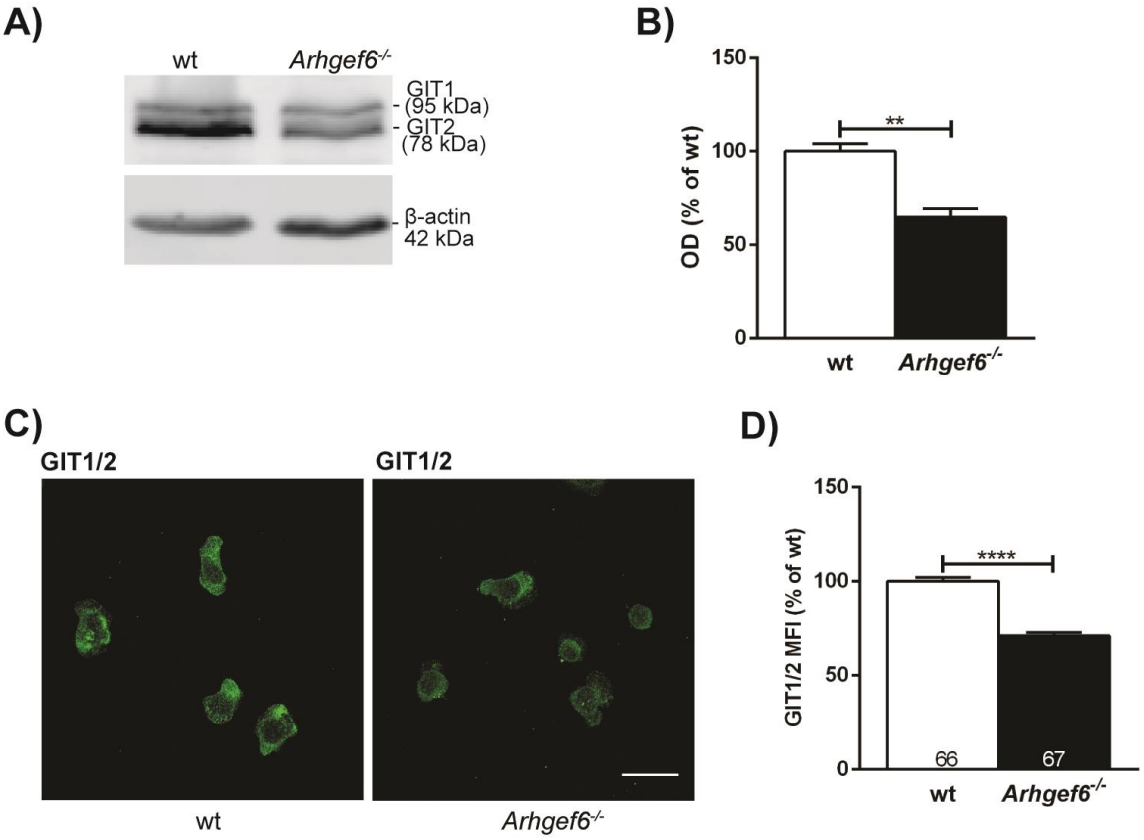

Figure 26. Reduced GIT1 and GIT2 expression levels in *Arhgef6*$^{-/-}$ CD4^{+} T cells
A) Immunoblots of expression level of GIT1 and GIT2 in cell lysates from wt and *Arhgef6*$^{-/-}$ CD4^{+} T cells. B) Quantification of GIT1 and GIT2 signal normalized to β-actin, which was used as a loading control. Statistics was done by using Mann–Whitney test. ** $p<0.01$. C) Representative confocal images of GIT1 and GIT2 staining in wt and *Arhgef6*$^{-/-}$ CD4^{+} T cells. D) Quantitative analysis showed significant decrease of GIT1 and GIT2 IF in *Arhgef6*$^{-/-}$. Data on the graph represent mean ± SEM and originate from 3 independent experiments. The numbers within bars denote the number of analyzed cells. Student's t-test was used for statistics. **** $p<0.0001$. Scale bar, 20 µm.

3.9 Paxillin and phospho-paxillin in *Arhgef6*$^{-/-}$ CD4^{+} T cells

Central to the assembly of focal contacts is the recruitment and subsequent phosphorylation of paxillin at Tyr118, mediated by focal adhesion kinase (FAK) (Bellis et al., 1995). Therefore, we analyzed expression, phosphorylation status and localization of paxillin. Expression of total paxillin in CD4^{+} T cells was not significantly different between wt and *Arhgef6*$^{-/-}$ as assessed by WB (Figure 27A). Also, using a specific antibody recognizing paxillin Tyr118 phosphorylationin the same samples, we could not detect a significant reduction of global paxillin phosphorylation in *Arhgef6*$^{-/-}$ T cells (Figure 27A,B). However, immunostaining of migrating T cells

showed significantly lower overall levels of phospho-paxillin (p-paxillin) in *Arhgef6*$^{-/-}$ cells (79.5±1.2% of control) (Figure 27C,D).

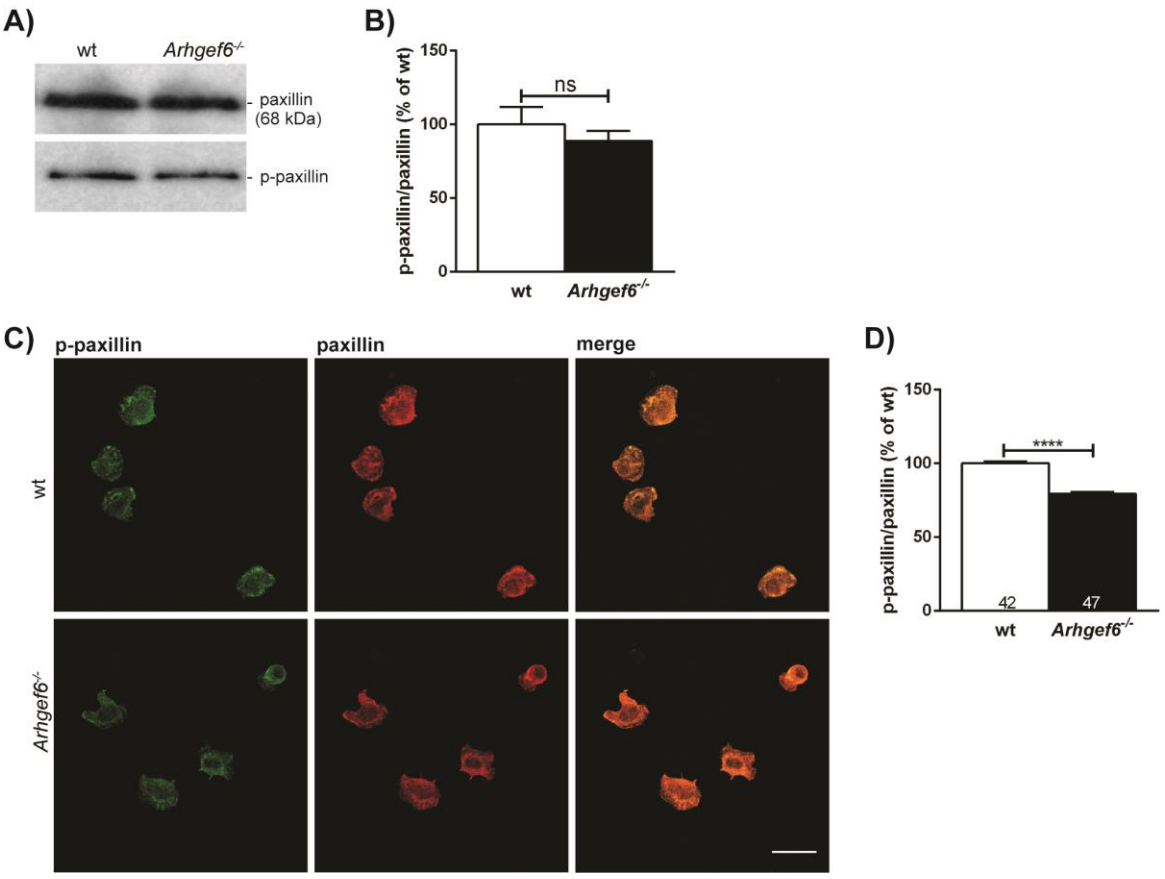

Figure 27. Reduced phospho-paxillin level in *Arhgef6*$^{-/-}$ CD4^{+} T cells
A) Representative immunoblots and B) quantification of paxillin and p-paxillin in wt and *Arhgef6*$^{-/-}$ CD4^{+} T cells lysates. The bar graph displays pooled data from 4 independent experiments. Within each experiment the signal of phosphorylated paxillin was normalized to the level of the total paxillin in each genotype and expressed as % of the mean of the signal in wt cells. Statistics was done by using Student's t-test. C) An example of confocal images of migrating wt and *Arhgef6*$^{-/-}$ CD4^{+} T cells stained for p-paxillin (green), paxillin (red) and overlay. D) Quantification of normalized p-paxillin/paxillin IF signal in wt and *Arhgef6*$^{-/-}$ CD4^{+} T cells. Data on the graph represent mean ± SEM obtained from 3 independent experiments. In each experiment data were normalized and expressed as % of the mean of wt cells. The numbers within bars show the number of analyzed cells. Statistics was done by using Student's t-test. **** $p<0.0001$. Scale bar, 20 µm.

In order to investigate the presence of paxillin and p-paxillin more specifically in focal contacts, we performed TIRF imaging. TIRF images showing immunostaining for endogenous paxillin again did not reveal a significant difference in the total amount of paxillin at the contact area of the whole cell and the substrate (Figure 28A and B). However, there was a significant reduction in total paxillin expression at the TIRF plane of lamellipodia regions from *Arhgef6*$^{-/-}$ cells compared to wt cells (78.5±3.3% of control) (Figure 28A and B). Moreover, the level of paxillin phosphorylation was reduced in *Arhgef6*$^{-/-}$ CD4^{+} T cells at the TIRF plane of both the whole cell body and

the lamellipodia (the whole cell 73.9±7.9% of control; lamellipodia 78.1±9.2% of control) (Figure 28C and D). Less available paxillin and less paxillin phosphorylation at surface contact area in lamellipodia indicate that *Arhgef6* deficient CD4$^+$ T cells may have less mature and increased turnover of contacts sites, which might refer to altered focal contacts.

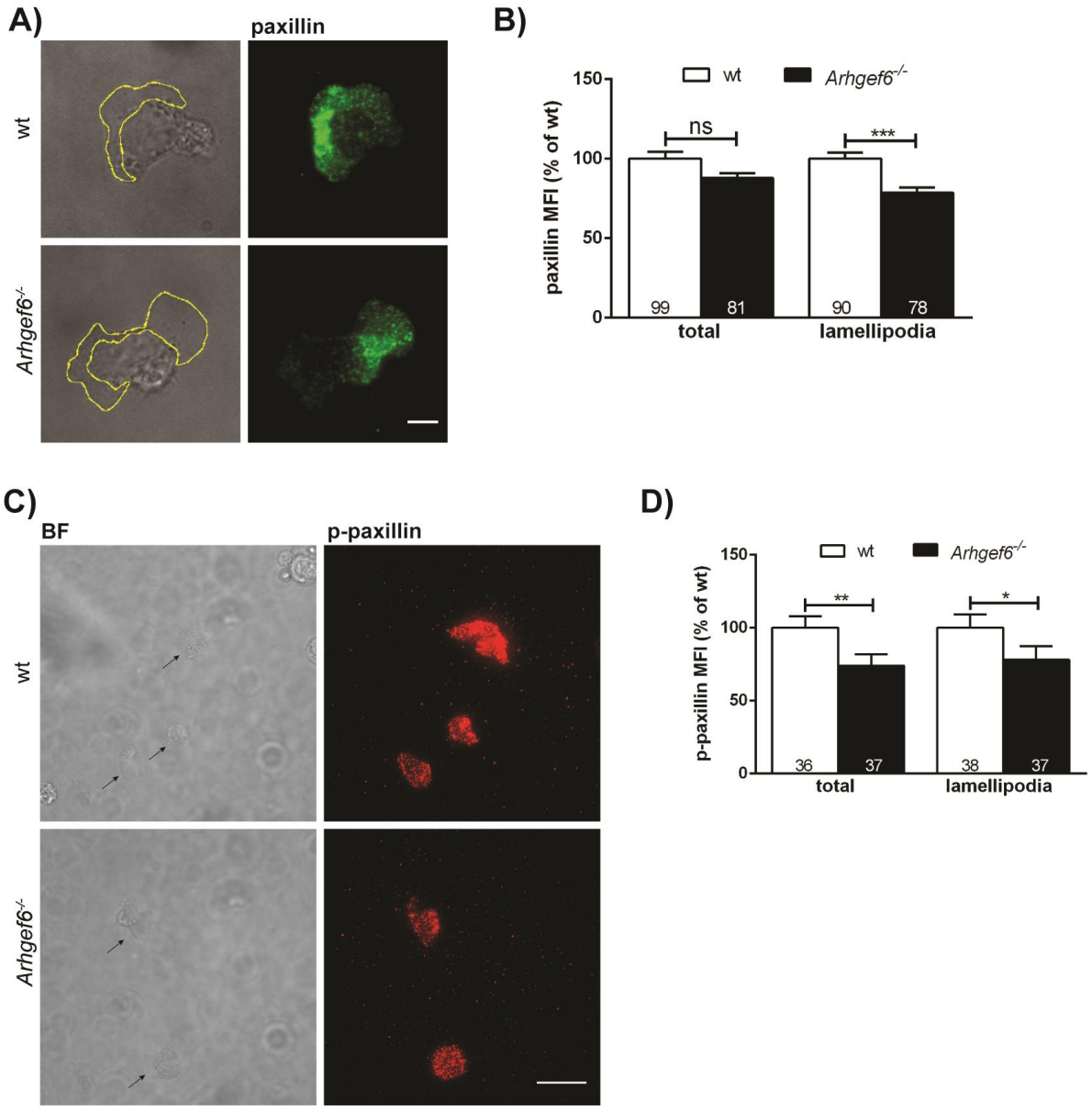

Figure 28. Reduction of paxillin and phospho-paxillin at surface contact area of *Arhgef6*$^{-/-}$ CD4$^+$ T cells

A) Single cell bright field and TIRF images of wt and *Arhgef6*$^{-/-}$ CD4$^+$ T cells stained for paxillin. B) Quantification of paxillin IF in the whole cell and lamellipodia. Data on the graph represent mean ± SEM obtained from 3 independent experiments. In each experiment the signal in *Arhgef6*$^{-/-}$ cells was normalized to the mean of wt cells and expressed as % of the mean. The numbers within bars show the number of cells used for analysis. Statistical significance was assessed by Mann–Whitney test. *** $p<0.001$. Scale bar, 5 µm. C) Bright field and TIRF images of wt and *Arhgef6*$^{-/-}$ CD4$^+$ T cells stained for p-paxillin. The cells are assigned with arrows on BF image. D) Graphs represent the level of p-paxillin IF in the whole cell and lamellipodia. Data on the graph represent mean ± SEM obtained from

3 independent experiments. The numbers within bars denote the number of cells used for analysis. Statistical significance was assessed by Mann–Whitney test. * p<0.05; ** p<0.01. Scale bar, 20 µm.

In order to visualize paxillin turnover we introduced a paxillin-GFP biosensor by lentiviral transduction into our cultured primary murine wt and *Arhgef6*$^{-/-}$ CD4^{+} T cells. As observed by TIRF imaging of fixed cells immunostained for endogenous paxillin, live cell TIRF imaging of GFP positive cells migrating on ICAM-1 reflected a similar global reduction of ectopically expressed paxillin in *Arhgef6*$^{-/-}$ T cells (Figure 29; Supplemental movies 7 and 8). Generally, focal paxillin signals were mainly concentrated in the central and rear part of the cell body with much lower intensity in *Arhgef6*$^{-/-}$ T cells compared to wt cells. At the same time, wt cells frequently showed several stable paxillin spots in the lamellipodium, whereas we could never detect comparable focal signals in *Arhgef6* deficient T cells. These data therefore support the idea that ARHGEF6 is required to stabilize contact sites and to limit their turnover in migrating T cells.

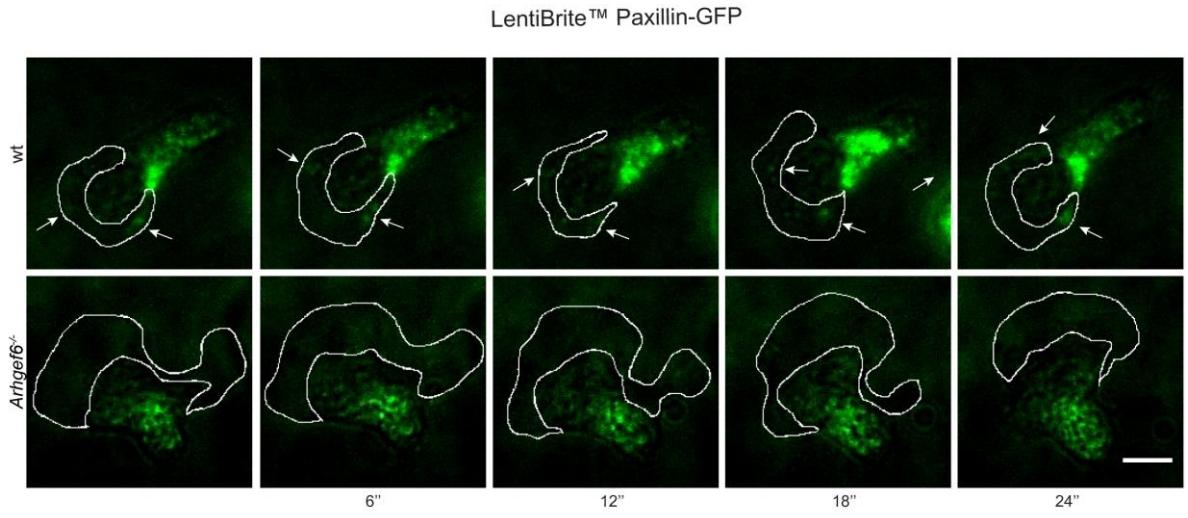

Figure 29. Higher paxillin turnover in lamellipodia of *Arhgef6*$^{-/-}$ CD4^{+} T cells
Consecutive TIRF images of live wt (upper row) and *Arhgef6*$^{-/-}$ (lower row) CD4^{+} T cells transduced with paxillin-GFP biosensor and migrating on ICAM-1 coated surface. White lines delineate lamellipodia. Arrows indicate higher paxillin-GFP signal at lamellipodial surface contact area of wt cells. Images were cropped from movies of equal duration and frame rate in intervals of 6 seconds. Scale bar, 5 µm.

3.10 Vinculin in *Arhgef6*$^{-/-}$ CD4^{+} T cells

As a good measure for the maturity of contact sites we also analyzed the presence of vinculin at surface contact area. This protein connects filamentous (F)-actin to the

integrin-binding protein talin, thereby transmitting forces between the actin cytoskeleton and the ECM (Humphries et al., 2007).

To analyze this in more detail, we applied immunocytochemistry. Confocal imaging of vinculin immunostaining showed an overall increase of vinculin levels in *Arhgef6*$^{-/-}$ T cells (136.1±7.4% of control) (Figure 30A,B). TIRF imaging, however, showed a strong reduction of vinculin in *Arhgef6*$^{-/-}$ cells to almost half of the level of wt cells at the surface contact plane both of the whole cell (56.9±4.4% of control) and specifically in lamellipodia (57.8±7.8% of control) (Figure 30C,D). Altogether, our data therefore suggest that *Arhgef6*$^{-/-}$ T cells form less stable contact sites.

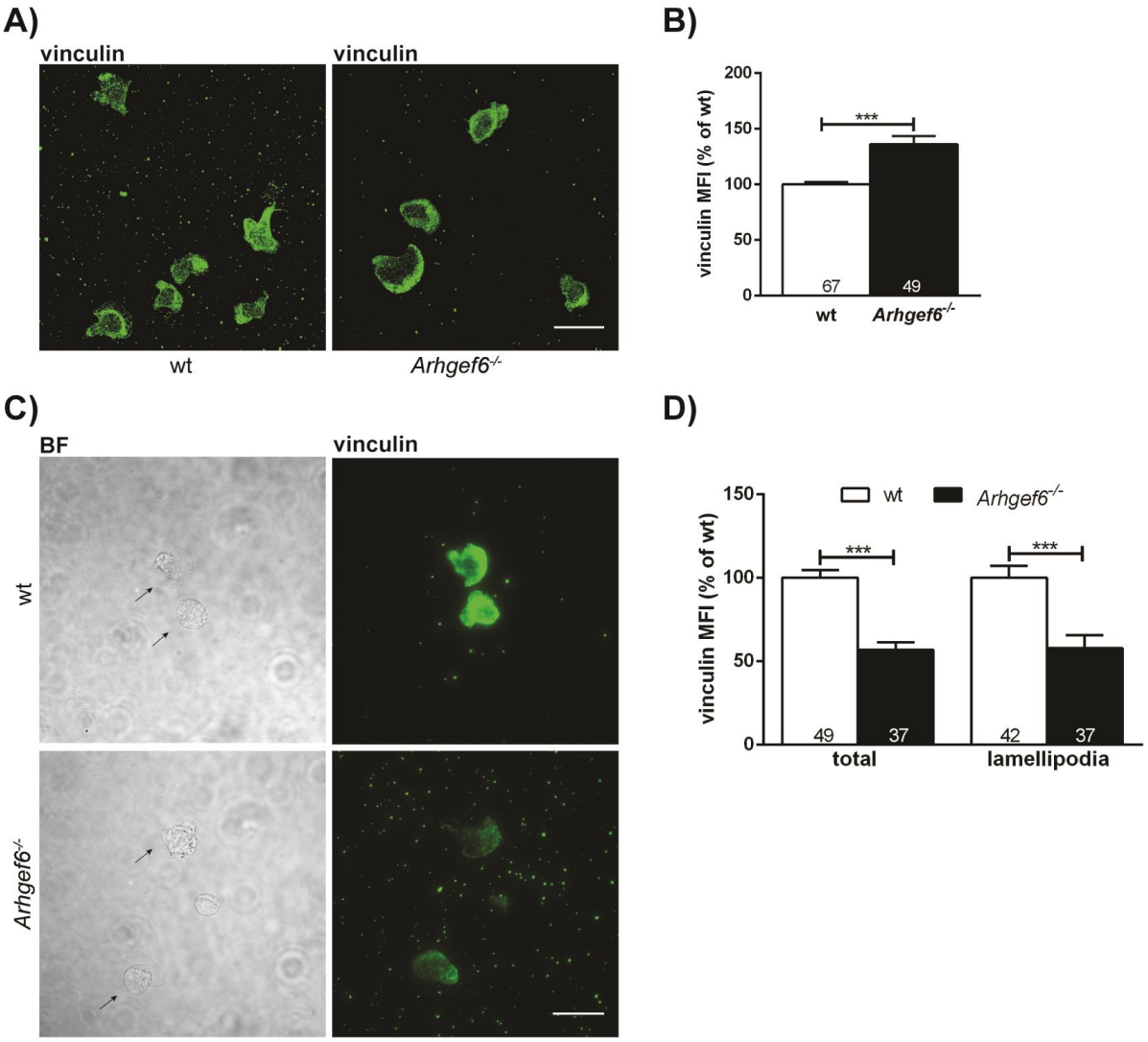

Figure 30. Vinculin expression level in the whole cell and at surface contact area
A) Representative confocal images of vinculin staining in wt and *Arhgef6*$^{-/-}$ CD4^{+} T cells. B) Quantitative analysis showed significant increase of vinculin IF in *Arhgef6*$^{-/-}$. Data originate from 3 independent experiments. The numbers within bars denote the number of cells used for statistics. Statistical significance was done by using Mann–Whitney test. *** $p<0.001$. Scale bar, 20 µm. C) Representative bright field and TIRF images of wt and *Arhgef6*$^{-/-}$ CD4^{+} T cells stained for vinculin. The cells are assigned with arrows on BF image. D) Graph represents the level of vinculin IF in the whole

cell and lamellipodia. Data on the graph represent mean ± SEM obtained from 3 independent experiments. The numbers within bars show the number of cells used for analysis. Statistical significance was assessed by Mann–Whitney test. *** p<0.001. Scale bar, 20 µm.

3.11 Altered lamellipodia morphology in *Arhgef6*$^{-/-}$ CD4^{+} T cells

Although we observed the differences at surface contact area (higher paxillin turnover in lamellipodia and reduced vinculin expression), the most prominent change was impairment of PAK2/LIMK1/cofilin signaling to actin in *Arhgef6*$^{-/-}$ T cells. Therefore, we wondered how the altered actin turnover observed in *Arhgef6* deficient T cells would affect their morphology. During our studies using ICC or live cell imaging we frequently observed morphological differences between wt and *Arhgef6*$^{-/-}$ CD4^{+} T cells, which are particularly related to irregular dynamics of lamellipodia in *Arhgef6*$^{-/-}$ CD4^{+} T cells (Supplemental movies 3, 4 and Figure 31A). During migration, wt T cells usually spread a newly formed lamellipodium while retracting a previously formed overlapping lamellipodium (Figure 31A), which results in a “zick-zick” but overall straight migration course (Supplemental movie 1). In contrast, migrating *Arhgef6*$^{-/-}$ T cells often displayed 2 lamellipodia spreading simultaneously in opposite directions giving *Arhgef6*$^{-/-}$ T cells an extra-wide “hammer-head-like” appearance (Figure 31A) making it difficult to anticipate in which direction *Arhgef6*$^{-/-}$ cell turns (Supplemental movie 2). Cells with such irregular lamellipodia were more frequent among *Arhgef6*$^{-/-}$ than wt T cells (wt 15.9±2.1% of all cells; *Arhgef6*$^{-/-}$ 68.1±2.7% of all cells) (Figure 31B).

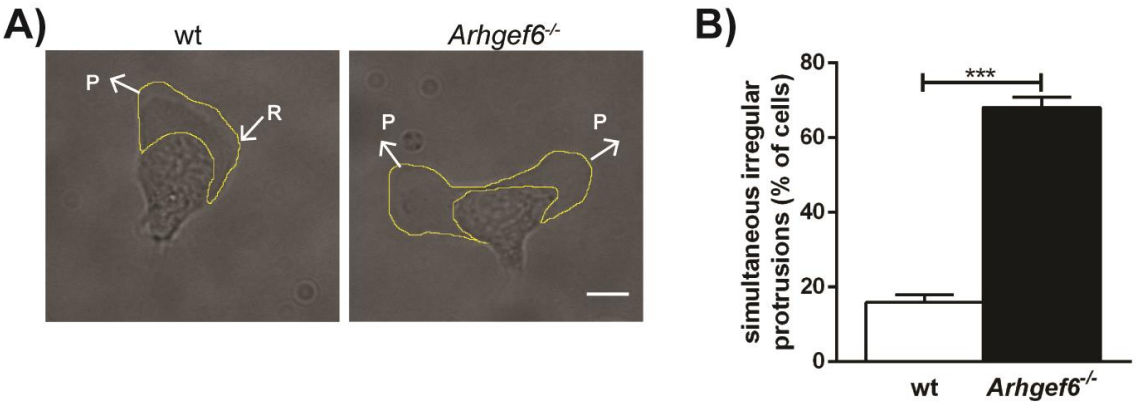

Figure 31. Lamellipodia defects in *Arhgef6*$^{-/-}$ T cells
A) Representative bright field images (100X magnification) of CD4^{+} T cells showing lamellipodial defect in *Arhgef6*$^{-/-}$ versus wt control. Extra-wide “hammer-head-like” appearance in *Arhgef6*$^{-/-}$ cells. Arrows indicate protrusion (P) and retraction (R). Scale bar, 5 µm. B) Quantification of simultaneous irregular protrusions expressed as % of total cells within each genotype. Statistical significance was assessed by Mann–Whitney test. *** p<0.001.

When looking at freeze-frames of single live migrating cells, *Arhgef6*$^{-/-}$ lamellipodia are often unusually large and wide, covering more area than wt lamellipodia. In order to describe these morphological differences between wt and *Arhgef6*$^{-/-}$, we quantified width, depth and total area of the lamellipodia of single cells randomly captured at instant moments during migration, and we also measured the angle between consecutive (or simultaneous) lamellipodia as depicted in Figure 32A. The quantification revealed that the mean width and area of lamellipodia in *Arhgef6*$^{-/-}$ cells were larger than in wt cells whereas the depth did not differ (width: wt, 13.3±0.6 µm vs *Arhgef6*$^{-/-}$, 15.3±0.6 µm; area: wt, 63.6±5.1 µm^2 vs *Arhgef6*$^{-/-}$, 98.7±6.5 µm^2) (Figure 32B,C,D). Notably, the median area revealed an even 80% increase in *Arhgef6*$^{-/-}$ lamellipodia size (wt: 53.9 µm^2 vs *Arhgef6*$^{-/-}$: 96.8 µm^2), indicating that most *Arhgef6*$^{-/-}$ cells have larger lamellipodia than the majority of wt cells. By using arbitrary definition of small (<70 µm^2), and large size (>70 µm^2) lamellipodia, we identified that 73% of wt CD4$^+$ T cells show small and only 27% large lamellipodia. In contrast, even 80% of *Arhgef6*$^{-/-}$ cells showed large lamellipodia (Figure 32E). In wt cells, newly formed lamellipodia were formed at angle of approximately 90° (Figure 32F). This angle was increased to 145° in *Arhgef6*$^{-/-}$ cells, which seems to be a striking qualitative difference indicating conflictive directionality and predisposition for a less directional migration phenotype.

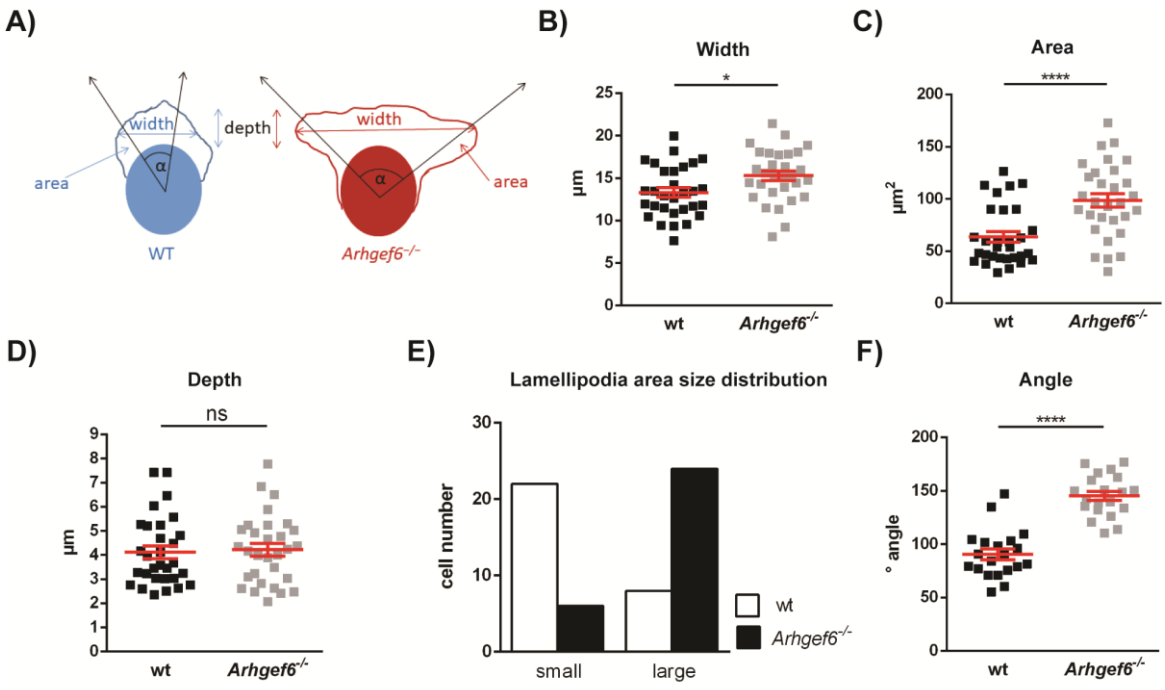

Figure 32. Morphological differences of lamellipodia between wt and *Arhgef6*$^{-/-}$ CD4$^+$ T cells
A) Diagram of quantified parameters in lamellipodia and usual extra-long-wide lamellipodia present in *Arhgef6*$^{-/-}$. Quantification of lamellipodia size parameters showing mean ± SEM of B) width, C) area

and D) depth in wt and *Arhgef6*$^{-/-}$ CD4^{+} T cells. The bar graphs display the pooled data from ≥3 experiments. Statistical significance was assessed by Student's t-test. * p<0.05; **** p<0.0001. E) Histogram of small and large size lamellipodia discriminated by area threshold of 70 µm^2. F) Quantification of lamellipodia angle in wt and *Arhgef6*$^{-/-}$ CD4^{+} T cells. The bar graphs display the pooled data from 3 experiments. Statistics was done by using Student's t-test. **** p<0.0001.

Observed morphological changes (width, area and angle) between wt and *Arhgef6*$^{-/-}$ lamellipodia are in line with above described over-activation of cofilin and increased actin turnover in the absence of ARHGEF6. However, we wondered whether defective LIMK1 signaling was also sufficient to induce the same phenotype in wt as in *Arhgef6*$^{-/-}$ cells and therefore we tested the impact of LIMKi3 on lamellipodia size parameters. Addition of LIMKi3 to wt cells indeed mimicked the *Arhgef6*$^{-/-}$ phenotype regarding the width (untreated wt 11.8±0.4 µm; untreated *Arhgef6*$^{-/-}$ 15.3±0.6 µm; treated wt 15.8±0.6 µm; treated *Arhgef6*$^{-/-}$ 17.1±0.5 µm) and area (untreated wt 56.4±3.6 µm^2; untreated *Arhgef6*$^{-/-}$ 98.7±6.5 µm^2; treated wt 96.4±6.7 µm^2; treated *Arhgef6*$^{-/-}$ 101.2±5.8 µm^2) of lamellopodia (Figure 33A,C; Supplemental movies 3 and 4). There was no significant effect of the inhibitor on the width or area of *Arhgef6*$^{-/-}$ cells compared to untreated *Arhgef6*$^{-/-}$ cells suggesting that the described parameters are LIMK dependent and LIMKi3 did not have further effect on LIMK activity in *Arhgef6*$^{-/-}$ cells, as described in the figure 21F. Also, LIMKi3 did not significantly influence the depth of lamellipodia in any of the genotypes (Figure 33B). In summary, these results suggest that impaired LIMK activation in migrating CD4^{+} T cells leads to the morphological changes observed in *Arhgef6*$^{-/-}$ T cells migrating on ICAM-1 coated 2D surfaces.

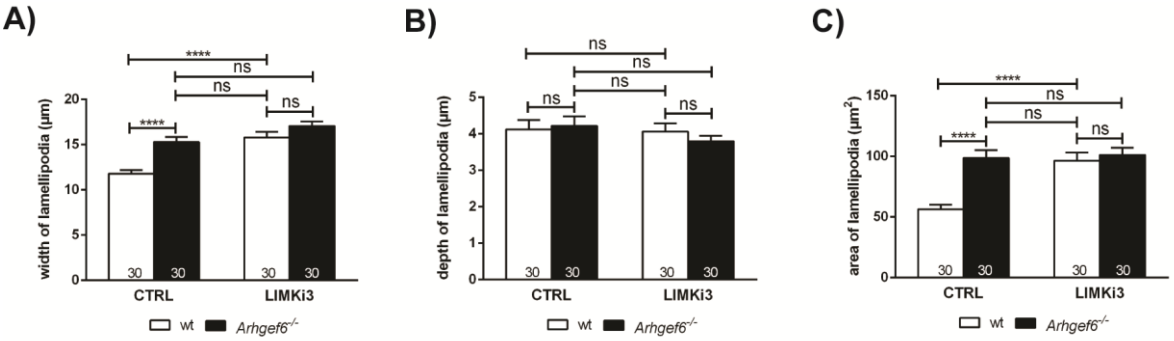

Figure 33. Lamellipodia size parameters in wt and *Arhgef6*$^{-/-}$ T cells with or without LIMKi3
Quantification of A) lamellipodia width, B) depth and C) area in wt and *Arhgef6*$^{-/-}$ CD4^{+} T cells treated with control solution or LIMKi3 (10 µM, 4h). The bar graphs display the pooled data from ≥3 experiments and represent mean ± SEM. Statistical significance was assessed by two-way ANOVA followed by Bonferroni's *post hoc* test. **** p<0.0001.

3.12 Role of LIMK on cellular motility of CD4$^+$ T cells

Our data cleary showed that the absence of ARHGEF6 exerts morphological changes and alters LIMK signaling in CD4$^+$ T cells. As shown above (Figure 33), lamellipodia size parameters are LIMK dependent and reduced LIMK1 activity in *Arhgef6*$^{-/-}$ cells is responsible for their specific phenotype. Therefore our next question was whether altered LIMK signaling pathway in *Arhgef6*$^{-/-}$ cells could also be linked to the migration defects observed in these cells (Figure 13).

To do so, we again performed live-cell imaging of wt and *Arhgef6*$^{-/-}$ CD4$^+$ T cells randomly migrating on ICAM-1 in the presence or absence of LIMKi3. First, we investigated the migratory behavior at a high time and space resolution at 100x magnification and tracked cells at time intervals of 0.375s over a total period of 5 min (Figure 34A). As expected, upon control treatment, *Arhgef6*$^{-/-}$ T cells displayed higher velocity and lower directionality than wt cells (Figure 34B and C) in line with altered lamellipodia dynamics. LIMK inhibition of wt cells indeed resulted in a significant increase of the median velocity up to the level of untreated *Arhgef6*$^{-/-}$ cells, whereas LIMKi3 treatment had no significant impact on the velocity of *Arhgef6*$^{-/-}$ cells (treated wt 17.7±0.9; treated *Arhgef6*$^{-/-}$ 19.9±1.3) (Figure 34B). Likewise, LIMKi3 treatment reduced the straightness of wt cells almost to the level of untreated *Arhgef6*$^{-/-}$ cells, whereas it had no effect on *Arhgef6*$^{-/-}$ cells (treated wt 0.67±0.04; treated *Arhgef6*$^{-/-}$ 0.61±0.04) (Figure 34C).

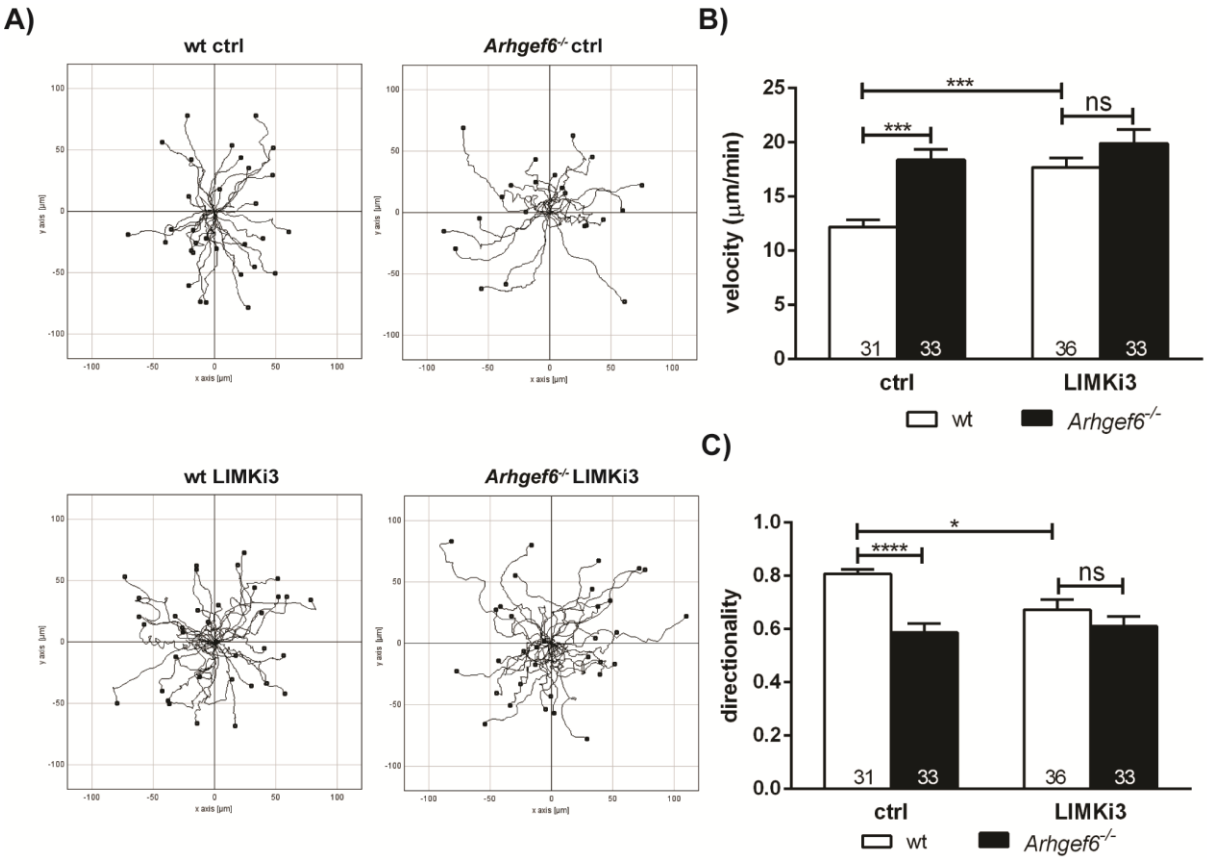

Figure 34. Directionality and velocity of wt and *Arhgef6*$^{-/-}$ CD4^{+} T cells with or without LIMKi3 inhibitor at 100x

A) Live cell imaging tracks of wt and *Arhgef6*$^{-/-}$ CD4^{+} T cell migration on 2D substrates in the presence and absence of LIMKi3. Cells were plated on immobilized ICAM-1 and images were recorded at 100X magnification every 0,375 s for 5 min. B) The bar graphs display quantification of velocity and C) directionality of 4 groups described in A. Numbers within bars present number of analyzed cells obtained from pooled data of 3 independent experiments. Data on the graph represent mean ± SEM. Statistics was done by using two-way ANOVA followed by Bonferroni's post hoc test. * p<0.05; *** p<0.001; **** p<0.0001.

In order to test if LIMKi3 treatment also affected the migration over longer distances, we repeated the experiments using 10x magnification. Tracking of control cells nicely reproduced the results from Figure 13 with very similar increase of the median overall velocity and decrease of the median directionality of fast moving *Arhgef6*$^{-/-}$ T cells (Figure 35B,C). Again, LIMKi3 treatment increased velocity of wt cells to the same level of control *Arhgef6*$^{-/-}$ cells, but it had no effect on the velocity of *Arhgef6*$^{-/-}$ cells (Figure 35B). Additionally, LIMK inhibition also resulted in decreased directionality of wt cells (Figure 35C). This effect was milder not fully reflecting the strong 'twist-and-turn' migration phenotype observed for untreated *Arhgef6*$^{-/-}$ cells. Moreover, in this setting, LIMK inhibition led to a further reduction of directionality in *Arhgef6*$^{-/-}$ cells (Figure 35C). However, as a result of the reciprocal effects of LIMKi3 treatment on velocity and directionality, the overall displacement of both wt and *Arhgef6*$^{-/-}$, respectively, was unaltered (Figure 35D).

Taken together, our results strongly imply that ARHGEF6 is indispensable for maintaining T cell migration pattern and morphology. ARHGEF6 deficiency leads to migratory defects characterized by increased velocity and decreased straightness of migrating $CD4^+$ T cells (on 2D ICAM-1 substrate) accompanied with altered lamellipodia morphology. Moreover, our data clearly showed that the observed migratory and morphological phenotype in *Arhgef6*$^{-/-}$ cells is a consequence of impaired LIMK activity and defective PAK2/LIMK1/cofilin signaling to actin dynamics.

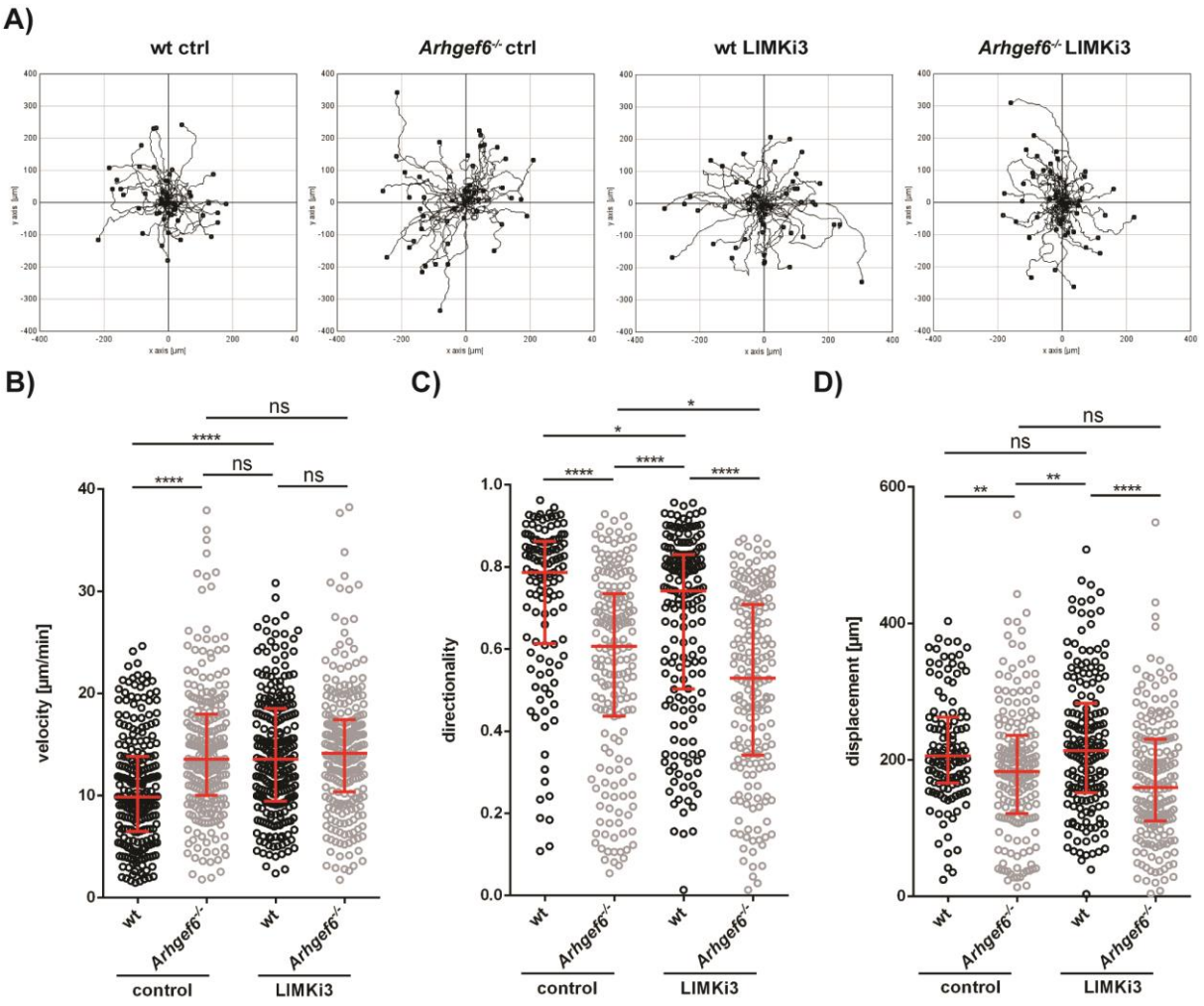

Figure 35. Migration parameters of wt and *Arhgef6*$^{-/-}$ $CD4^+$ T cells with or without LIMKi3 inhibitor at 10x (data provided by Dr. Mark Korthals)
Wt and *Arhgef6*$^{-/-}$ $CD4^+$ T cell were preincubated with solvent alone (ethanol control) or solvent containing 10 µM LIMKi3 for 4h before migration on ICAM-1. Migration was recorded at 10x magnification for 20 min. Cells were manually tracked in 20s intervals. A) Representative track plots from one experiment of control or LIMKi3 treated wt and *Arhgef6*$^{-/-}$ T cells migrating on ICAM-1. B) Quantification of the overall velocity of all cells tracked (control: 250 wt cells, 250 *Arhgef6*$^{-/-}$ cells; LIMKi3 treated: 250 wt cells, 247 *Arhgef6*$^{-/-}$ cells). C) and D) Quantification of directionality and displacement, respectively, only of cells moving faster than 10 µm/min (control: 120 wt cells, 188 *Arhgef6*$^{-/-}$ cells; LIMKi3 treated: 179 wt cells, 188 *Arhgef6*$^{-/-}$ cells). Scatter plots show results of all single cells derived from 4 independent experiments with red lines representing median with interquartile range. Significance was assessed by Mann–Whitney test. * p<0.05; ** p<0.01; *** p<0.001; **** p<0.0001.

3.13 Supplementary figures and movies

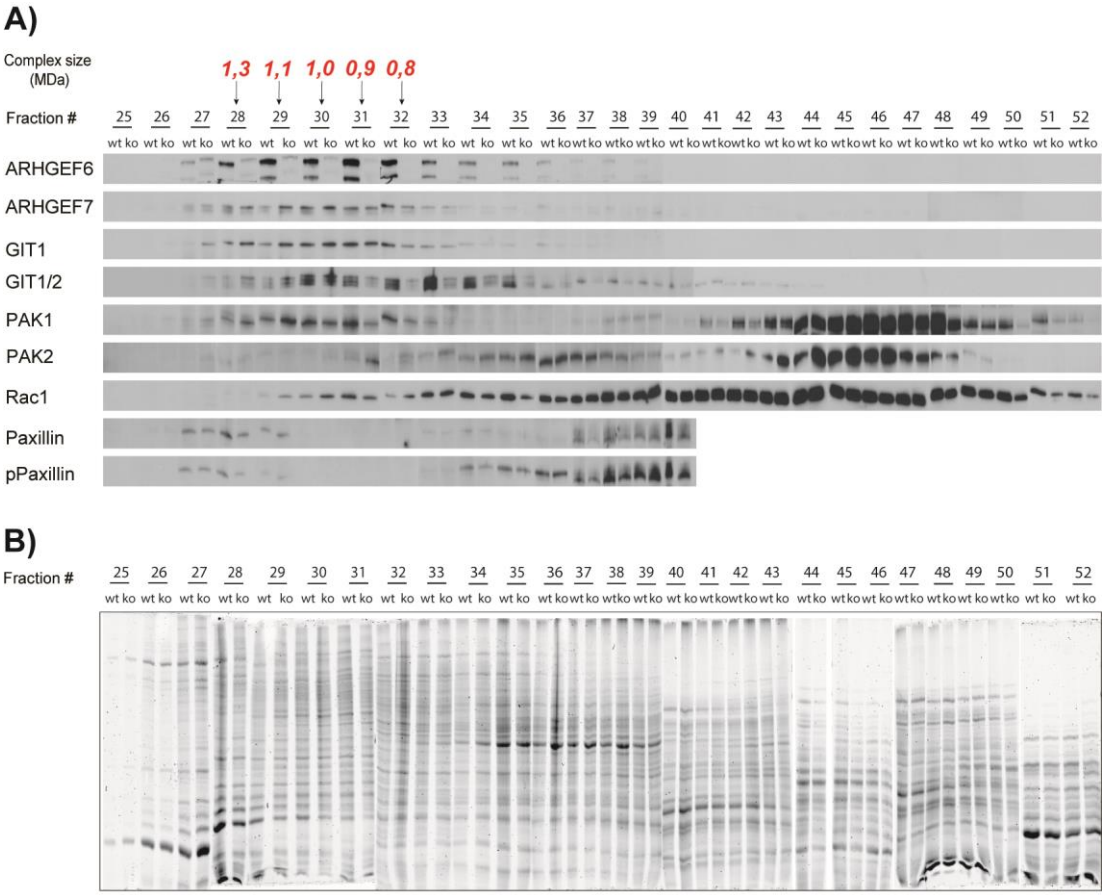

Supplementary figure 1. Distribution of PIX/GIT complex members in the presence and absence of ARHGEF6

A) Western blots showing gel filtration elution profiles of wt and *Arhgef6*$^{-/-}$ (ko) thymocytes using appropriate antibodies (as indicated on the left). The complex size is marked on the top. B) Coomassie gels of FPLC purification fractions (25-52) loaded in A. Equal amount of cell lysates was loaded in each fraction of both wt and *Arhgef6*$^{-/-}$ thymocytes.

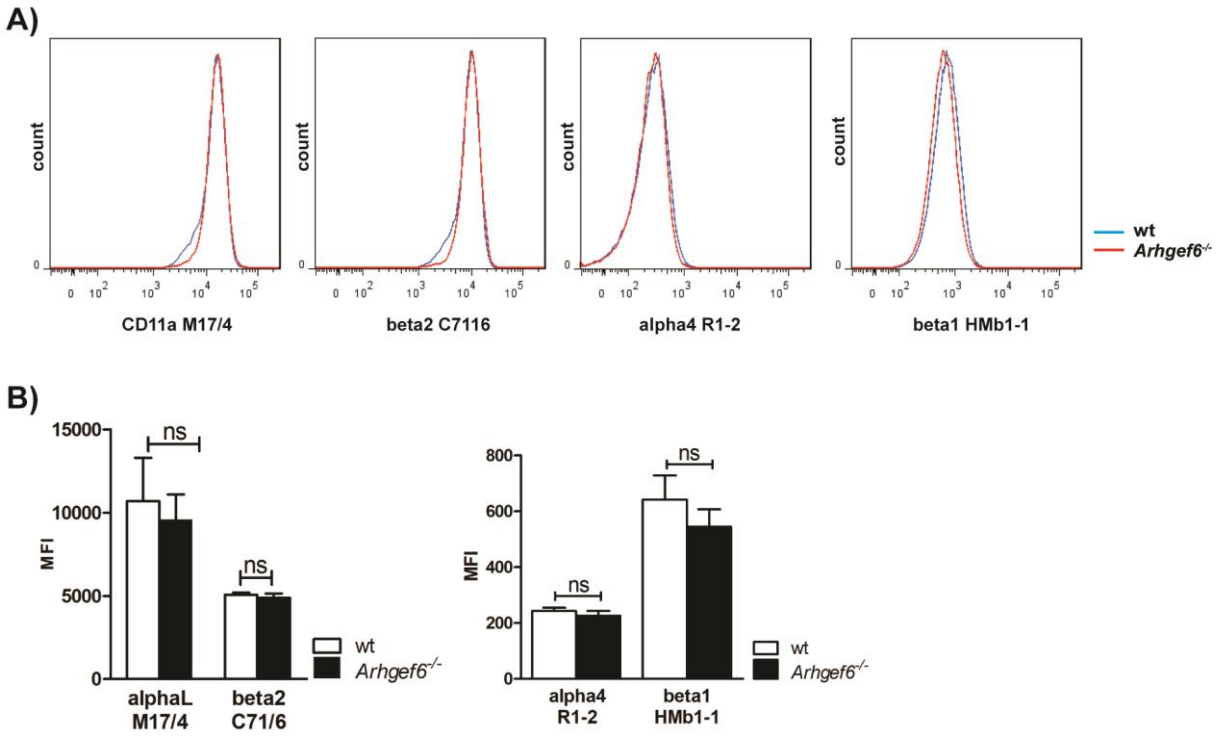

Supplementary figure 2. Unaltered integrin expression level in *Arhgef6*$^{-/-}$ compared to wt CD4^{+} T cells

A) Representative FACS histograms of wt (blue) and *Arhgef6*$^{-/-}$ (red) CD4^{+} T cells gated on CD4^{+} T cell population and stained for integrins with following antibodies: LFA-1 (CD11a) M17/4 Rat Anti-Mouse, Integrin β2 chain C7116 Rat Anti-Mouse-FITC, CD49d clone R1-2 Rat Anti-Mouse and Integrin β1 chain HMb1-1. B) Quantification of integrin expression level shown in A. Data on the graph represent mean ± SEM obtained from 3 independent experiments.

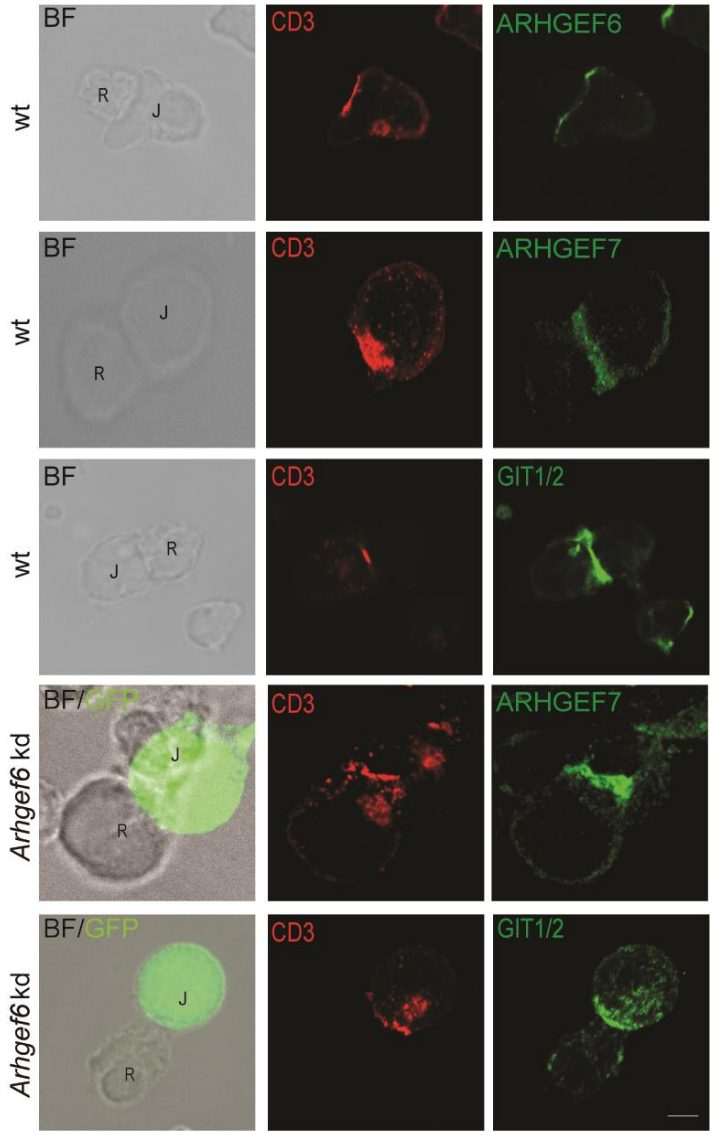

Supplementary figure 3. Recruitment of PIX/GIT proteins in immune synapse
Representative confocal images of ARHGEF6, ARHGEF7 and GIT1/2 immunofluorescence in wt and *Arhgef6* kd Jurkat cells, each forming immunosynapse with Raji cells. CD3 immunofluorescence indicates location of Jurkat cells and both Jurkat (J) and Raji (R) cells were labeled in bright field images. Transfected Jurkat cell- *Arhgef6* kd were represented with bright field/GFP overlay image. Scale bar, 5 µm.

Supplemental movies (attached CD)

Supplemental Movies 1 and 2: Bright field live cell imaging of a typical wt and *Arhgef6*$^{-/-}$ CD4^{+} T cells, magnification 10x.

Supplemental Movies 3 and 4: Bright field live cell imaging of wt and *Arhgef6*$^{-/-}$ CD4^{+} T cells, magnification 100x.

Supplemental Movies 5 and 6: TIRF live cell imaging of wt and *Arhgef6*$^{-/-}$ CD4^{+} T cells harboring Lifeact-GFP, magnification 100x.

Supplemental Movies 7 and 8: TIRF live cell imaging of wt and *Arhgef6*$^{-/-}$ CD4^{+} T cells harboring LentiBrite Paxillin-GFP, magnification 100x.

4. DISCUSSION

T cell migration is essential for efficient immune responses. It is strictly regulated and governed by mechanisms that are optimized for both the activation stage of the cell and for environment-specific cues (Krummel et al., 2016). The cellular movement is accomplished by integration of the extracellular and intracellular signals that lead to reorganization of the cellular structure, primarily actin cytoskeleton in lamellipodia at the leading edge and uropod at the trailing edge (Ratner et al., 1997; Sanchez-Madrid and del Pozo, 1999). It has been very well established that Rho family of small GTPases together with Rho GEFs play a central role in cell migration (Goicoechea et al., 2014; Hanna and El-Sibai, 2013; Ridley, 2015). Among Rho GEFs, ARHGEF7 which belongs to the PIX family of Rho GEFs, is one of the most extensively studied for its ubiquitious role in cell migration. The best known is the signaling through trimolecular GIT–PIX–PAK complex, which promotes Rac1 activity upon the interaction of GIT with paxillin in integrin-containing focal adhesions (Frank and Hansen, 2008; Kuo et al., 2011). ARHGEF7 drives cell migration by promoting lamellipodial protrusion and focal adhesion turnover in adherent cells, such as fibroblasts (Kuo et al., 2011).

Our group is interested in the role of another member of the PIX Rho GEF family, ARHGEF6, which besides ARHGEF7 is expressed only in immune cells and neurons. Our aim was therefore to decipher its role in lymphocyte migration and to understand why immune cells, which are highly motile, specifically express a second PIX variant. Although other groups observed impaired directional migration of Arhgef6 deficient neutrophils (Li et al., 2003), our first study showed that *Arhgef6* deficient T and B cells display increased basal migration as well as chemokinesis and chemotaxis in transwell assays (Missy et al., 2008). The following study demonstrated that also thymocyte migration was greatly increased in *Arhgef6* deficient mice in vitro as well as in live explanted thymic lobes. Moreover, increased motility of *Arhgef6* deficient thymocytes came along with increased displacement and decreased arrest intervals. Together, these data suggested that ARHGEF6 rather limits lymphocyte migration.

The present study was undertaken in order to further elucidate the role of ARHGEF6 in subcellular and molecular mechanism underlying migration of T cells. By in vitro live cell imaging on ICAM-1 coated 2D surfaces, we corroborated that TCR activated

Arhgef6$^{-/-}$ CD4^{+} T cells migrate faster than wt cells and, in addition, display a 'twist-and-turn' migration pattern resulting in reduced directionality – an unusual phenotype because most studies showed either that increased velocity was associated with straighter migration or that impaired directionality was associated with impaired overall motility. Using biochemical and fluorescence imaging techniques we detected several alterations in the expression level, molecular interactions and subcellular localization of typical ARHGEF6 interaction partners. In summary, our results led us to the conclusion that ARHGEF6 balances 3 signaling pathways in parallel, which together control speed and directionality of T cells (see also model Figure 36):
1. ARHGEF6 is required for PAK2 activation and subsequent LIMK dependent inactivation of cofilin. 2. At the same time, ARHGEF6 restricts lamellipodial Rac1 activity partially displacing ARHGEF7. 3. ARHGEF6 promotes assembly of focal complexes probably via its interaction with GIT2. On a cell biological level, we show that the ARHGEF6/Rac1/PAK2/LIMK/cofilin signaling module limits actin turnover by confining both lamellipodial actin polymerization and depolymerisation, enables formation of stable polarized lamellipodia, and promotes focal contact formation. As a consequence, ARHGEF6 facilitates straighter migration but also restricts migration speed. This study therefore establishes ARHGEF6 as an important regulator of migration in immune cells, which competes with ARHGEF7 functions by compensatory and complementary mechanisms.

4.1 ARHGEF6 controls PAK2 signaling in T cell migration

The most striking biochemical observation in T cells lacking ARHGEF6 was a dramatic decrease of active PAK2 levels. This was first shown in thymocyte samples, which display reduced PAK1/2 Thr423/402 phosphorylation and lower activity in a PAK2 kinase activity assay both under resting conditions as well as within minutes after TCR stimulation. In addition samples of cultured and in vitro activated CD4^{+} T cells showed strong specific reduction of PAK2 Thr402 phosphorylation. This result was surprising since WB and IF analyses of Arhgef6 deficient T cells at the same time revealed increased levels of total PAK2, increased levels of ARHGEF7, increased levels of active Rac1, and even accumulation of all 3 in lamellipodia. PAK2 interacts with the SH3 domain of both ARHGEF7 (Hoelz et al., 2006; Mott et al., 2005) and ARHGEF6 (Figure 14 *results*), therefore the interaction with ARHGEF7

may be responsible for its recruitment and localization in lamellipodia of *Arhgef6* deficient cells. However, in the absence of ARHGEF6, over-activated Rac1 is apparently not sufficient to induce full activity of PAK2 in T cells. These data are still in a line with experimental evidences showing that ARHGEF6 strongly stimulates PAK activity while ARHGEF7 has only a permissive effect (Daniels et al., 1999; Feng et al., 2002). This is also in line with a reported study showing that full PAK activation is regulated by both Rac1-dependent and Rac1-independent mechanisms (Itakura et al., 2013).

As a consequence of reduced PAK2 activity in *Arhgef6* deficient cells, we also observed reduced LIMK1 phosphorylation at Thr508 and, most prominently, reduced cofilin phosphorylation at Ser3 (by ~75% in qWB and ~50% in IF), especially within the lamellipodia region. The phosphorylation status of LIMK only partially correlates with its activity. Interestingly, reduced levels pLIMK1 in *Arhgef6* deficient cells was comparable to the level of pLIMK1 in wt cells treated with LIMKi3 inhibitor, whereas the same inhibitor did not influence LIMK1 phosphorylation in *Arhgef6* deficient cells. This suggests that LIMK1 was already inactive at the basal condition of *Arhgef6*$^{-/-}$ cells. Additional experiments (e.g. LIMK1 activity assay) are needed to corroborate this assumption. However, indirect evidence of reduced LIMK activity is the dramatic reduction of phosphorylation of its target molecule cofilin.

Using kinase specific inhibitors, we corroborated that ARHGEF6 indeed controls the canonical PAK/LIMK pathway to cofilin phosphorylation in murine T cells both in wt and *Arhgef6*$^{-/-}$. Besides LIMK, also the kinase TESK1, which is also expressed in T cells (www.immgen.org; (Heng et al., 2008)), was shown to phosphorylate cofilin at the same residue (Ser3) (Toshima et al., 2001a). However, our immunofluorescence data revealed a ~75% reduction of p-cofilin in wt cells upon inhibition of LIMK with LIMKi3 and further reduction in *Arhgef6*$^{-/-}$ cells to the same level. This reduction may even be underestimated (e.g. as compared to WB results), due to some degree of unspecific background binding of primary antibodies, which we could not exclude. Therefore, LIM kinases seem to be the major, if not the only kinases, involved in phosphorylation of cofilin Ser3 in both wt and *Arhgef6*$^{-/-}$ T cells. LIM kinases themselves may be activated via a number of routes involving many different kinases, including PAK and ROCK (Amano et al., 2001; Edwards et al., 1999; Ohashi et al., 2000; Scott and Olson, 2007). However, our results imply that reduced cofilin Ser3 phosphorylation in *Arhgef6* deficient T cells is exclusively based on reduced

PAK activity, because PAK inhibition by IPA3 in wt cells mimicked reduction of p-cofilin level in *Arhgef6*$^{-/-}$ cells, while the same treatment did not result in a further decrease in *Arhgef6*$^{-/-}$ cells. On the other hand, remaining p-cofilin levels after IPA3 treatment indicate the presence of other mechanisms probably involving Rho/ROCK (Thauland et al., 2017), which contribute to cofilin phosphorylation (via activation of LIMK), which are independent from ARHGEF6/PAK2 signaling.

Another possible explanation of decreased cofilin Ser3 phosphorylation in *Arhgef6*$^{-/-}$ T cells might be increased dephosphorylation of cofilin. The most prominent phosphatases involved in this cofilin activation process is slingshot (Mizuno, 2013), which in addition may also downregulate LIMK1 activity (Soosairajah et al., 2005) as well as PP1 and PP2A, which can dephosphorylate cofilin in T cells (Ambach et al., 2000). Indeed, our preliminary data showed slightly increased level of Slingshot in *Arhgef6* deficient T cells, especially in lamellipodia regions (not shown). Further investigation of phosphatase activity is required to test the significance of this observation. It has been shown in neurons that PAK4, a group II PAK family member, can phosphorylate both LIMK as well as Slingshot, thereby activating LIMK and inhibiting slingshot, which together strongly promotes inactivation of cofilin (Soosairajah et al., 2005). Therefore, it would be interesting to know if ARHGEF6/Rac1/PAK2 signaling may also play a role in the inactivation of cofilin phosphatases in T cells.

Cofilin is activated in human primary T cells via a Ras/MEK/PI3K pathway upon TCR activation in the presence of costimulation or upon chemokine stimulation (Klemke et al., 2010; Wabnitz et al., 2006). In our migration experiments we used murine primary in vitro activated CD4^{+} T cells, which should favour cofilin activation. Our results, however, demonstrate that under these conditions ARHGEF6 is still required to limit cofilin activation. Since ARHGEF6 and PAK2 are also involved in TCR signaling (Missy et al., 2008), and since PAK1/2 can phosphorylate members of the Ras/MAPK pathway (Beeser et al., 2005; Slack-Davis et al., 2003; Sun et al., 2000), the interplay of these pathways might balance the cofilin activity status in activated T cells. It will be particularly important to know, if the presence or absence of costimulation differentially affects PAK2 and PI3K activation.

Several studies show that both cofilin and PAK2 are required for motility in general and especially in directed migration. Cell directionality is maintained by limiting membrane protrusion to one direction and increasing cofilin activity locally in

lamellipodia at the leading edge during directed migration of T cells and neutrophils (Nishita et al., 2005; Tang et al., 2011). Particularly, the homeostatic balance between LIMK1 and slinghshot has a crucial role in lamellipodium formation and directional cell migration (Nishita et al., 2005). It has also been reported that PAK activity has an important role in chemotaxis of human neutrophils and that its inhibition leads to loss of their directionality (Itakura et al., 2013). PAK and PI3K are also both involved in the spatially confined promotion of Rac and/or Cdc42 activation required for the establishment of cell polarity, directional sensing and chemotaxis in neutrophils and fibroblasts (Campa et al., 2015; Cau and Hall, 2005; Itakura et al., 2013; Li et al., 2003; Xu et al., 2003).

Interestingly, the PAK2/LIMK/cofilin pathway can be hijacked by lentiviruses to evade immune responses. Binding of Nef proteins to PAK2 leads to PAK2 over-activation, LIMK dependent cofilin inactivation, impairment of membrane ruffling and inhibition of motility in human T cells and other cells (Stolp et al., 2009). These defects could partially be rescued by simultaneous knockdown or co-expression of a dominant negative PAK2 mutant. In addition, impaired membrane ruffling could also partially be mimicked by expression of a constitutively active PAK2 mutant. This study therefore supports our observation that signaling via ARHGEF6/PAK2/LIMK/cofilin limits migration in T cells. Interestingly, Nef proteins have also been found to interact with the PIX-GIT complex (Brown et al., 1999; Vincent et al., 2006) and block thymocyte development, thereby resembling the phenotypes of *Arhgef6* deficient mice (Korthals et al., 2014) and mice with T cell-specific PAK2 deficiency (Phee et al., 2014). The latter study revealed that PAK2-dependent actin rearrangements are required for normal TCR (and IL-2) signaling via PLCγ1 and Ras/MAPK pathways, but the relevant target of PAK2 kinase activity in this process have not yet been identified. It would be interesting to know, on the one hand, if ARHGEF6 also regulates these pathways, and, on the other hand, if LIMK dependent cofilin inhibition is involved in thymocyte signaling. Surprisingly, although PAK2 deficiency reveals maturation defects in thymocytes, which may lead to defective egress from the thymus. It is not known however, how motility of PAK2 deficient lymphocytes is affected. We may speculate that, similar to *Arhgef6*$^{-/-}$ cells, these cells are also more motile than their wild-type counterparts. Cofilin is highly expressed in thymocytes (Brieher et al., 2006) and plays a specific role in early T cell development (Seeland et al., 2018).

Increased cofilin activity in immune cells might have different impact when comparing migration in 2D vs 3D substrates or less spatially confined vs strongly confined surroundings or when looking at cells with different activation status. Klemke et al. (2010) found that interference with cofilin activation specifically reduced speed and directionality of freshly prepared human T cells chemotactically migrating in a 3D matrix while chemokine-induced 2D amoeboid T cell migration was not affected. The authors argued that (unconfined) 2D amoeboid migration compared to 3D migration is mainly driven by adhesion and actino-myosin mediated contraction than by actin polymerization, thereby limiting the requirement for actin turnover. Sidani et al. (2007) on the other hand, found that cofilin knockdown in apolar randomly moving amoeboid metastatic tumor cells (MTLn3) induced an elongated polar morphology and the switch to even faster but also straighter mesenchymal-type mode of migration on a 2D surface. However, under all conditions we tested, 2D, transwell and in vivo migration (only thymocytes), *Arhgef6* deficient murine thymocytes, naïve and activated T cells, B cells and human T cell lines showed generally increased basal as well as chemokine induced migration ((Korthals et al., 2014; Missy et al., 2008; Tedford et al., 2017); this study). Our cultured activated $CD4^+$ T cell blasts are already highly motile on 2D even in the absence of chemokines (or serum) and are very sensitive to LIMKi3 inhibition, which implies that these cells already use pronounced actin polymerization. By providing actin monomers and barbed ends, active cofilin may accelerate actin polymerization in the lamellipodium. Indeed, cofilin and Rac mediated actin polymerization synergize with each other in promoting an increased actin network in lamellipodium (Bravo-Cordero et al., 2013). Indeed, we detected strong actin accumulation at the TIRF excitation zone (up to 200 nm penetration depth corresponding to the level of focal contacts) in lamellipodia of *Arhgef6*$^{-/-}$ T cells. Moreover, this LIMK-dependent increase of actin dynamics led to more numerous, wider and larger lamellipodia often displaying an extra-long wide “hammer-head” -like form. Finally, our data convincingly proved that these morphological changes, the increased overall motility but impaired directionality of activated *Arhgef6* deficient T cells migrating on 2D surfaces were indeed attributable to impaired LIMK1 dependent inactivation of cofilin, because treatment with LIMKi3 mimicked all phenotypes in wt cells without affecting *Arhgef6*$^{-/-}$ T cells. Yet, we found additional alterations in signaling modules, which may act independently from the

LIMK/cofilin pathway, and may contribute to some phenotypical aspects of *Arhgef6* deficient cell migration.

4.2 ARHGEF6 regulates ARHGEF7 signaling in T cell migration

The finding that deletion of ARHGEF6 in both thymocytes and $CD4^+$ T cells results in higher expression of ARHGEF7 and increased GTP-Rac1 levels led us to the hypothesis that in *Arhgef6*$^{-/-}$ cells ARHGEF7 can replace ARHGEF6 in the PIX/GIT complex and can recruit and activate Rac1. Both BN-PAGE and FPLC clearly showed that in the absence of ARHGEF6 the PIX/GIT complex becomes larger and is particularly enriched with ARHGEF7 indicating that both PIX variants may compete for binding to the complex. Together with our observation that both ARHGEF7 and active Rac1 were prominently concentrated in lamellipodia of *Arhgef6* deficient $CD4^+$ T cells, these data suggest that ARHGEF7 not only compensates for the loss of ARHGEF6, but also governs the subcellular localization of the PIX/GIT complex towards the leading edge of the migratory cell resulting in Rac over-activation in the lamellipodium.

Rac1 activates the WAVE complex at the leading edge, which in turn recruits and activates the Arp2/3 complex (Ridley, 2011). The role of this complex in assembly and protrusion of a branched actin network at the leading edge has been well established in both adherent and motile cells, such as fibroblasts and Jurkat T lymphocytes, respectively (Nicholson-Dykstra and Higgs, 2008). Active Rac1 thus affects lamellipodia dynamics being responsible for membrane ruffling and generating sheet-like protrusions, thereby influencing cellular migration (Pankov et al., 2005; Steffen et al., 2013). Particularly, it was shown in primary human fibroblasts, that lower Rac activity facilitates directionality with variable velocities and higher Rac activity promotes random migration with medium velocity (Pankov et al., 2005). Interestingly, over-expression of ARHGEF7 in fibroblasts or neurons, respectively, was also shown to induce increased Rac activity, and both overexpression of ARHGEF7 or expression of constitutively active Rac1 lead to formation of multiple protrusions (Cau and Hall, 2005; Zhang et al., 2003). Accordingly, knockdown of Arhgef7 in fibroblasts and epithelial cells results in speed reduction and directionality defects probably due to Rac1 mislocalization (Cau and Hall, 2005; ten Klooster et al., 2006; Yu et al., 2015). Therefore, ARHGEF7-induced

over-activation of Rac1 may contribute to the observed phenotypes in *Arhgef6* deficient $CD4^+$ T cells, such as larger and more numerous lamellipodia and hyper motility. Of course, we cannot rule out that other GEFs, such as Vav or Dock family members among many others, which are also expressed in T cells (Nimnual et al., 1998), may participate in altered Rac activity in *Arhgef6*$^{-/-}$ T cells.

Rac hyperactivity in *Arhgef6*$^{-/-}$ T cells may not only be explained by a mere overexpression of ARHGEF7 but also by altered regulation of ARHGEF7 itself. Indeed, it is possible that this could be mediated by PAK2, since both ARHGEF6 and ARHGEF7 have been described as a phosphorylation target for PAK2 (Koh et al., 2001; Rennefahrt et al., 2007; Shin et al., 2002). An interesting observation in T cell specific *PAK2*$^{-/-}$ mice was that Rac activity was indeed increased in *PAK2*$^{-/-}$ thymocytes, resulting also in increased F-actin levels (Phee et al., 2014). Such a negative feedback has also been observed in human cell lines, where PAK mediated phosphorylation of the Rac GEF PREX2 leads to Rac inhibition (Barrows et al., 2015).

ARHGEF7, like ARHGEF6, is also known as an activator for Cdc42. In astrocytes, it was shown that ARHGEF7 is targeted to the leading edge by interaction with the polarity protein hScrib (which does not bind to ARHGEF6) (Osmani et al., 2006). This interaction was required for Cdc42 recruitment to the leading edge, Cdc42 activation, local protrusion formation and establishment of a polarized phenotype during migration. Our data revealed less GTP-bound Cdc42 in the absence of ARHGEF6, which is in line with our observation that lamellipodia formation is less confined in *Arhgef6* deficient T cells. ARHGEF6 is indeed also directly involved in the local Cdc42 activation at the leading edge of neutrophils by PAK1 mediated recruitment upon chemokine receptor signaling (Li et al., 2003). Interestingly, knockdown of Cdc42 in neutrophils or genetic ablation of Cdc42 in DCs results in formation of multiple short-lived active Rac containing leading edges (Lammermann et al., 2009; Srinivasan et al., 2003) resembling the morphological phenotypes induced by ARHGEF7 overexpression. The presence of ARHGEF6 is therefore required for balanced activation of Rac1 and Cdc42 in the establishment of T cell polarity and directed migration.

Taken together, ARHGEF7/Rac1 dependent signaling defects could also explain most of the morphological and migratory phenotypes in *Arhgef6* deficient T cells. As pointed out above, Rac and cofilin cooperate in promoting actin turnover during

migration, so that over-activation of both should amplify actin turnover, protrusion formation and migration speed but due to less spatial confinement also impairs clear polarization of the cell. Indeed, *Arhgef6*$^{-/-}$ T cells still migrated less straight than wt cells upon treatment with LIMKi3, which therefore could be explained by additional Rac over-activation.

The fact, however, that LIMK inhibition already phenocopied the morphological and most of the migratory defects of *Arhgef6* deficiency in wt T cells migrating on 2D suggests that under these conditions other mechanisms may limit the impact of increased actin turnover. Particularly, on unconfined 2D substrates, cells more strongly depend on adhesion and contractility than in confined 3D matrices (Lammermann and Sixt, 2009). Therefore, the contribution of both signaling defects may vary for example in 3D interstitial migration, where adhesive and contractile forces play only minor roles in the cellular locomotion. Further, in vitro imaging in 3D matrices, such as collagen gels with different pore sizes or 2-P imaging in vivo could be helpful to study ARHGEF6 function in immune cell migration under conditions, which are less dependent on adhesion but more dependent on coordinated actin polymerization. In addition, incorporation of immune cells with much more complex morphologies in these assays, such as DCs, microglia or dendritic epithelial T cells may also reveal cell type dependent requirements for ARHGEF6. For example, although Cdc42 deficiency in DCs results in morphological alterations resembling the *Arhgef6*$^{-/-}$ phenotypes and show normal (or even increased) actin turnover, their motility is dramatically impaired because they entangle in the ECM network (Lammermann et al., 2009).

4.3 Possible role of ARHGEF6 in adhesion formation

Besides actin turnover, locomotion of immune cell requires friction forces, which can be achieved by stickiness or pressure. On a 2D substrate this is mediated by adhesion and contractility of the cell. In a 3D surrounding, spatial confinement may be sufficient, unless the matrix meshwork becomes too dense, which can only be overcome by contractile forces squeezing cell body and nucleus through the gaps (Lammermann et al., 2008). Although lymphocytes are only weakly adherent and do not show large stable focal adhesion structures, they use transient adhesions during migration on 2D surfaces (Smith et al., 2005; Smith et al., 2007; Stanley et al., 2008).

LFA-1 mediated adhesion to ICAM-1 in migrating T cells is organized in a way that LFA-1 is enriched at a central focal zone (mid zone), where it is also present in the most active open conformation. In the lamellipodium LFA-1 is much less abundant, visible as transient focal dots, and displaying the closed intermediate active conformation. Most LFA-1 molecules are located in the uropod, where they are most probably inactive and not in contact with the ligand. In contrast to strongly adherent cells, this more dynamic contact formation permits high speed migration and rapid turning of immune cells.

Motility of cells on 2D substrates is a function of adhesion with highest motility at intermediate adhesion strength. This relation is nicely demonstrated by the fact that LFA-1 blockage in vitro or ICAM-1 deficiency in vivo (Katakai et al., 2013) as well as expression of a constitutively active LFA-1 mutant in mice (Semmrich et al., 2005) all result in reduced T cell migration speed and very similar immune phenotypes. Therefore, small or severe changes in the intrinsic regulation of adhesion dynamics may alter the dependency of migration speed and directionality on adhesion strength.

The PIX/GIT complex, as part of the 'molecular clutch' described in chapter 1.5, functions as a "molecular hub", which mobilizes proteins involved in the maturation and turnover of focal contacts (Frank and Hansen, 2008). Therefore, it is not surprising that our study revealed impaired localization of main focal contacts components in *Arhgef6*$^{-/-}$ T cells on ICAM-1. Specifically, by TIRF microscopy of immunostained fixed cells and live cells expressing a paxillin biosensor, we observed paxillin enrichment in the mid zone and short-lived, spot-like signals in the lamellipodia of wt cells, which matches the expected pattern of LFA-1-ICAM-1 binding of migrating T cells. In contrast, *Arhgef6* deficient T cells displayed a global reduction of total paxillin, p-paxillin (Tyr118), and vinculin in the mid zone as well as in the lamellipodium, and completely lacked focal signals of the paxillin biosensor in the lamellipodium.

Paxillin and vinculin are main components of focal adhesions, the first involved in assembly and disassembly (dynamics) (Steffen et al., 2013), the latter involved in maintenance (Carisey and Ballestrem, 2011; Turner et al., 1990) of focal contacts. Both colocalize with each other and with both LFA-1 or VLA-4 mediated adhesions in Jurkat T cells (Jankowska et al., 2018). Paxillin binds to α4 integrin subunit of VLA-4 integrin upon the binding of this integrin to its ligand, VCAM-1. This event supports LFA-1 integrin mediated T cell migration (Rose et al., 2003). In our initial 2D

migration experiments, cells migrating on combined ICAM-1 and VCAM-1 were generally slightly faster and straighter than on ICAM-1 alone, whereas VCAM-1 alone did not support migration. In our model, we used only ICAM-1. However, paxillin may have an impact in an indirect manner on LFA-1 integrin by controlling actin-dependent LFA-1 clustering (Romanova and Mushinski, 2011). Although overall surface expression of both LFA-1 and VLA-4 was not changed in *Arhgef6* deficiency, their avidity might be altered leading to reduced adhesion.

Indeed, fibroblasts isolated from both paxillin null mice (Hagel et al., 2002) or from vinculin knock-out mouse embryos (Xu et al., 1998) displayed smaller focal adhesions and impaired cell spreading. Although FAK-dependent phosphorylation of paxillin Tyr118 has been shown to be required for focal adhesion formation and reorganization of the cytoskeleton in motile cells (Nakamura et al., 2000; Zaidel-Bar et al., 2003; Zaidel-Bar et al., 2007), vinculin deficient embryonic fibroblasts or carcinoma cells displayed even faster migration. The fact that tight adhesion via LFA-1-ICAM-1 interaction rather forces T cells to stop migration (e.g. in response to TCR stimulation) supports our idea that loosened adhesion of *Arhgef6* deficient T cells makes them more motile. We have already shown that *Arhgef6*$^{-/-}$ T cells do not efficiently build and organize an immune synapse and resist TCR-mediated stop signals (Korthals et al., 2014; Missy et al., 2008). But we can only indirectly deduce the molecular mechanism of how ARHGEF6 controls focal contact stability. However, these adhesion defects are clearly in line with the alterations in the stoichiometry of the PIX/GIT complex in the absence of ARHGEF6 and also with all ARHGEF6 dependent signaling defects we observed.

First, it has been reported that paxillin binds to both GIT1 and GIT2, thus recruiting the PIX/GIT complex to focal adhesions where it functions to regulate their maturation and disassembly (Schmalzigaug et al., 2007). GIT2 is higher expressed than GIT1 in murine T cells but *Arhgef6* deficiency leads to GIT2 protein destabilization (Missy et al., 2008). A direct role for GIT2 in LFA-1 mediated adhesion has not been investigated so far. But interestingly GIT2 and ARHGEF6 play very similar roles in LFA-1 dependent processes: GIT2 and ARHGEF6 together are recruited to the immune synapse ((Kong et al., 2014; Ku et al., 2001); this study). And finally, *GIT2*$^{-/-}$ thymocytes and T cells, respectively, are more motile on ICAM-1 coated substrates in vitro even in the presence of stop signals ((Phee et al., 2010);

and own unpublished data). It is therefore very reasonable to conclude that ARHGEF6 is required for GIT2-mediated stabilization of LFA-1 dependent adhesion.

Increased Rac activity may additionally contribute to the phenotypes of ARHGEF6 deficiency via its effect on the turnover of focal contacts. Using different cell lines, ten Klooster et al. (2006) have shown that ARHGEF7 interaction with Rac1 is required for Rac1 targeting to focal adhesions. They also demonstrated reduced Rac1 activity after adhesion in mouse embryonal fibroblast where *Arhgef7* was silenced, supporting an important role of ARHGEF7 in adhesion-induced Rac1 activation. The importance of ARHGEF7 in promoting focal adhesion turnover required for fibroblast migration Kuo et al. (2011) could also be relevant in lymphocytes.

A third possible explanation for impaired adhesion of *Arhgef6*$^{-/-}$ T cells is given again by the reduced PAK2 activity. Among the many targets of PAK2 are also regulatory myosin light chain, e.g. in Jurkat T cells (Chew et al., 1998; Ramos et al., 1997), as well as paxillin (Lee et al., 2013). In addition, since PAK1 can phosphorylate GIT1 (Webb et al., 2006), it is tempting to speculate that PAK2 may also phosphorylate GIT2. It is therefore highly likely that PAK2 additionally regulates PIX/GIT function in the turnover of focal contacts via phosphorylation of paxillin and GIT2.

Although we can only speculate about the exact molecular mechanism, ARHGEF6 seems to be required for proper adhesion formation not only during immune synapse formation (Missy et al., 2008) but also during integrin dependent migration.

Imaging migration under conditions where adhesion becomes much more relevant, could help to complete the picture of the specific impact of ARHGEF6 on different modes of immune cell migration. For example, live imaging of antigen specific T cells in LN of immunized mice could be used to analyze if ARHGEF6 plays a role in the switch from an explorative to a more confined exploiting migration mode and further to a complete arrest. Particularly, it would be interesting, if in this 3D setting increased speed or increased meandering of *Arhgef6*$^{-/-}$ cells may dominate and thereby alter the overall displacement. The same model could also be used to study the re-acquisition of high motility after completion of activation.

The switch between different migration modes is also relevant for migration on the inner vessel walls where T cells are exposed to the shear force applied by the blood flow. This situation involves a complex interplay of tight LFA-1 dependent adhesion (required for resistance against the flow), which is yet accompanied by active migration on the endothelial surface followed by arrest, spreading, invasive

pseudopod formation and final chemokine attracted extravasation. In vitro model systems for flow or transendothelial migration could be used to investigate a possible role of ARHGEF6 in the coordination of these processes.

4.4 Conclusion and future outlook

Our data provided molecular evidences that explain the defective morphology and migration phenotype of *Arhgef6* deficient $CD4^+$ T cells. In these cells the signaling pathway involving Rac1/PAK2/LIMK/cofilin to actin and focal contact dynamics is greatly impaired. The absence of ARHGEF6 leads to increased ARHGEF7 and Rac1 activation, reduced PAK2 and LIMK1 activity and increased cofilin activation. Subsequently, that changed actin remodeling in lamellipodium at the leading edge. The absence of ARHGEF6 also altered the level of paxillin and vinculin, which are central for the assembly of focal contacts. These cytoskeletal signaling defects elucidates the observed migratory phenotype of *Arhgef6*$^{-/-}$ $CD4^+$ T cells (Figure 36). Although ARHGEF6 seems to control several signaling pathways in parallel, it is possible that the major effector involved in these pathways is PAK2, making the ARHGEF6/PAK2 a master signaling module that balances migration and adhesion in immune cells.

Assuming that ARHGEF6 might be an import player in the switch between different modes of T cell migration, expression or activity of ARHGEF6 should be tightly regulated. Interestingly, transcript databases imply that ARHGEF6 is a much more regulated protein in immune cells than ARHGEF7 (www.immgen.org; (Heng et al., 2008)). For example ARHGEF6 seems to be upregulated during thymocyte positive selection or in activated T cells, where probably increased adhesion capacity is required in order to allow for transient or stable interaction with antigen-presenting cells (Korthals et al., 2014). This could also be relevant for firm attachment of activated T cells to integrin ligands on endothelial cells in order to resist the blood flow and to transmigrate through the vessel wall into inflamed tissue. To date, there is only little known about the functional regulation of ARHGEF6. Recruitment of ARHGEF6 by signals through the TCR, integrins or chemokine receptors clearly imply that presence of ARHGEF6 is particularly required when strong adhesion or directional movement is wanted. In some studies it has been published that ARHGEF6 (next to other signaling molecules also including PAK2) can be

phosphorylated upon stimulation of TCR signaling (Mayya et al., 2009) or chemokine receptor signaling (Wojcechowskyj et al., 2011). It will be interesting to find out the relevant kinases and if these phosphorylation events are significant modulations of ARHGEF6 activity.

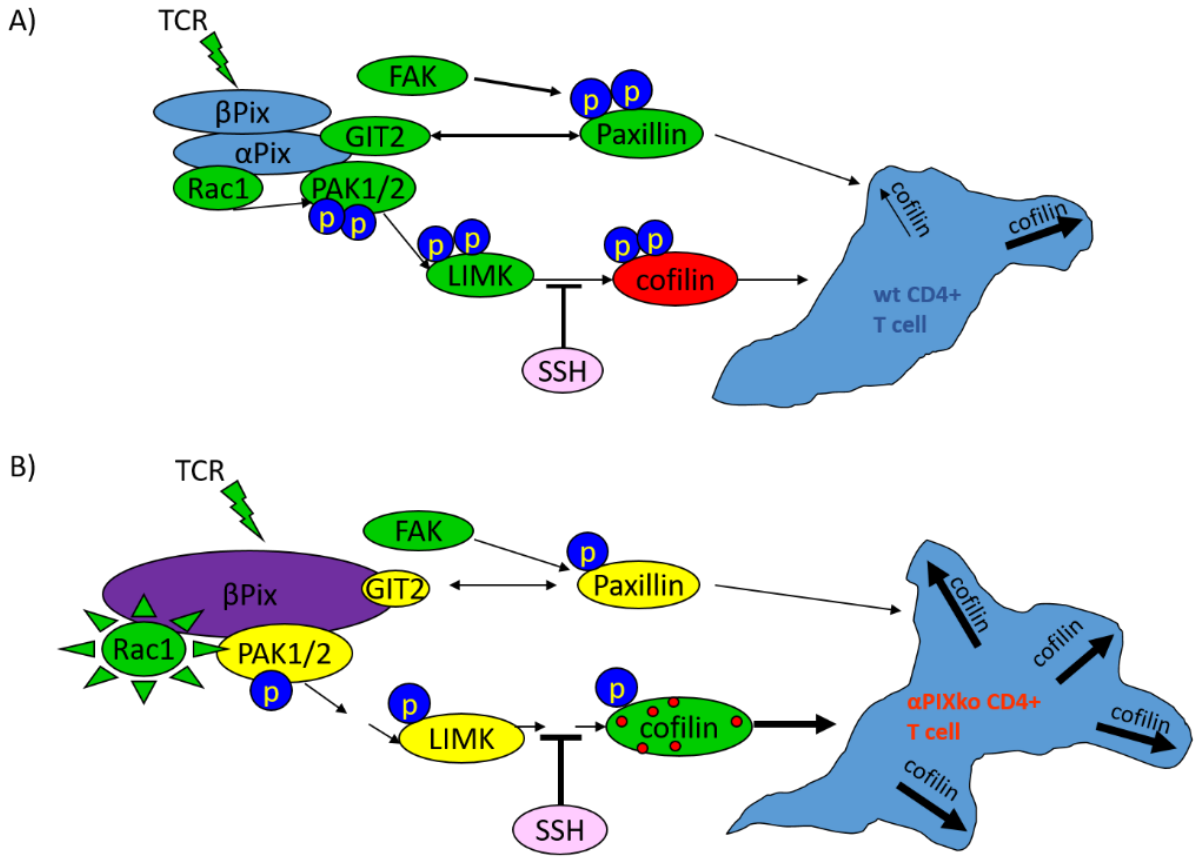

Figure 36. Model showing the role of ARHGEF6 in balancing distinct signaling pathways regulating lymphocyte morphology and migration
A) In wt cells ARHGEF6 maintains GIT2 stability and proper signaling through Rac1/PAK2/LIMK/cofilin thereby influencing actin and paxillin turnover. B) The absence of ARHGEF6 leads to ARHGEF7 accumulation, increased activity of Rac1, decreased activity of PAK2 and LIMK, over-activation of cofilin resulting in altered actin dynamics and paxillin turnover. The cell is dominated with several simultaneous protrusion directions leading to impaired morphology and migration pattern. *Bold arrows denote enhanced activation or inhibition.*

Future studies should also reveal the role of other PIX/GIT complex components and their downstream targets in immune synapse formation, synapse maintenance and subsequent impact of this on immune response. Especially, it is important to decipher the specific role of ARHGEF7 in this process. ARHGEF7 is upregulated in cells with *Arhgef6* deficiency and some of the observed phenotypes (e.g. Rac1 over-activation) might be attributed to its overexpression. As previously described, the reduction of ARHGEF7 in fibroblasts and epithelial cells results in speed reduction and

directionality defect probably due to Rac1 mislocalization (Cau and Hall, 2005; ten Klooster et al., 2006; Yu et al., 2015). Therefore, future experiments should employ *Arhgef7*$^{-/-}$ as well as double *Arhgef6*$^{-/-}$/*Arhgef7*$^{-/-}$ CD4^{+} T cells.

As previously described, ARHGEF6 harbors several specific domains involved in assembly of multimolecular complexes controlling cytoskeleton organization, cell polarity and migratory behavior. Further interest will be to dissect the role of specific ARHGEF6 domain(s) in T cell migration and to identify which domain(s) may preclude observed defects in *Arhgef6* deficiency. For this purpose shRNA together with simultaneous rescue expression may be used.

We believe that our study brought new insights into understanding how ARHGEF6 integrates different signaling pathways affecting morphology, motility and adhesion of immune cells, which are required for proper immune response.

5. ABBREVIATIONS

2D BN PAGE	2D blue native polyacrylamide gel electrophoresis
ADF	actin-depolymerizing factor
ADHD	attention deficit hyperactivity disorder
APC	antigen presenting cell
Arf	ADP-ribosylation factor
ArfGAP	Arf GTPase-activating protein
Arp2/3	actin-related protein-2/3
ATP	adenosine triphosphate
BF	bright field
BM	bone marrow
CCL	chemokine (C-C motif) ligand
Cdc42	cell division control protein 42 homolog
CH	calponin homology domain
co-IP	co-immunoprecipitation
CRIB	Cdc42/Rac1 interaction/binding region
cTEC	cortical thymic epithelial cell
CXCL12	C-X-C motif chemokine 12
DC	dendritic cell
DH	Dbl homology domain
DN	double negative
DP	double positive
ECM	extracellular matrix
ETP	early thymocyte progenitors
FA	focal adhesion
FACS	fluorescence-activated cell sorter
F-actin	filamentous actin

FAK	focal adhesion kinase
FPLC	fast performance liquid chromatography
GAPDH	glyceraldehyde 3-phosphate dehydrogenase
GDP	guanosine diphosphate
GFP	green fluorescent protein
GIT	G protein–coupled receptor kinase–interacting protein
GPCR	G protein-coupled receptor
GTP	guanosine triphosphate
ICAM-1	intercellular adhesion molecule 1
IF	immunofluorescence
IFN-γ	interferon gamma
IL	interleukin
ILK	integrin-linked kinase
KID	kinase inhibitory region
LFA-1	lymphocyte function-associated antigen 1
LIMK1	LIM domain kinase 1
MAPK	mitogen-activated protein kinase
MEK	mitogen-activated protein kinase kinase
MHC	major histocompatibility complex
mTEC	medullary thymic epithelial cell
PAK	p21-activated kinase
PH	pleckstrin homology domain
PI3K	phosphoinositide 3-kinase
PIX	PAK-interacting exchange factor
PKL	paxillin-kinase linker protein
PLC	phospholipase C
PP1	protein phosphatase 1
PP2A	protein phosphatase 2A

PtdIns(4,5)P2	phosphatidylinositol 4,5-bisphosphate
qWB	quantitative western blot
Rac1	Ras-related C3 botulinum toxin substrate 1
Rho	Ras homologous protein
RhoGAP	RhoGTPase activating protein
RhoGDI	RhoGTPase guanosine nucleotide dissociation inhibitor
RhoGEF	RhoGTPase guanine nucleotide exchange factor
ROCK	Rho-associated protein kinase
S1P	sphingosine-1-phosphate
S1PR1	sphingosine-1-phosphate receptor 1
SDS-PAGE	sodium dodecyl sulphate polyacrylamide gel electrophoresis
SH3	Src homology 3 domain
shRNA	short hairpin RNA
SP	single positive
SSH1L	Slingshot-1
TCR	T cell receptor
TESK	testis-specific protein kinase
TGFβ	transforming growth factor beta
Th	T helper
TIRF	total internal reflection fluorescence
VCAM-1	vascular cell adhesion molecule 1
VLA-4	very late antigen-4
wt	wild-type

6. REFERENCES

Allende, M.L., J.L. Dreier, S. Mandala, and R.L. Proia. 2004. Expression of the sphingosine 1-phosphate receptor, S1P1, on T-cells controls thymic emigration. *J Biol Chem*. 279:15396-15401.

Amano, T., K. Tanabe, T. Eto, S. Narumiya, and K. Mizuno. 2001. LIM-kinase 2 induces formation of stress fibres, focal adhesions and membrane blebs, dependent on its activation by Rho-associated kinase-catalysed phosphorylation at threonine-505. *Biochem J*. 354:149-159.

Ambach, A., J. Saunus, M. Konstandin, S. Wesselborg, S.C. Meuer, and Y. Samstag. 2000. The serine phosphatases PP1 and PP2A associate with and activate the actin-binding protein cofilin in human T lymphocytes. *Eur J Immunol*. 30:3422-3431.

Arber, S., F.A. Barbayannis, H. Hanser, C. Schneider, C.A. Stanyon, O. Bernard, and P. Caroni. 1998. Regulation of actin dynamics through phosphorylation of cofilin by LIM-kinase. *Nature*. 393:805-809.

Audebert, S., C. Navarro, C. Nourry, S. Chasserot-Golaz, P. Lecine, Y. Bellaiche, J.L. Dupont, R.T. Premont, C. Sempere, J.M. Strub, A. Van Dorsselaer, N. Vitale, and J.P. Borg. 2004. Mammalian Scribble forms a tight complex with the betaPIX exchange factor. *Curr Biol*. 14:987-995.

Bagrodia, S., S.J. Taylor, K.A. Jordon, L. Van Aelst, and R.A. Cerione. 1998. A novel regulator of p21-activated kinases. *J Biol Chem*. 273:23633-23636.

Baird, D., Q. Feng, and R.A. Cerione. 2005. The Cool-2/alpha-Pix protein mediates a Cdc42-Rac signaling cascade. *Curr Biol*. 15:1-10.

Bajenoff, M., J.G. Egen, L.Y. Koo, J.P. Laugier, F. Brau, N. Glaichenhaus, and R.N. Germain. 2006. Stromal cell networks regulate lymphocyte entry, migration, and territoriality in lymph nodes. *Immunity*. 25:989-1001.

Bajenoff, M., N. Glaichenhaus, and R.N. Germain. 2008. Fibroblastic reticular cells guide T lymphocyte entry into and migration within the splenic T cell zone. *J Immunol*. 181:3947-3954.

Barrows, D., S.M. Schoenfeld, C. Hodakoski, A. Silkov, B. Honig, A. Couvillon, A. Shymanets, B. Nurnberg, J.M. Asara, and R. Parsons. 2015. p21-activated Kinases (PAKs) Mediate the Phosphorylation of PREX2 Protein to Initiate Feedback Inhibition of Rac1 GTPase. *J Biol Chem*. 290:28915-28931.

Beeser, A., Z.M. Jaffer, C. Hofmann, and J. Chernoff. 2005. Role of group A p21-activated kinases in activation of extracellular-regulated kinase by growth factors. *J Biol Chem*. 280:36609-36615.

Bellis, S.L., J.T. Miller, and C.E. Turner. 1995. Characterization of tyrosine phosphorylation of paxillin in vitro by focal adhesion kinase. *J Biol Chem*. 270:17437-17441.

Bompard, G., and E. Caron. 2004. Regulation of WASP/WAVE proteins: making a long story short. *J Cell Biol*. 166:957-962.

Bousso, P., and E. Robey. 2003. Dynamics of CD8+ T cell priming by dendritic cells in intact lymph nodes. *Nat Immunol*. 4:579-585.

Bravo-Cordero, J.J., M.A. Magalhaes, R.J. Eddy, L. Hodgson, and J. Condeelis. 2013. Functions of cofilin in cell locomotion and invasion. *Nat Rev Mol Cell Biol*. 14:405-415.

Brieher, W.M., H.Y. Kueh, B.A. Ballif, and T.J. Mitchison. 2006. Rapid actin monomer-insensitive depolymerization of Listeria actin comet tails by cofilin, coronin, and Aip1. *J Cell Biol*. 175:315-324.

Britschgi, M.R., A. Link, T.K. Lissandrin, and S.A. Luther. 2008. Dynamic modulation of CCR7 expression and function on naive T lymphocytes in vivo. *J Immunol*. 181:7681-7688.

Brown, A., X. Wang, E. Sawai, and C. Cheng-Mayer. 1999. Activation of the PAK-related kinase by human immunodeficiency virus type 1 Nef in primary human peripheral blood lymphocytes and macrophages leads to phosphorylation of a PIX-p95 complex. *J Virol*. 73:9899-9907.

Burbach, B.J., R.B. Medeiros, K.L. Mueller, and Y. Shimizu. 2007. T-cell receptor signaling to integrins. *Immunol Rev*. 218:65-81.

Cahalan, M.D., and I. Parker. 2008. Choreography of cell motility and interaction dynamics imaged by two-photon microscopy in lymphoid organs. *Annu Rev Immunol*. 26:585-626.

Campa, C.C., E. Ciraolo, A. Ghigo, G. Germena, and E. Hirsch. 2015. Crossroads of PI3K and Rac pathways. *Small GTPases*. 6:71-80.

Carisey, A., and C. Ballestrem. 2011. Vinculin, an adapter protein in control of cell adhesion signalling. *European journal of cell biology*. 90:157-163.

Castellino, F., A.Y. Huang, G. Altan-Bonnet, S. Stoll, C. Scheinecker, and R.N. Germain. 2006. Chemokines enhance immunity by guiding naive CD8+ T cells to sites of CD4+ T cell-dendritic cell interaction. *Nature*. 440:890-895.

Cau, J., and A. Hall. 2005. Cdc42 controls the polarity of the actin and microtubule cytoskeletons through two distinct signal transduction pathways. *J Cell Sci*. 118:2579-2587.

Chapman, N.M., and J.C. Houtman. 2014. Functions of the FAK family kinases in T cells: beyond actin cytoskeletal rearrangement. *Immunol Res*. 59:23-34.

Chen, L., M. Vicente-Manzanares, L. Potvin-Trottier, P.W. Wiseman, and A.R. Horwitz. 2012. The integrin-ligand interaction regulates adhesion and migration through a molecular clutch. *PLoS One*. 7:e40202.

Cherfils, J., and M. Zeghouf. 2013. Regulation of small GTPases by GEFs, GAPs, and GDIs. *Physiol Rev*. 93:269-309.

Chew, T.L., R.A. Masaracchia, Z.M. Goeckeler, and R.B. Wysolmerski. 1998. Phosphorylation of non-muscle myosin II regulatory light chain by p21-activated kinase (gamma-PAK). *J Muscle Res Cell Motil*. 19:839-854.

Chiarugi, P., and E. Giannoni. 2008. Anoikis: a necessary death program for anchorage-dependent cells. *Biochemical pharmacology*. 76:1352-1364.

Chong, C., L. Tan, L. Lim, and E. Manser. 2001. The mechanism of PAK activation. Autophosphorylation events in both regulatory and kinase domains control activity. *J Biol Chem*. 276:17347-17353.

Chu, P.C., J. Wu, X.C. Liao, J. Pardo, H. Zhao, C. Li, M.K. Mendenhall, E. Pali, M. Shen, S. Yu, V.C. Taylor, G. Aversa, S. Molineaux, D.G. Payan, and E.S. Masuda. 2004. A novel role for p21-activated protein kinase 2 in T cell activation. *J Immunol*. 172:7324-7334.

Ciobanasu, C., B. Faivre, and C. Le Clainche. 2012. Actin dynamics associated with focal adhesions. *Int J Cell Biol*. 2012:941292.

Dan, C., A. Kelly, O. Bernard, and A. Minden. 2001. Cytoskeletal changes regulated by the PAK4 serine/threonine kinase are mediated by LIM kinase 1 and cofilin. *J Biol Chem*. 276:32115-32121.

Dang, I., R. Gorelik, C. Sousa-Blin, E. Derivery, C. Guerin, J. Linkner, M. Nemethova, J.G. Dumortier, F.A. Giger, T.A. Chipysheva, V.D. Ermilova, S. Vacher, V. Campanacci, I. Herrada, A.G. Planson, S. Fetics, V. Henriot, V. David, K. Oguievetskaia, G. Lakisic, F. Pierre, A. Steffen, A. Boyreau, N. Peyrieras, K. Rottner, S. Zinn-Justin, J. Cherfils, I. Bieche, A.Y. Alexandrova, N.B. David, J.V. Small, J. Faix, L. Blanchoin,

and A. Gautreau. 2013. Inhibitory signalling to the Arp2/3 complex steers cell migration. *Nature*. 503:281-284.

Daniels, R.H., F.T. Zenke, and G.M. Bokoch. 1999. alphaPix stimulates p21-activated kinase activity through exchange factor-dependent and -independent mechanisms. *J Biol Chem*. 274:6047-6050.

Deakin, N.O., and C.E. Turner. 2008. Paxillin comes of age. *J Cell Sci*. 121:2435-2444.

Dong, T.X., S. Othy, M.L. Greenberg, A. Jairaman, C. Akunwafo, S. Leverrier, Y. Yu, I. Parker, J.L. Dynes, and M.D. Cahalan. 2017. Intermittent Ca(2+) signals mediated by Orai1 regulate basal T cell motility. *Elife*. 6.

Eden, S., R. Rohatgi, A.V. Podtelejnikov, M. Mann, and M.W. Kirschner. 2002. Mechanism of regulation of WAVE1-induced actin nucleation by Rac1 and Nck. *Nature*. 418:790-793.

Edwards, D.C., L.C. Sanders, G.M. Bokoch, and G.N. Gill. 1999. Activation of LIM-kinase by Pak1 couples Rac/Cdc42 GTPase signalling to actin cytoskeletal dynamics. *Nat Cell Biol*. 1:253-259.

Feng, Q., J.G. Albeck, R.A. Cerione, and W. Yang. 2002. Regulation of the Cool/Pix proteins: key binding partners of the Cdc42/Rac targets, the p21-activated kinases. *J Biol Chem*. 277:5644-5650.

Feng, Q., D. Baird, and R.A. Cerione. 2004. Novel regulatory mechanisms for the Dbl family guanine nucleotide exchange factor Cool-2/alpha-Pix. *EMBO J*. 23:3492-3504.

Filipenko, N.R., S. Attwell, C. Roskelley, and S. Dedhar. 2005. Integrin-linked kinase activity regulates Rac- and Cdc42-mediated actin cytoskeleton reorganization via alpha-PIX. *Oncogene*. 24:5837-5849.

Flanders, J.A., Q. Feng, S. Bagrodia, M.T. Laux, A. Singavarapu, and R.A. Cerione. 2003. The Cbl proteins are binding partners for the Cool/Pix family of p21-activated kinase-binding proteins. *FEBS letters*. 550:119-123.

Frank, S.R., and S.H. Hansen. 2008. The PIX-GIT complex: a G protein signaling cassette in control of cell shape. *Seminars in cell & developmental biology*. 19:234-244.

Germain, R.N. 1994. MHC-dependent antigen processing and peptide presentation: providing ligands for T lymphocyte activation. *Cell*. 76:287-299.

Giannone, G., R.M. Mege, and O. Thoumine. 2009. Multi-level molecular clutches in motile cell processes. *Trends Cell Biol*. 19:475-486.

Giannoni, E., P. Chiarugi, G. Cozzi, L. Magnelli, M.L. Taddei, T. Fiaschi, F. Buricchi, G. Raugei, and G. Ramponi. 2003. Lymphocyte function-associated antigen-1-mediated T cell adhesion is impaired by low molecular weight phosphotyrosine phosphatase-dependent inhibition of FAK activity. *J Biol Chem*. 278:36763-36776.

Gohla, A., J. Birkenfeld, and G.M. Bokoch. 2005. Chronophin, a novel HAD-type serine protein phosphatase, regulates cofilin-dependent actin dynamics. *Nat Cell Biol*. 7:21-29.

Goicoechea, S.M., S. Awadia, and R. Garcia-Mata. 2014. I'm coming to GEF you: Regulation of RhoGEFs during cell migration. *Cell Adh Migr*. 8:535-549.

Gringel, A., D. Walz, G. Rosenberger, A. Minden, K. Kutsche, P. Kopp, and S. Linder. 2006. PAK4 and alphaPIX determine podosome size and number in macrophages through localized actin regulation. *Journal of cellular physiology*. 209:568-579.

Gu, C., S.G. Tangye, X. Sun, Y. Luo, Z. Lin, and J. Wu. 2006. The X-linked lymphoproliferative disease gene product SAP associates with PAK-interacting exchange factor and participates in T cell activation. *Proc Natl Acad Sci U S A*. 103:14447-14452.

Gurniak, C.B., E. Perlas, and W. Witke. 2005. The actin depolymerizing factor n-cofilin is essential for neural tube morphogenesis and neural crest cell migration. *Dev Biol*. 278:231-241.

Hagel, M., E.L. George, A. Kim, R. Tamimi, S.L. Opitz, C.E. Turner, A. Imamoto, and S.M. Thomas. 2002. The adaptor protein paxillin is essential for normal development in the mouse and is a critical transducer of fibronectin signaling. *Mol Cell Biol*. 22:901-915.

Hanna, S., and M. El-Sibai. 2013. Signaling networks of Rho GTPases in cell motility. *Cell Signal*. 25:1955-1961.

Harris, T.H., E.J. Banigan, D.A. Christian, C. Konradt, E.D. Tait Wojno, K. Norose, E.H. Wilson, B. John, W. Weninger, A.D. Luster, A.J. Liu, and C.A. Hunter. 2012. Generalized Levy walks and the role of chemokines in migration of effector CD8+ T cells. *Nature*. 486:545-548.

Hart, M.J., A. Eva, D. Zangrilli, S.A. Aaronson, T. Evans, R.A. Cerione, and Y. Zheng. 1994. Cellular transformation and guanine nucleotide exchange activity are catalyzed by a common domain on the dbl oncogene product. *J Biol Chem*. 269:62-65.

Hashimoto-Tane, A., M. Sakuma, H. Ike, T. Yokosuka, Y. Kimura, O. Ohara, and T. Saito. 2016. Micro-adhesion rings surrounding TCR microclusters are essential for T cell activation. *J Exp Med*. 213:1609-1625.

Haston, W.S., J.M. Shields, and P.C. Wilkinson. 1982. Lymphocyte locomotion and attachment on two-dimensional surfaces and in three-dimensional matrices. *J Cell Biol*. 92:747-752.

Heasman, S.J., and A.J. Ridley. 2008. Mammalian Rho GTPases: new insights into their functions from in vivo studies. *Nat Rev Mol Cell Biol*. 9:690-701.

Heath, J.P., and G.A. Dunn. 1978. Cell to substratum contacts of chick fibroblasts and their relation to the microfilament system. A correlated interference-reflexion and high-voltage electron-microscope study. *J Cell Sci*. 29:197-212.

Heng, T.S., M.W. Painter, and C. Immunological Genome Project. 2008. The Immunological Genome Project: networks of gene expression in immune cells. *Nat Immunol*. 9:1091-1094.

Hoefen, R.J., and B.C. Berk. 2006. The multifunctional GIT family of proteins. *J Cell Sci*. 119:1469-1475.

Hoelz, A., J.M. Janz, S.D. Lawrie, B. Corwin, A. Lee, and T.P. Sakmar. 2006. Crystal structure of the SH3 domain of betaPIX in complex with a high affinity peptide from PAK2. *J Mol Biol*. 358:509-522.

Hofmann, C., M. Shepelev, and J. Chernoff. 2004. The genetics of Pak. *J Cell Sci*. 117:4343-4354.

Hogg, N., I. Patzak, and F. Willenbrock. 2011. The insider's guide to leukocyte integrin signalling and function. *Nat Rev Immunol*. 11:416-426.

Hons, M., A. Kopf, R. Hauschild, A. Leithner, F. Gaertner, J. Abe, J. Renkawitz, J.V. Stein, and M. Sixt. 2018. Chemokines and integrins independently tune actin flow and substrate friction during intranodal migration of T cells. *Nat Immunol*. 19:606-616.

Hu, K., L. Ji, K.T. Applegate, G. Danuser, and C.M. Waterman-Storer. 2007. Differential transmission of actin motion within focal adhesions. *Science*. 315:111-115.

Hu, Z., J.N. Lancaster, C. Sasiponganan, and L.I. Ehrlich. 2015. CCR4 promotes medullary entry and thymocyte-dendritic cell interactions required for central tolerance. *J Exp Med*. 212:1947-1965.

Humphries, J.D., P. Wang, C. Streuli, B. Geiger, M.J. Humphries, and C. Ballestrem. 2007. Vinculin controls focal adhesion formation by direct interactions with talin and actin. *J Cell Biol*. 179:1043-1057.

Itakura, A., J.E. Aslan, B.T. Kusanto, K.G. Phillips, J.E. Porter, P.K. Newton, X. Nan, R.H. Insall, J. Chernoff, and O.J. McCarty. 2013. p21-Activated kinase (PAK) regulates cytoskeletal reorganization and directional migration in human neutrophils. *PLoS One*. 8:e73063.

Jankowska, K.I., E.K. Williamson, N.H. Roy, D. Blumenthal, V. Chandra, T. Baumgart, and J.K. Burkhardt. 2018. Integrins Modulate T Cell Receptor Signaling by Constraining Actin Flow at the Immunological Synapse. *Front Immunol*. 9:25.

Jozic, D., N. Cardenes, Y.L. Deribe, G. Moncalian, D. Hoeller, Y. Groemping, I. Dikic, K. Rittinger, and J. Bravo. 2005. Cbl promotes clustering of endocytic adaptor proteins. *Nature structural & molecular biology*. 12:972-979.

Kaibuchi, K., S. Kuroda, and M. Amano. 1999. Regulation of the cytoskeleton and cell adhesion by the Rho family GTPases in mammalian cells. *Annu Rev Biochem*. 68:459-486.

Katakai, T., K. Habiro, and T. Kinashi. 2013. Dendritic cells regulate high-speed interstitial T cell migration in the lymph node via LFA-1/ICAM-1. *J Immunol*. 191:1188-1199.

Katakai, T., N. Kondo, Y. Ueda, and T. Kinashi. 2014. Autotaxin produced by stromal cells promotes LFA-1-independent and Rho-dependent interstitial T cell motility in the lymph node paracortex. *J Immunol*. 193:617-626.

Kelly, M.L., and J. Chernoff. 2012. Mouse models of PAK function. *Cell Logist*. 2:84-88.

Kim, C.H., L.S. Rott, I. Clark-Lewis, D.J. Campbell, L. Wu, and E.C. Butcher. 2001. Subspecialization of CXCR5+ T cells: B helper activity is focused in a germinal center-localized subset of CXCR5+ T cells. *J Exp Med*. 193:1373-1381.

Kinashi, T. 2005. Intracellular signalling controlling integrin activation in lymphocytes. *Nat Rev Immunol*. 5:546-559.

Klein, L., B. Kyewski, P.M. Allen, and K.A. Hogquist. 2014. Positive and negative selection of the T cell repertoire: what thymocytes see (and don't see). *Nat Rev Immunol*. 14:377-391.

Klemke, M., E. Kramer, M.H. Konstandin, G.H. Wabnitz, and Y. Samstag. 2010. An MEK-cofilin signalling module controls migration of human T cells in 3D but not 2D environments. *EMBO J*. 29:2915-2929.

Klemke, M., G.H. Wabnitz, F. Funke, B. Funk, H. Kirchgessner, and Y. Samstag. 2008. Oxidation of cofilin mediates T cell hyporesponsiveness under oxidative stress conditions. *Immunity*. 29:404-413.

Koh, C.G., E. Manser, Z.S. Zhao, C.P. Ng, and L. Lim. 2001. Beta1PIX, the PAK-interacting exchange factor, requires localization via a coiled-coil region to promote microvillus-like structures and membrane ruffles. *J Cell Sci*. 114:4239-4251.

Kong, K.F., G. Fu, Y. Zhang, T. Yokosuka, J. Casas, A.J. Canonigo-Balancio, S. Becart, G. Kim, J.R. Yates, 3rd, M. Kronenberg, T. Saito, N.R. Gascoigne, and A. Altman. 2014. Protein kinase C-eta controls CTLA-4-mediated regulatory T cell function. *Nat Immunol*. 15:465-472.

Korthals, M., K. Schilling, P. Reichardt, D. Mamula, T. Schluter, M. Steiner, K. Langnase, U. Thomas, E. Gundelfinger, R.T. Premont, K. Tedford, and K.D. Fischer. 2014. alphaPIX RhoGEF supports positive selection by restraining migration and promoting arrest of thymocytes. *J Immunol*. 192:3228-3238.

Kozai, M., Y. Kubo, T. Katakai, H. Kondo, H. Kiyonari, K. Schaeuble, S.A. Luther, N. Ishimaru, I. Ohigashi, and Y. Takahama. 2017. Essential role of CCL21 in establishment of central self-tolerance in T cells. *J Exp Med*. 214:1925-1935.

Krueger, A., S. Willenzon, M. Lyszkiewicz, E. Kremmer, and R. Forster. 2010. CC chemokine receptor 7 and 9 double-deficient hematopoietic progenitors are severely impaired in seeding the adult thymus. *Blood*. 115:1906-1912.

Krummel, M.F., F. Bartumeus, and A. Gerard. 2016. T cell migration, search strategies and mechanisms. *Nat Rev Immunol*. 16:193-201.

Ku, G.M., D. Yablonski, E. Manser, L. Lim, and A. Weiss. 2001. A PAK1-PIX-PKL complex is activated by the T-cell receptor independent of Nck, Slp-76 and LAT. *EMBO J*. 20:457-465.

Kuo, J.C., X. Han, C.T. Hsiao, J.R. Yates, 3rd, and C.M. Waterman. 2011. Analysis of the myosin-II-responsive focal adhesion proteome reveals a role for beta-Pix in negative regulation of focal adhesion maturation. *Nat Cell Biol*. 13:383-393.

Kurd, N., and E.A. Robey. 2016. T-cell selection in the thymus: a spatial and temporal perspective. *Immunol Rev*. 271:114-126.

Kurita, S., Y. Watanabe, E. Gunji, K. Ohashi, and K. Mizuno. 2008. Molecular dissection of the mechanisms of substrate recognition and F-actin-mediated activation of cofilin-phosphatase Slingshot-1. *J Biol Chem*. 283:32542-32552.

Kutsche, K., H. Yntema, A. Brandt, I. Jantke, H.G. Nothwang, U. Orth, M.G. Boavida, D. David, J. Chelly, J.P. Fryns, C. Moraine, H.H. Ropers, B.C. Hamel, H. van Bokhoven, and A. Gal. 2000. Mutations in ARHGEF6, encoding a guanine nucleotide exchange factor for Rho GTPases, in patients with X-linked mental retardation. *Nat Genet*. 26:247-250.

Ladi, E., X. Yin, T. Chtanova, and E.A. Robey. 2006. Thymic microenvironments for T cell differentiation and selection. *Nat Immunol*. 7:338-343.

Laemmli, U.K. 1970. Cleavage of structural proteins during the assembly of the head of bacteriophage T4. *Nature*. 227:680-685.

Lammermann, T., B.L. Bader, S.J. Monkley, T. Worbs, R. Wedlich-Soldner, K. Hirsch, M. Keller, R. Forster, D.R. Critchley, R. Fassler, and M. Sixt. 2008. Rapid leukocyte migration by integrin-independent flowing and squeezing. *Nature*. 453:51-55.

Lammermann, T., J. Renkawitz, X. Wu, K. Hirsch, C. Brakebusch, and M. Sixt. 2009. Cdc42-dependent leading edge coordination is essential for interstitial dendritic cell migration. *Blood*. 113:5703-5710.

Lammermann, T., and M. Sixt. 2009. Mechanical modes of 'amoeboid' cell migration. *Curr Opin Cell Biol*. 21:636-644.

Lancaster, J.N., Y. Li, and L.I.R. Ehrlich. 2018. Chemokine-Mediated Choreography of Thymocyte Development and Selection. *Trends in immunology*. 39:86-98.

Lee, J.H., S. Wittki, T. Brau, F.S. Dreyer, K. Kratzel, J. Dindorf, I.C. Johnston, S. Gross, E. Kremmer, R. Zeidler, U. Schlotzer-Schrehardt, M. Lichtenheld, K. Saksela, T. Harrer, G. Schuler, M. Federico, and A.S. Baur. 2013. HIV Nef, paxillin, and Pak1/2 regulate activation and secretion of TACE/ADAM10 proteases. *Mol Cell*. 49:668-679.

Lei, M., W. Lu, W. Meng, M.C. Parrini, M.J. Eck, B.J. Mayer, and S.C. Harrison. 2000. Structure of PAK1 in an autoinhibited conformation reveals a multistage activation switch. *Cell*. 102:387-397.

Ley, K., C. Laudanna, M.I. Cybulsky, and S. Nourshargh. 2007. Getting to the site of inflammation: the leukocyte adhesion cascade updated. *Nat Rev Immunol*. 7:678-689.

Li, Z., M. Hannigan, Z. Mo, B. Liu, W. Lu, Y. Wu, A.V. Smrcka, G. Wu, L. Li, M. Liu, C.K. Huang, and D. Wu. 2003. Directional sensing requires G beta gamma-mediated PAK1 and PIX alpha-dependent activation of Cdc42. *Cell*. 114:215-227.

Lim, K., Y.M. Hyun, K. Lambert-Emo, T. Capece, S. Bae, R. Miller, D.J. Topham, and M. Kim. 2015. Neutrophil trails guide influenza-specific CD8(+) T cells in the airways. *Science*. 349:aaa4352.

Lim, Y., S.T. Lim, A. Tomar, M. Gardel, J.A. Bernard-Trifilo, X.L. Chen, S.A. Uryu, R. Canete-Soler, J. Zhai, H. Lin, W.W. Schlaepfer, P. Nalbant, G. Bokoch, D. Ilic, C. Waterman-Storer, and D.D. Schlaepfer. 2008. PyK2 and FAK connections to p190Rho guanine nucleotide exchange factor regulate RhoA activity, focal adhesion formation, and cell motility. *J Cell Biol*. 180:187-203.

Lopez-Colome, A.M., I. Lee-Rivera, R. Benavides-Hidalgo, and E. Lopez. 2017. Paxillin: a crossroad in pathological cell migration. *J Hematol Oncol*. 10:50.

Lorentzen, A., J. Bamber, A. Sadok, I. Elson-Schwab, and C.J. Marshall. 2011. An ezrin-rich, rigid uropod-like structure directs movement of amoeboid blebbing cells. *J Cell Sci*. 124:1256-1267.

Luther, S.A., H.L. Tang, P.L. Hyman, A.G. Farr, and J.G. Cyster. 2000. Coexpression of the chemokines ELC and SLC by T zone stromal cells and deletion of the ELC gene in the plt/plt mouse. *Proc Natl Acad Sci U S A*. 97:12694-12699.

Manning, G., D.B. Whyte, R. Martinez, T. Hunter, and S. Sudarsanam. 2002. The protein kinase complement of the human genome. *Science*. 298:1912-1934.

Manser, E., T.H. Loo, C.G. Koh, Z.S. Zhao, X.Q. Chen, L. Tan, I. Tan, T. Leung, and L. Lim. 1998. PAK kinases are directly coupled to the PIX family of nucleotide exchange factors. *Mol Cell*. 1:183-192.

Mardilovich, K., M. Baugh, D. Crighton, D. Kowalczyk, M. Gabrielsen, J. Munro, D.R. Croft, F. Lourenco, D. James, G. Kalna, L. McGarry, O. Rath, E. Shanks, M.J. Garnett, U. McDermott, J. Brookfield, M. Charles, T. Hammonds, and M.F. Olson. 2015. LIM kinase inhibitors disrupt mitotic microtubule organization and impair tumor cell proliferation. *Oncotarget*. 6:38469-38486.

Matloubian, M., C.G. Lo, G. Cinamon, M.J. Lesneski, Y. Xu, V. Brinkmann, M.L. Allende, R.L. Proia, and J.G. Cyster. 2004. Lymphocyte egress from thymus and peripheral lymphoid organs is dependent on S1P receptor 1. *Nature*. 427:355-360.

Mayor, R., and C. Carmona-Fontaine. 2010. Keeping in touch with contact inhibition of locomotion. *Trends Cell Biol*. 20:319-328.

Mayya, V., D.H. Lundgren, S.I. Hwang, K. Rezaul, L. Wu, J.K. Eng, V. Rodionov, and D.K. Han. 2009. Quantitative phosphoproteomic analysis of T cell receptor signaling reveals system-wide modulation of protein-protein interactions. *Sci Signal*. 2:ra46.

Mazaki, Y., S. Hashimoto, K. Okawa, A. Tsubouchi, K. Nakamura, R. Yagi, H. Yano, A. Kondo, A. Iwamatsu, A. Mizoguchi, and H. Sabe. 2001. An ADP-ribosylation factor GTPase-activating protein Git2-short/KIAA0148 is involved in subcellular localization of paxillin and actin cytoskeletal organization. *Mol Biol Cell*. 12:645-662.

Mazaki, Y., S. Hashimoto, T. Tsujimura, M. Morishige, A. Hashimoto, K. Aritake, A. Yamada, J.M. Nam, H. Kiyonari, K. Nakao, and H. Sabe. 2006. Neutrophil direction sensing and superoxide production linked by the GTPase-activating protein GIT2. *Nat Immunol*. 7:724-731.

Mempel, T.R., S.E. Henrickson, and U.H. Von Andrian. 2004. T-cell priming by dendritic cells in lymph nodes occurs in three distinct phases. *Nature*. 427:154-159.

Millar, F.R., S.M. Janes, and A. Giangreco. 2017. Epithelial cell migration as a potential therapeutic target in early lung cancer. *Eur Respir Rev*. 26.

Miller, M.J., S.H. Wei, I. Parker, and M.D. Cahalan. 2002. Two-photon imaging of lymphocyte motility and antigen response in intact lymph node. *Science*. 296:1869-1873.

Missy, K., B. Hu, K. Schilling, A. Harenberg, V. Sakk, K. Kuchenbecker, K. Kutsche, and K.D. Fischer. 2008. AlphaPIX Rho GTPase guanine nucleotide exchange factor regulates lymphocyte functions and antigen receptor signaling. *Mol Cell Biol*. 28:3776-3789.

Mitchison, T., and M. Kirschner. 1988. Cytoskeletal dynamics and nerve growth. *Neuron*. 1:761-772.

Mizuno, K. 2013. Signaling mechanisms and functional roles of cofilin phosphorylation and dephosphorylation. *Cell Signal*. 25:457-469.

Moreau, H.D., F. Lemaitre, K.R. Garrod, Z. Garcia, A.M. Lennon-Dumenil, and P. Bousso. 2015. Signal strength regulates antigen-mediated T-cell deceleration by distinct mechanisms to promote local exploration or arrest. *Proc Natl Acad Sci U S A*. 112:12151-12156.

Moriyama, K., K. Iida, and I. Yahara. 1996. Phosphorylation of Ser-3 of cofilin regulates its essential function on actin. *Genes Cells*. 1:73-86.

Mott, H.R., D. Nietlispach, K.A. Evetts, and D. Owen. 2005. Structural analysis of the SH3 domain of beta-PIX and its interaction with alpha-p21 activated kinase (PAK). *Biochemistry*. 44:10977-10983.

Mueller, S.N., and R.N. Germain. 2009. Stromal cell contributions to the homeostasis and functionality of the immune system. *Nat Rev Immunol*. 9:618-629.

Mueller, S.N., K.A. Hosiawa-Meagher, B.T. Konieczny, B.M. Sullivan, M.F. Bachmann, R.M. Locksley, R. Ahmed, and M. Matloubian. 2007. Regulation of homeostatic chemokine expression and cell trafficking during immune responses. *Science*. 317:670-674.

Nagata-Ohashi, K., Y. Ohta, K. Goto, S. Chiba, R. Mori, M. Nishita, K. Ohashi, K. Kousaka, A. Iwamatsu, R. Niwa, T. Uemura, and K. Mizuno. 2004. A pathway of neuregulin-induced activation of cofilin-phosphatase Slingshot and cofilin in lamellipodia. *J Cell Biol*. 165:465-471.

Nakamura, K., H. Yano, H. Uchida, S. Hashimoto, E. Schaefer, and H. Sabe. 2000. Tyrosine phosphorylation of paxillin alpha is involved in temporospatial regulation of paxillin-containing focal adhesion formation and F-actin organization in motile cells. *J Biol Chem*. 275:27155-27164.

Nayal, A., D.J. Webb, C.M. Brown, E.M. Schaefer, M. Vicente-Manzanares, and A.R. Horwitz. 2006. Paxillin phosphorylation at Ser273 localizes a GIT1-PIX-PAK complex and regulates adhesion and protrusion dynamics. *J Cell Biol*. 173:587-589.

Ngoc, P.L., D.R. Gold, A.O. Tzianabos, S.T. Weiss, and J.C. Celedon. 2005. Cytokines, allergy, and asthma. *Curr Opin Allergy Clin Immunol*. 5:161-166.

Nicholson-Dykstra, S.M., and H.N. Higgs. 2008. Arp2 depletion inhibits sheet-like protrusions but not linear protrusions of fibroblasts and lymphocytes. *Cell Motil Cytoskeleton*. 65:904-922.

Nimnual, A.S., B.A. Yatsula, and D. Bar-Sagi. 1998. Coupling of Ras and Rac guanosine triphosphatases through the Ras exchanger Sos. *Science*. 279:560-563.

Nishita, M., H. Aizawa, and K. Mizuno. 2002. Stromal cell-derived factor 1alpha activates LIM kinase 1 and induces cofilin phosphorylation for T-cell chemotaxis. *Mol Cell Biol*. 22:774-783.

Nishita, M., C. Tomizawa, M. Yamamoto, Y. Horita, K. Ohashi, and K. Mizuno. 2005. Spatial and temporal regulation of cofilin activity by LIM kinase and Slingshot is critical for directional cell migration. *J Cell Biol*. 171:349-359.

Ohashi, K., K. Nagata, M. Maekawa, T. Ishizaki, S. Narumiya, and K. Mizuno. 2000. Rho-associated kinase ROCK activates LIM-kinase 1 by phosphorylation at threonine 508 within the activation loop. *J Biol Chem*. 275:3577-3582.

Ory, S., and S. Gasman. 2011. Rho GTPases and exocytosis: what are the molecular links? *Seminars in cell & developmental biology*. 22:27-32.

Osmani, N., N. Vitale, J.P. Borg, and S. Etienne-Manneville. 2006. Scrib controls Cdc42 localization and activity to promote cell polarization during astrocyte migration. *Curr Biol*. 16:2395-2405.

Pals, S.T., D.J. de Gorter, and M. Spaargaren. 2007. Lymphoma dissemination: the other face of lymphocyte homing. *Blood*. 110:3102-3111.

Paluch, E.K., and E. Raz. 2013. The role and regulation of blebs in cell migration. *Curr Opin Cell Biol*. 25:582-590.

Pankov, R., Y. Endo, S. Even-Ram, M. Araki, K. Clark, E. Cukierman, K. Matsumoto, and K.M. Yamada. 2005. A Rac switch regulates random versus directionally persistent cell migration. *J Cell Biol*. 170:793-802.

Park, E., M. Na, J. Choi, S. Kim, J.R. Lee, J. Yoon, D. Park, M. Sheng, and E. Kim. 2003. The Shank family of postsynaptic density proteins interacts with and promotes synaptic accumulation of the beta PIX guanine nucleotide exchange factor for Rac1 and Cdc42. *J Biol Chem*. 278:19220-19229.

Parsons, J.T., A.R. Horwitz, and M.A. Schwartz. 2010. Cell adhesion: integrating cytoskeletal dynamics and cellular tension. *Nat Rev Mol Cell Biol*. 11:633-643.

Phee, H., R.T. Abraham, and A. Weiss. 2005. Dynamic recruitment of PAK1 to the immunological synapse is mediated by PIX independently of SLP-76 and Vav1. *Nat Immunol*. 6:608-617.

Phee, H., B.B. Au-Yeung, O. Pryshchep, K.L. O'Hagan, S.G. Fairbairn, M. Radu, R. Kosoff, M. Mollenauer, D. Cheng, J. Chernoff, and A. Weiss. 2014. Pak2 is required for actin cytoskeleton remodeling, TCR signaling, and normal thymocyte development and maturation. *Elife*. 3:e02270.

Phee, H., I. Dzhagalov, M. Mollenauer, Y. Wang, D.J. Irvine, E. Robey, and A. Weiss. 2010. Regulation of thymocyte positive selection and motility by GIT2. *Nat Immunol*. 11:503-511.

Pirruccello, M., H. Sondermann, J.G. Pelton, P. Pellicena, A. Hoelz, J. Chernoff, D.E. Wemmer, and J. Kuriyan. 2006. A dimeric kinase assembly underlying autophosphorylation in the p21 activated kinases. *J Mol Biol*. 361:312-326.

Pollard, T.D., and G.G. Borisy. 2003. Cellular motility driven by assembly and disassembly of actin filaments. *Cell*. 112:453-465.

Premont, R.T., S.J. Perry, R. Schmalzigaug, J.T. Roseman, Y. Xing, and A. Claing. 2004. The GIT/PIX complex: an oligomeric assembly of GIT family ARF GTPase-activating proteins and PIX family Rac1/Cdc42 guanine nucleotide exchange factors. *Cell Signal*. 16:1001-1011.

Prockop, S.E., S. Palencia, C.M. Ryan, K. Gordon, D. Gray, and H.T. Petrie. 2002. Stromal cells provide the matrix for migration of early lymphoid progenitors through the thymic cortex. *J Immunol*. 169:4354-4361.

Radu, M., G. Semenova, R. Kosoff, and J. Chernoff. 2014. PAK signalling during the development and progression of cancer. *Nat Rev Cancer*. 14:13-25.

Raftopoulou, M., and A. Hall. 2004. Cell migration: Rho GTPases lead the way. *Dev Biol*. 265:23-32.

Ramakers, G.J., D. Wolfer, G. Rosenberger, K. Kuchenbecker, H.J. Kreienkamp, J. Prange-Kiel, G. Rune, K. Richter, K. Langnaese, S. Masneuf, M.R. Bosl, K.D. Fischer, H.J. Krugers, H.P. Lipp, E. van Galen, and K. Kutsche. 2012. Dysregulation of Rho GTPases in the alphaPix/Arhgef6 mouse model of X-linked intellectual disability is paralleled by impaired structural and synaptic plasticity and cognitive deficits. *Human molecular genetics*. 21:268-286.

Ramos, E., R.B. Wysolmerski, and R.A. Masaracchia. 1997. Myosin phosphorylation by human cdc42-dependent S6/H4 kinase/gammaPAK from placenta and lymphoid cells. *Recept Signal Transduct*. 7:99-110.

Ratner, S., W.S. Sherrod, and D. Lichlyter. 1997. Microtubule retraction into the uropod and its role in T cell polarization and motility. *J Immunol*. 159:1063-1067.

Reichardt, P., I. Patzak, K. Jones, E. Etemire, M. Gunzer, and N. Hogg. 2013. A role for LFA-1 in delaying T-lymphocyte egress from lymph nodes. *EMBO J*. 32:829-843.

Renkawitz, J., and M. Sixt. 2010. Mechanisms of force generation and force transmission during interstitial leukocyte migration. *EMBO reports*. 11:744-750.

Rennefahrt, U.E., S.W. Deacon, S.A. Parker, K. Devarajan, A. Beeser, J. Chernoff, S. Knapp, B.E. Turk, and J.R. Peterson. 2007. Specificity profiling of Pak kinases allows identification of novel phosphorylation sites. *J Biol Chem*. 282:15667-15678.

Rhee, S., S.J. Yang, S.J. Lee, and D. Park. 2004. betaPix-b(L), a novel isoform of betaPix, is generated by alternative translation. *Biochem Biophys Res Commun*. 318:415-421.

Ridley, A.J. 2011. Life at the leading edge. *Cell*. 145:1012-1022.

Ridley, A.J. 2015. Rho GTPase signalling in cell migration. *Curr Opin Cell Biol*. 36:103-112.

Rodriguez-Fernandez, J.L., M. Gomez, A. Luque, N. Hogg, F. Sanchez-Madrid, and C. Cabanas. 1999. The interaction of activated integrin lymphocyte function-associated antigen 1 with ligand intercellular adhesion molecule 1 induces activation and redistribution of focal adhesion kinase and proline-rich tyrosine kinase 2 in T lymphocytes. *Mol Biol Cell*. 10:1891-1907.

Romanova, L.Y., and J.F. Mushinski. 2011. Central role of paxillin phosphorylation in regulation of LFA-1 integrins activity and lymphocyte migration. *Cell Adh Migr*. 5:457-462.

Rose, D.M., S. Liu, D.G. Woodside, J. Han, D.D. Schlaepfer, and M.H. Ginsberg. 2003. Paxillin binding to the alpha 4 integrin subunit stimulates LFA-1 (integrin alpha L beta 2)-dependent T cell migration by augmenting the activation of focal adhesion kinase/proline-rich tyrosine kinase-2. *J Immunol*. 170:5912-5918.

Rosenberger, G., A. Gal, and K. Kutsche. 2005. AlphaPIX associates with calpain 4, the small subunit of calpain, and has a dual role in integrin-mediated cell spreading. *J Biol Chem*. 280:6879-6889.

Rosenberger, G., I. Jantke, A. Gal, and K. Kutsche. 2003. Interaction of alphaPIX (ARHGEF6) with beta-parvin (PARVB) suggests an involvement of alphaPIX in integrin-mediated signaling. *Human molecular genetics*. 12:155-167.

Rosenberger, G., and K. Kutsche. 2006. AlphaPIX and betaPIX and their role in focal adhesion formation. *European journal of cell biology*. 85:265-274.

Rozenblum, G.T., and M. Gimona. 2008. Calponins: adaptable modular regulators of the actin cytoskeleton. *Int J Biochem Cell Biol*. 40:1990-1995.

Sakuma, M., Y. Shirai, K. Yoshino, M. Kuramasu, T. Nakamura, T. Yanagita, K. Mizuno, I. Hide, Y. Nakata, and N. Saito. 2012. Novel PKCalpha-mediated phosphorylation site(s) on cofilin and their potential role in terminating histamine release. *Mol Biol Cell*. 23:3707-3721.

Sanchez-Madrid, F., and M.A. del Pozo. 1999. Leukocyte polarization in cell migration and immune interactions. *EMBO J*. 18:501-511.

Sander, E.E., J.P. ten Klooster, S. van Delft, R.A. van der Kammen, and J.G. Collard. 1999. Rac downregulates Rho activity: reciprocal balance between both GTPases determines cellular morphology and migratory behavior. *J Cell Biol*. 147:1009-1022.

Schlenker, O., and K. Rittinger. 2009. Structures of dimeric GIT1 and trimeric beta-PIX and implications for GIT-PIX complex assembly. *J Mol Biol*. 386:280-289.

Schmalzigaug, R., M.L. Garron, J.T. Roseman, Y. Xing, C.E. Davidson, S.T. Arold, and R.T. Premont. 2007. GIT1 utilizes a focal adhesion targeting-homology domain to bind paxillin. *Cell Signal*. 19:1733-1744.

Schmidt, A., and A. Hall. 2002. Guanine nucleotide exchange factors for Rho GTPases: turning on the switch. *Genes & development*. 16:1587-1609.

Schwarz, B.A., A. Sambandam, I. Maillard, B.C. Harman, P.E. Love, and A. Bhandoola. 2007. Selective thymus settling regulated by cytokine and chemokine receptors. *J Immunol*. 178:2008-2017.

Scimone, M.L., I. Aifantis, I. Apostolou, H. von Boehmer, and U.H. von Andrian. 2006. A multistep adhesion cascade for lymphoid progenitor cell homing to the thymus. *Proc Natl Acad Sci U S A*. 103:7006-7011.

Scott, R.W., and M.F. Olson. 2007. LIM kinases: function, regulation and association with human disease. *J Mol Med (Berl)*. 85:555-568.

Seeland, I., Y. Xiong, C. Orlik, D. Deibel, S. Prokosch, G. Kublbeck, B. Jahraus, D. De Stefano, S. Moos, F.C. Kurschus, B. Arnold, and Y. Samstag. 2018. The actin remodeling protein cofilin is crucial for thymic alphabeta but not gammadelta T-cell development. *PLoS Biol*. 16:e2005380.

Semmrich, M., A. Smith, C. Feterowski, S. Beer, B. Engelhardt, D.H. Busch, B. Bartsch, M. Laschinger, N. Hogg, K. Pfeffer, and B. Holzmann. 2005. Importance of integrin LFA-1 deactivation for the generation of immune responses. *J Exp Med*. 201:1987-1998.

Shah, D.K., and J.C. Zuniga-Pflucker. 2014. An overview of the intrathymic intricacies of T cell development. *J Immunol*. 192:4017-4023.

Shin, E.Y., K.S. Shin, C.S. Lee, K.N. Woo, S.H. Quan, N.K. Soung, Y.G. Kim, C.I. Cha, S.R. Kim, D. Park, G.M. Bokoch, and E.G. Kim. 2002. Phosphorylation of p85 beta PIX, a Rac/Cdc42-specific guanine nucleotide exchange factor, via the Ras/ERK/PAK2 pathway is required for basic fibroblast growth factor-induced neurite outgrowth. *J Biol Chem*. 277:44417-44430.

Shulman, Z., S.J. Cohen, B. Roediger, V. Kalchenko, R. Jain, V. Grabovsky, E. Klein, V. Shinder, L. Stoler-Barak, S.W. Feigelson, T. Meshel, S.M. Nurmi, I. Goldstein, O. Hartley, C.G. Gahmberg, A. Etzioni, W. Weninger, A. Ben-Baruch, and R. Alon. 2011. Transendothelial migration of lymphocytes mediated by intraendothelial vesicle stores rather than by extracellular chemokine depots. *Nat Immunol*. 13:67-76.

Sidani, M., D. Wessels, G. Mouneimne, M. Ghosh, S. Goswami, C. Sarmiento, W. Wang, S. Kuhl, M. El-Sibai, J.M. Backer, R. Eddy, D. Soll, and J. Condeelis. 2007. Cofilin determines the migration behavior and turning frequency of metastatic cancer cells. *J Cell Biol*. 179:777-791.

Slack-Davis, J.K., S.T. Eblen, M. Zecevic, S.A. Boerner, A. Tarcsafalvi, H.B. Diaz, M.S. Marshall, M.J. Weber, J.T. Parsons, and A.D. Catling. 2003. PAK1 phosphorylation of MEK1 regulates fibronectin-stimulated MAPK activation. *J Cell Biol*. 162:281-291.

Smith, A., Y.R. Carrasco, P. Stanley, N. Kieffer, F.D. Batista, and N. Hogg. 2005. A talin-dependent LFA-1 focal zone is formed by rapidly migrating T lymphocytes. *J Cell Biol*. 170:141-151.

Smith, A., P. Stanley, K. Jones, L. Svensson, A. McDowall, and N. Hogg. 2007. The role of the integrin LFA-1 in T-lymphocyte migration. *Immunol Rev*. 218:135-146.

Soosairajah, J., S. Maiti, O. Wiggan, P. Sarmiere, N. Moussi, B. Sarcevic, R. Sampath, J.R. Bamburg, and O. Bernard. 2005. Interplay between components of a novel LIM kinase-slingshot phosphatase complex regulates cofilin. *EMBO J*. 24:473-486.

Srinivasan, S., F. Wang, S. Glavas, A. Ott, F. Hofmann, K. Aktories, D. Kalman, and H.R. Bourne. 2003. Rac and Cdc42 play distinct roles in regulating PI(3,4,5)P3 and polarity during neutrophil chemotaxis. *J Cell Biol*. 160:375-385.

Stanley, P., A. Smith, A. McDowall, A. Nicol, D. Zicha, and N. Hogg. 2008. Intermediate-affinity LFA-1 binds alpha-actinin-1 to control migration at the leading edge of the T cell. *EMBO J*. 27:62-75.

Steffen, A., M. Ladwein, G.A. Dimchev, A. Hein, L. Schwenkmezger, S. Arens, K.I. Ladwein, J. Margit Holleboom, F. Schur, J. Victor Small, J. Schwarz, R. Gerhard, J. Faix, T.E. Stradal, C. Brakebusch, and K. Rottner. 2013. Rac function is crucial for cell migration but is not required for spreading and focal adhesion formation. *J Cell Sci*. 126:4572-4588.

Stolp, B., M. Reichman-Fried, L. Abraham, X. Pan, S.I. Giese, S. Hannemann, P. Goulimari, E. Raz, R. Grosse, and O.T. Fackler. 2009. HIV-1 Nef interferes with host cell motility by deregulation of Cofilin. *Cell Host Microbe*. 6:174-186.

Stradal, T.E., and G. Scita. 2006. Protein complexes regulating Arp2/3-mediated actin assembly. *Curr Opin Cell Biol*. 18:4-10.

Sumi, T., K. Matsumoto, Y. Takai, and T. Nakamura. 1999. Cofilin phosphorylation and actin cytoskeletal dynamics regulated by rho- and Cdc42-activated LIM-kinase 2. *J Cell Biol*. 147:1519-1532.

Sun, H., A.J. King, H.B. Diaz, and M.S. Marshall. 2000. Regulation of the protein kinase Raf-1 by oncogenic Ras through phosphatidylinositol 3-kinase, Cdc42/Rac and Pak. *Curr Biol*. 10:281-284.

Swaminathan, V., and C.M. Waterman. 2016. The molecular clutch model for mechanotransduction evolves. *Nat Cell Biol*. 18:459-461.

Swamy, M., and W.W. Schamel. 2009. Purification of the T cell antigen receptor and analysis by blue-native PAGE. *Methods in molecular biology*. 514:135-150.

Swamy, M., G.M. Siegers, S. Minguet, B. Wollscheid, and W.W. Schamel. 2006. Blue native polyacrylamide gel electrophoresis (BN-PAGE) for the identification and analysis of multiprotein complexes. *Science's STKE : signal transduction knowledge environment*. 2006:pl4.

Tang, W., Y. Zhang, W. Xu, T.K. Harden, J. Sondek, L. Sun, L. Li, and D. Wu. 2011. A PLCbeta/PI3Kgamma-GSK3 signaling pathway regulates cofilin phosphatase slingshot2 and neutrophil polarization and chemotaxis. *Dev Cell*. 21:1038-1050.

Tedford, K., M. Steiner, S. Koshutin, K. Richter, L. Tech, Y. Eggers, I. Jansing, K. Schilling, A.E. Hauser, M. Korthals, and K.D. Fischer. 2017. The opposing forces of shear flow and sphingosine-1-phosphate control marginal zone B cell shuttling. *Nat Commun*. 8:2261.

ten Klooster, J.P., Z.M. Jaffer, J. Chernoff, and P.L. Hordijk. 2006. Targeting and activation of Rac1 are mediated by the exchange factor beta-Pix. *J Cell Biol*. 172:759-769.

Thauland, T.J., K.H. Hu, M.A. Bruce, and M.J. Butte. 2017. Cytoskeletal adaptivity regulates T cell receptor signaling. *Sci Signal*. 10.

Toshima, J., J.Y. Toshima, T. Amano, N. Yang, S. Narumiya, and K. Mizuno. 2001a. Cofilin phosphorylation by protein kinase testicular protein kinase 1 and its role in integrin-mediated actin reorganization and focal adhesion formation. *Mol Biol Cell*. 12:1131-1145.

Toshima, J., J.Y. Toshima, K. Takeuchi, R. Mori, and K. Mizuno. 2001b. Cofilin phosphorylation and actin reorganization activities of testicular protein kinase 2 and its predominant expression in testicular Sertoli cells. *J Biol Chem*. 276:31449-31458.

Totaro, A., S. Tavano, G. Filosa, A. Gartner, R. Pennucci, P. Santambrogio, A. Bachi, C.G. Dotti, and I. de Curtis. 2012. Biochemical and functional characterisation of alphaPIX, a specific regulator of axonal and dendritic branching in hippocampal neurons. *Biology of the cell / under the auspices of the European Cell Biology Organization*. 104:533-552.

Trampont, P.C., A.C. Tosello-Trampont, Y. Shen, A.K. Duley, A.E. Sutherland, T.P. Bender, D.R. Littman, and K.S. Ravichandran. 2010. CXCR4 acts as a costimulator during thymic beta-selection. *Nat Immunol*. 11:162-170.

Turner, C.E. 2000. Paxillin interactions. *J Cell Sci*. 113 Pt 23:4139-4140.

Turner, C.E., J.R. Glenney, Jr., and K. Burridge. 1990. Paxillin: a new vinculin-binding protein present in focal adhesions. *J Cell Biol*. 111:1059-1068.

Tybulewicz, V.L., and R.B. Henderson. 2009. Rho family GTPases and their regulators in lymphocytes. *Nat Rev Immunol*. 9:630-644.

Valdes, J.L., J. Tang, M.I. McDermott, J.C. Kuo, S.P. Zimmerman, S.M. Wincovitch, C.M. Waterman, S.L. Milgram, and M.P. Playford. 2011. Sorting nexin 27 protein regulates trafficking of a p21-activated kinase (PAK) interacting exchange factor (beta-Pix)-G protein-coupled receptor kinase interacting protein (GIT) complex via a PDZ domain interaction. *J Biol Chem*. 286:39403-39416.

van Rheenen, J., X. Song, W. van Roosmalen, M. Cammer, X. Chen, V. Desmarais, S.C. Yip, J.M. Backer, R.J. Eddy, and J.S. Condeelis. 2007. EGF-induced PIP2 hydrolysis releases and activates cofilin locally in carcinoma cells. *J Cell Biol*. 179:1247-1259.

Vicente-Manzanares, M., K. Newell-Litwa, A.I. Bachir, L.A. Whitmore, and A.R. Horwitz. 2011. Myosin IIA/IIB restrict adhesive and protrusive signaling to generate front-back polarity in migrating cells. *J Cell Biol*. 193:381-396.

Vincent, P., E. Priceputu, D. Kay, K. Saksela, P. Jolicoeur, and Z. Hanna. 2006. Activation of p21-activated kinase 2 and its association with Nef are conserved in murine cells but are not sufficient to induce an AIDS-like disease in CD4C/HIV transgenic mice. *J Biol Chem*. 281:6940-6954.

von Andrian, U.H., and T.R. Mempel. 2003. Homing and cellular traffic in lymph nodes. *Nat Rev Immunol*. 3:867-878.

Wabnitz, G.H., G. Nebl, M. Klemke, A.J. Schroder, and Y. Samstag. 2006. Phosphatidylinositol 3-kinase functions as a Ras effector in the signaling cascade that regulates dephosphorylation of the actin-remodeling protein cofilin after costimulation of untransformed human T lymphocytes. *J Immunol*. 176:1668-1674.

Webb, D.J., M. Kovalenko, L. Whitmore, and A.F. Horwitz. 2006. Phosphorylation of serine 709 in GIT1 regulates protrusive activity in cells. *Biochem Biophys Res Commun*. 346:1284-1288.

White, A.J., S. Baik, S.M. Parnell, A.M. Holland, F. Brombacher, W.E. Jenkinson, and G. Anderson. 2017. A type 2 cytokine axis for thymus emigration. *J Exp Med*. 214:2205-2216.

Whitehead, I.P., S. Campbell, K.L. Rossman, and C.J. Der. 1997. Dbl family proteins. *Biochimica et biophysica acta*. 1332:F1-23.

Wojcechowskyj, J.A., J.Y. Lee, S.H. Seeholzer, and R.W. Doms. 2011. Quantitative phosphoproteomics of CXCL12 (SDF-1) signaling. *PLoS One*. 6:e24918.

Won, H., W. Mah, E. Kim, J.W. Kim, E.K. Hahm, M.H. Kim, S. Cho, J. Kim, H. Jang, S.C. Cho, B.N. Kim, M.S. Shin, J. Seo, J. Jeong, S.Y. Choi, D. Kim, C. Kang, and E. Kim. 2011. GIT1 is associated with ADHD in humans and ADHD-like behaviors in mice. *Nature medicine*. 17:566-572.

Woolf, E., I. Grigorova, A. Sagiv, V. Grabovsky, S.W. Feigelson, Z. Shulman, T. Hartmann, M. Sixt, J.G. Cyster, and R. Alon. 2007. Lymph node chemokines promote sustained T lymphocyte motility without triggering stable integrin adhesiveness in the absence of shear forces. *Nat Immunol*. 8:1076-1085.

Worbs, T., T.R. Mempel, J. Bolter, U.H. von Andrian, and R. Forster. 2007. CCR7 ligands stimulate the intranodal motility of T lymphocytes in vivo. *J Exp Med*. 204:489-495.

Wu, C., S.B. Asokan, M.E. Berginski, E.M. Haynes, N.E. Sharpless, J.D. Griffith, S.M. Gomez, and J.E. Bear. 2012. Arp2/3 is critical for lamellipodia and response to extracellular matrix cues but is dispensable for chemotaxis. *Cell*. 148:973-987.

Wu, H., and Z.X. Wang. 2003. The mechanism of p21-activated kinase 2 autoactivation. *J Biol Chem*. 278:41768-41778.

Wurbel, M.A., B. Malissen, and J.J. Campbell. 2006. Complex regulation of CCR9 at multiple discrete stages of T cell development. *Eur J Immunol*. 36:73-81.

Xu, J., F. Wang, A. Van Keymeulen, P. Herzmark, A. Straight, K. Kelly, Y. Takuwa, N. Sugimoto, T. Mitchison, and H.R. Bourne. 2003. Divergent signals and cytoskeletal assemblies regulate self-organizing polarity in neutrophils. *Cell*. 114:201-214.

Xu, W., H. Baribault, and E.D. Adamson. 1998. Vinculin knockout results in heart and brain defects during embryonic development. *Development*. 125:327-337.

Yang, Y., and H. Jiang. 2017. Shape and Dynamics of Adhesive Cells: Mechanical Response of Open Systems. *Physical review letters*. 118:208102.

Yoo, Y., H.J. Ho, C. Wang, and J.L. Guan. 2010. Tyrosine phosphorylation of cofilin at Y68 by v-Src leads to its degradation through ubiquitin-proteasome pathway. *Oncogene*. 29:263-272.

York, I.A., and K.L. Rock. 1996. Antigen processing and presentation by the class I major histocompatibility complex. *Annu Rev Immunol*. 14:369-396.

Yoshii, S., M. Tanaka, Y. Otsuki, D.Y. Wang, R.J. Guo, Y. Zhu, R. Takeda, H. Hanai, E. Kaneko, and H. Sugimura. 1999. alphaPIX nucleotide exchange factor is activated by interaction with phosphatidylinositol 3-kinase. *Oncogene*. 18:5680-5690.

Yoshioka, K., V. Foletta, O. Bernard, and K. Itoh. 2003. A role for LIM kinase in cancer invasion. *Proc Natl Acad Sci U S A*. 100:7247-7252.

Yu, H.W., Y.Q. Chen, C.M. Huang, C.Y. Liu, A. Chiou, Y.K. Wang, M.J. Tang, and J.C. Kuo. 2015. beta-PIX controls intracellular viscoelasticity to regulate lung cancer cell migration. *J Cell Mol Med*. 19:934-947.

Yu, J.A., N.O. Deakin, and C.E. Turner. 2010. Emerging role of paxillin-PKL in regulation of cell adhesion, polarity and migration. *Cell Adh Migr*. 4:342-347.

Zaidel-Bar, R., C. Ballestrem, Z. Kam, and B. Geiger. 2003. Early molecular events in the assembly of matrix adhesions at the leading edge of migrating cells. *J Cell Sci*. 116:4605-4613.

Zaidel-Bar, R., R. Milo, Z. Kam, and B. Geiger. 2007. A paxillin tyrosine phosphorylation switch regulates the assembly and form of cell-matrix adhesions. *J Cell Sci*. 120:137-148.

Zamir, E., M. Katz, Y. Posen, N. Erez, K.M. Yamada, B.Z. Katz, S. Lin, D.C. Lin, A. Bershadsky, Z. Kam, and B. Geiger. 2000. Dynamics and segregation of cell-matrix adhesions in cultured fibroblasts. *Nat Cell Biol*. 2:191-196.

Zhang, H., D.J. Webb, H. Asmussen, and A.F. Horwitz. 2003. Synapse formation is regulated by the signaling adaptor GIT1. *J Cell Biol*. 161:131-142.

Zhao, Z.S., E. Manser, T.H. Loo, and L. Lim. 2000. Coupling of PAK-interacting exchange factor PIX to GIT1 promotes focal complex disassembly. *Mol Cell Biol*. 20:6354-6363.

Zheng, Y., D. Zangrilli, R.A. Cerione, and A. Eva. 1996. The pleckstrin homology domain mediates transformation by oncogenic dbl through specific intracellular targeting. *J Biol Chem*. 271:19017-19020.

Zhu, J., and W.E. Paul. 2008. CD4 T cells: fates, functions, and faults. *Blood*. 112:1557-1569.

Zlotoff, D.A., A. Sambandam, T.D. Logan, J.J. Bell, B.A. Schwarz, and A. Bhandoola. 2010. CCR7 and CCR9 together recruit hematopoietic progenitors to the adult thymus. *Blood*. 115:1897-1905.

Ehrenerklärung

Ich versichere hiermit, dass ich die vorliegende Arbeit ohne unzulässige Hilfe Dritter und ohne Benutzung anderer als der angegebenen Hilfsmittel angefertigt habe; verwendete fremde und eigene Quellen sind als solche kenntlich gemacht.

Ich habe insbesondere nicht wissentlich:

• Ergebnisse erfunden oder widersprüchlich Ergebnisse verschwiegen,
• statistische Verfahren absichtlich missbraucht, um Daten in ungerechtfertigter Weise zu
interpretieren,
• fremde Ergebnisse oder Veröffentlichungen plagiiert,
• fremde Forschungsergebnisse verzerrt wiedergegeben.

Mir ist bekannt, dass Verstöße gegen das Urheberrecht Unterlassungs- und Schadensersatzansprüche des Urhebers sowie eine strafrechtliche Ahndung durch die Strafverfolgungsbehörden begründen kann.

Ich erkläre mich damit einverstanden, dass die Arbeit ggf. mit Mitteln der elektronischen Datenverarbeitung auf Plagiate überprüft werden kann.

Die Arbeit wurde bisher weder im Inland noch im Ausland in gleicher oder ähnlicher Form als Dissertation eingereicht und ist als Ganzes auch noch nicht veröffentlicht.

_____ _____

(Ort, Datum) (Unterschrift)